

UNIVERSITÀ DEGLI STUDI DI MESSINA

DIPARTIMENTO DI INGEGNERIA



DOTTORATO DI RICERCA IN INGEGNERIA E CHIMICA DEI
MATERIALI E DELLE COSTRUZIONI (XXXVI CICLO)

SETTORE SCIENTIFICO DISCIPLINARE (SSD) – ING-IND/02
FSE – CUP G47C20000190002

*NUMERICAL AND EXPERIMENTAL ANALYSIS OF
COMPOSITE LIGHTWEIGHT STRUCTURES PRODUCED BY
INNOVATIVE ADDITIVE MANUFACTURING TECHNIQUES*

TUTOR:

PROF. VINCENZO CRUPI

CO-TUTOR:

PROF. GABRIELLA EPASTO

PROF. YORDAN GARBATOV

COORDINATORE:

PROF. EDOARDO PROVERBIO

TESI DI DOTTORATO DI:

ING. SIMONE SCATTAREGGIA MARCHESE

A.A. 2022/2023

Ai miei genitori,
per me fonte di luce

“Be the change you wish to see in the world”

Mahatma Gandhi

ABSTRACT

The present PhD thesis aims to understand to which extent the key enabling technology of Robotic Additive Manufacturing (RAM) can be utilized to produce multi-functional and multi-material composite structures with outstanding performances, oriented to specific applications. In particular, the main goal is to enhance navy ship structures and, in turn, navy ship capabilities.

The main vision driving the study is that the combination of robotics, additive manufacturing, and optimal design methodologies is the key to efficiently develop enhanced and application-oriented multi-functional and multi-material structures. In particular, the PhD work analyses the flexural response of Additive Manufactured Honeycomb Sandwich (AMHS) structures, which embed continuous fibre-reinforced skins and a honeycomb core. Such a structural solution has, interestingly, the potential to unlock the multifunctionality of the structure on both micro and macro scales. Raw materials and manufacturing processes can be purposely developed on the micro scale to satisfy specific structural requirements and functionalities. On the macro scale, multi-functional and multi-material sandwich structures, which integrate the identified raw materials, can be optimally designed and manufactured to satisfy advanced structural specifications.

The study has been conducted according to the following main phases:

- conceptual design of a robotic additive manufacturing platform tailored to satisfy the primary needs of the maritime sector (Chapter 4);
- assessment of the potential of multi-material deposition methods and related composite materials (Chapter 5);
- development of design and numerical optimization procedures for composite sandwich structures produced by additive manufacturing (Chapter 6);
- assessment of the potential of composite sandwich structures produced by additive manufacturing (Chapter 7).

The present PhD thesis provides a systematic methodology to assess to which extent innovative structural solutions and manufacturing procedures can be employed to satisfy the requirements of specific applications. A detailed framework for the optimal design and additive manufacturing of AMHS structures has been developed. Moreover, a comprehensive summary of advantages, drawbacks, challenges, and future research routes related to the addressed topics is given.

ACKNOWLEDGEMENTS

I wish to thank my thesis advisor, Prof. Vincenzo Crupi, for his constant availability and the valuable technical and non-technical advice provided over the years. He has always sustained and promoted my research vision, which has been inspiring.

I want to thank my thesis co-advisor, Prof. Gabriella Epasto, for her guidance through the complex and fascinating world of experimental structural mechanics.

I want to thank my thesis external co-advisor, Prof. Yordan Garbatov, for embracing my research vision and for the insight provided on ship design and optimization procedures. Our daily meetings have enormously contributed to strengthening and focusing the research objectives.

Finally, my profound gratitude goes to my parents and little sister for providing me with unfailing support and continuous motivation. Moreover, I wish to thank my father for being a source of inspiration and for sharing our deep passion for the sea.

ACRONYMS

Acronym	Description
ABS	Acrylonitrile Butadiene Styrene
AHS	Aluminium Honeycomb Sandwich
AM	Additive Manufacturing
AMHS	Additive Manufactured Honeycomb Sandwich
AMHSR	Additive Manufactured Honeycomb Sandwich Raw
ASTM	American Society of Testing and Materials
BTF	Buy-To-Fly
CAD	Computer-Aided Design
CF	Carbon Fiber
CFC	Continuous Fibre Co-extrusion
CFRP	Continuous Fibre-Reinforced Plastic
CFRTP	Continuous Fibre-Reinforced Thermoplastic
CFRTS	Continuous Fibre-Reinforced Thermoset
DIW	Direct Ink Writing
DM	Decision-Maker
DOF	Degrees Of Freedom
EA	Evolutionary Algorithms
EDA	European Defence Agency
EMOO	Evolutionary Multi-Objective Optimization
EO	Evolutionary Optimization
FDM	Fused Deposition Modelling

FI	Failure Index
FPV	Fast Patrol Vessel
FRP	Fibre Reinforced Plastics
FVF	Fibre Volume Fraction
GF	Glass Fiber
KF	Kevlar Fiber
LOM	Laminated Object Manufacturing
MCDM	Multiple Criteria Decision-Making
NSGA	Non-dominated Sorting Genetic Algorithms
OLP	Off-Line Programming
PA	Polyamide
PEEK	Polyether Ether Ketone
PhD	Doctor of Philosophy
PLA	Polylactic Acid
PUR	Polyurethane
PVC	Polyvinyl Chloride
RAM	Robotic Additive Manufacturing
RINA	Registro Italiano Navale
SLA	Stereolithography
SLS	Selective Laser Sintering
STL	Standard Triangulation Language
TP	Thermoplastic
TS	Thermoset
WAAM	Wire Arc Additive Manufacturing

CONTENTS

ABSTRACT	2
ACKNOWLEDGEMENTS.....	3
ACRONYMS	4
CONTENTS.....	6
1 INTRODUCTION	8
1.1 MOTIVATION	9
1.2 OBJECTIVES.....	10
1.3 THESIS FRAMEWORK	11
2 METHODOLOGY AND FUNDAMENTALS.....	13
2.1 CONCEPT DESIGN OF A RAM PLATFORM FOR MARINE APPLICATIONS	14
2.2 EXPERIMENTAL ASSESSMENT OF COMPOSITES PRODUCED BY AM.....	15
2.3 OPTIMAL DESIGN OF SANDWICH STRUCTURES PRODUCED BY AM	15
2.4 NUMERICAL ASSESSMENT OF SANDWICH STRUCTURES PRODUCED BY AM .	15
3 STATE OF THE ART	16
3.1 ADDITIVE MANUFACTURING TECHNOLOGY	17
3.2 ROBOTIC ADDITIVE MANUFACTURING AND THE MARITIME INDUSTRY	27
3.2.1 RAM CAPABILITIES FOR THE MARITIME INDUSTRY	28
3.2.2 RAM MAIN CHALLENGES AND RESEARCH DRIVERS.....	32
3.3 DESIGN METHODOLOGIES FOR SANDWICH STRUCTURES	33
3.3.1 SANDWICH GENERAL DESCRIPTION	33
3.3.2 BENDING AND SHEAR STRESSES	36
3.3.3 FLEXURAL DEFORMATION.....	39
3.3.4 FAILURE MODES	40
3.4 OPTIMIZATION PROCEDURES FOR SANDWICH STRUCTURES	44
3.5 DISCUSSION.....	49
4 CONCEPT DESIGN OF A RAM PLATFORM FOR MARINE APPLICATIONS	51
4.1 PHASE I: ADDITIVE MANUFACTURING TECHNIQUES FOR RAM	52

4.2	PHASE II: RAM PLATFORM DESIGN	55
4.3	DISCUSSION.....	59
5	EXPERIMENTAL ASSESSMENT OF COMPOSITES PRODUCED BY AM	62
5.1	CFC ADDITIVE MANUFACTURING PROCESS	63
5.2	MECHANICAL CHARACTERIZATION	64
5.2.1	CHOPPED FIBRE-REINFORCED PLASTIC	66
5.2.2	CONTINUOUS FIBRE-REINFORCED PLASTIC	70
5.3	DISCUSSION.....	77
6	OPTIMAL DESIGN OF SANDWICH STRUCTURES PRODUCED BY AM.....	82
6.1	MODELLING AND ADDITIVE MANUFACTURING	83
6.2	ANALYTICAL FORMULATIONS FOR DESIGN	87
6.2.1	DISPLACEMENT	88
6.2.2	FAILURE MODES	91
6.2.3	WEIGHT	97
6.2.4	COST	99
6.3	EXPERIMENTAL TESTING	101
6.3.1	DESIGN SOLUTION COMPARISON: AMHS VS AMHSR	102
6.3.2	RESULTS OF THE 3-POINT BENDING TESTING CAMPAIGN	105
6.4	OPTIMAL SANDWICH DESIGN	113
6.5	DISCUSSION.....	116
7	NUMERICAL ASSESSMENT OF SANDWICH STRUCTURES PRODUCED BY AM	118
7.1	ASSESSMENT OF AMHS FOR FPV MIDSHIP SECTION DESIGN	120
7.2	COMPARISON AGAINST RINA RULES AND TRADITIONAL STRUCTURES.....	128
7.3	DISCUSSION.....	131
8	CONCLUSIONS.....	133
8.1	FUTURE RESEARCH ROUTES.....	136
	REFERENCES	137
	LIST OF FIGURES.....	143

1 INTRODUCTION

Additive Manufacturing (AM) is a disruptive technology which is drastically reshaping the traditional way of designing, manufacturing and supplying components. While many industrial sectors are successfully leveraging its potential to develop and manufacture more efficient products through cutting-edge technologies, the maritime sector seems to be at its infancy regarding industrial applications. This has to be primarily brought back to robust design procedures, consolidated manufacturing methods and stringent regulations that have prevented the full integration of this technology and, in turn, the potential improvement of structural performances and manufacturing and supply chain efficiency.

With this scenario in mind, the present PhD study consistently attempts to pave the way for the integration of multi-functional and multi-material composite lightweight structures, produced by innovative manufacturing technologies, in the maritime field. In particular, the study is focused on Additive Manufactured Honeycomb Sandwich (AMHS) structures, which embed continuous fibre-reinforced skins and a honeycomb core. Such structures have been manufactured by innovative AM techniques (Chapter 5) to be integrated into a purposely conceived Robotic Additive Manufacturing platform (Chapter 4) and have been designed through ad-hoc developed optimal design methodologies (Chapter 6).

A detailed framework for the optimal design and additive manufacturing of AMHS structures has been developed within this research work, with the primary aim of assessing to which extent innovative structural solutions and manufacturing procedures can be employed to satisfy the requirements of a specific naval application, enhancing its capabilities (Chapter 7).

It is worth mentioning that the PhD work has been conducted within a collaboration framework among the Department of Engineering, University of Messina, Messina (IT), the Centre for Marine Technology and Ocean Engineering at Instituto Superior Técnico, University of Lisbon, Lisbon (PT) and the research-intensive company Signo Motus Srl, Messina (IT).

1.1 MOTIVATION

The main vision driving the present PhD study is the following:

“The combination of robotics, additive manufacturing and optimal design methodologies is the key to enable an efficient development of enhanced and application-oriented multi-functional and multi-material structures.”

In the context of the present PhD work, multi-functional and multi-material structures are tailored to enhance the capabilities of navy vessels. In particular, the work deals with Additive Manufactured Honeycomb Sandwiches (AMHS) to be produced employing Robotic Additive Manufacturing (RAM) techniques.

The utilization of the RAM technology opens up unprecedented possibilities concerning the potential to tune the structural and functional requirements of the sandwich within and through the layers that build up the whole structure. Moreover, it enlarges the range of employable core cellular topologies and usable composite materials for the skins and core. A further evolution of currently employed sandwich structures may be achieved using more efficient and sustainable materials, based on different matrix systems, functionalized by additives and-or reinforced by fibres. Such innovative raw materials, integrated into purposely designed and manufactured sandwich structural solutions, may achieve enhanced structural performances (e.g., weight savings, impact resistance), sustainability, recyclability and multifunctionality (e.g., fire resistance, radar invisibility, corrosion resistance, etc.).

Among the research areas to be addressed for achieving the mentioned objectives, the development of advanced design solutions and efficient manufacturing methods are the most relevant, as they may lead to attain outstanding structural performances, which, in turn, encourage the integration of multi-functional and multi-material solutions in industrial fields. Moreover, identifying key design parameters is of unprecedented importance to guide the development of materials and manufacturing procedures, oriented to maximize structural capacity and to fulfil advanced requirements.

Given the above framework, the PhD thesis has focused on the development of optimal design procedures for AMHS and of a framework for the robotic additive manufacturing of such innovative structural solutions.

1.2 OBJECTIVES

The present PhD thesis aims to understand to which extent the key enabling technology of Robotic Additive Manufacturing (RAM) can be utilized to produce multi-functional and multi-material composite structures with outstanding performances, oriented to specific structural applications. In particular, the work deals with Additive Manufactured Honeycomb Sandwich (AMHS) structures, which embed continuous fibre-reinforced skins and a honeycomb core, to be employed as structural elements in navy ships.

The objectives will be pursued by means the following main steps:

- State-of-the-art analysis, tailored to:
 - understand the key features of additive manufacturing technology, giving particular attention to processes suited to robotic applications;
 - highlight the potential of robotic additive manufacturing technology in fulfilling the main needs of the maritime sector;
 - identify suited design methodologies for sandwich structures;
 - identify suited optimization procedures for the design of sandwich structures.
- conceptual design of a robotic additive manufacturing platform tailored to satisfy the primary needs of the maritime sector;
- assessment of the potential of multi-material deposition methods and related materials, accounting for significative variables governing the process and minimum material requirements from Classification Societies Rules;
- development of design and numerical optimization procedures for composite sandwich structures produced by additive manufacturing, to be used as structural elements in the maritime field;
- assessment of the potential of composite sandwich structures produced by additive manufacturing, by comparison against traditional primary structures employed in the midship section of navy ships, minimum material requirements from Classification Societies Rules and current providers of similar structural solutions.

1.3 THESIS FRAMEWORK

The present section highlights the main contents of the present PhD thesis.

Chapter 1

This chapter provides an introduction on the research topic, defining the motivation and the main objectives of the work.

Chapter 2

This chapter describes in detail the methodology adopted to achieve the goals of the study, addressing the main contents and objectives of each phase of the work.

Chapter 3

This chapter reports the literature research that has been conducted concerning:

- additive manufacturing technology;
- the potential of the robotic additive manufacturing technology in fulfilling the main needs of the maritime sector;
- design methodologies for sandwich structures;
- optimization procedures for the design of sandwich structures.

Chapter 4

This chapter describes the conceptual design of a robotic additive manufacturing platform, which has been developed to fulfil the primary needs of the maritime sector.

Chapter 5

This chapter reports the assessment, conducted through systematic experimental testing, of the potential of multi-material deposition methods and related materials. The work accounts for significant variables governing the AM process and minimum material requirements from Classification Societies Rules.

Chapter 6

This chapter describes the development of design procedures for composite sandwich structures, which embed continuous fibre-reinforced skins and a honeycomb core. The method is built upon multi-objective optimization algorithms, which utilize purposely developed analytical equations calibrated through a systematic experimental testing campaign.

Chapter 7

This chapter reports the assessment of the potential of composite sandwich structures produced by AM. Different sandwich solutions are numerically developed and compared against traditional primary structures employed in the midship section of navy ships, minimum material requirements from Classification Societies Rules and current providers of similar structural solutions.

Chapter 8

This chapter reports the conclusions of the thesis work and defines future research routes and relative challenges to be addressed.

2 METHODOLOGY AND FUNDAMENTALS

The main objective of this chapter is to describe the methodology followed to assess to which extent the key enabling technology of Robotic Additive Manufacturing (RAM) can be utilized to produce multi-functional and multi-material composite structures with outstanding performances, oriented to naval structural applications.

The PhD thesis work takes its steps from an in-depth analysis of the state-of-the-art, which has been focused on the following main topics:

- additive manufacturing technology (section 3.1);
- the potential of the robotic additive manufacturing technology in fulfilling the main needs of the maritime sector (section 3.2);
- design methodologies for sandwich structures (section 3.3);
- optimization procedures for the design of sandwich structures (section 3.4).

The first two blocks of the state-of-the-art study have been oriented to identify to which extent additive manufacturing and robotics may be efficiently combined to satisfy the main needs of the maritime sector. The main research drivers and related challenges to achieve such an objective have been identified.

The development of an efficient design workflow for lightweight structures produced by AM is one of the main research drivers to achieve the integration of the Robotic Additive Manufacturing (RAM) technology in the maritime sector. Therefore, the study has thus been oriented to understand how lightweight structures are currently designed to match structural requirements. In particular, the main focus has been on sandwich structures, as they represent promising structural solutions, particularly suited to the RAM technology and the maritime sector.

The last block of the state-of-the-art study has been oriented to analyse optimization procedures for the design of sandwich structures. In particular, the main focus has been on multi-objective optimization methods and evolutionary algorithms.

The analysis of the state-of-the-art has allowed to develop the necessary knowledge to build a systematic workflow to achieve the objectives of the work.

As mentioned, the main vision driving the present PhD study is the combination of robotics, additive manufacturing and optimal design methodologies is the key to enable an efficient development of enhanced and application-oriented multi-functional and multi-material structures.

To validate the above-stated vision, the following activities have been conducted:

- conceptual design of a robotic additive manufacturing platform tailored to satisfy the primary needs of the maritime sector (Chapter 4);
- assessment of the potential of multi-material deposition methods and related composite materials, accounting for significant variables governing the process and minimum material requirements from Classification Societies Rules (Chapter 5);
- development of design and numerical optimization procedures for composite sandwich structures produced by additive manufacturing, to be used as structural elements in the maritime field (Chapter 6);
- assessment of the potential of composite sandwich structures produced by additive manufacturing, by comparison against traditional primary structures employed in the midship section of navy ships, minimum material requirements from Classification Societies Rules and current providers of similar structural solutions (Chapter 7).

The objectives of the mentioned activities are addressed in the following sections.

2.1 CONCEPT DESIGN OF A RAM PLATFORM FOR MARINE APPLICATIONS

The main purpose of the work is to develop the conceptual design of a robotic additive manufacturing platform suited to marine applications. Such a design is given in terms of design and manufacturing workflow description. A design and manufacturing methodology that leverages robotics, additive manufacturing and optimal design procedures is proposed with the aim to improve structural performances and manufacturing efficiency.

A relevant output of this study is the identification of additive manufacturing techniques suited to robotics and marine applications. Moreover, key research areas to be addressed to achieve the full integration of the RAM technology in the maritime sector are highlighted.

2.2 EXPERIMENTAL ASSESSMENT OF COMPOSITES PRODUCED BY AM

The main purpose of the work is to highlight the potential of multi-material deposition methods for composite lightweight structures. Such AM techniques have been previously identified as promising solutions for RAM applications in the maritime sector. Therefore, the main goal is to assess their potential, before their integration in RAM platforms, to enhance the capabilities of the process.

The promising “Continuous Fibre Co-extrusion” (CFC) technique is selected for the additive manufacturing of composite lightweight structures for marine applications. A mechanical characterization campaign is conducted to assess the tensile response of continuous and chopped carbon fibre-reinforced composites manufactured by such a technology, accounting for the influence of the main process parameters. Finally, the results are compared to minimum material requirements from Classification Societies Rules and traditionally manufactured composites.

2.3 OPTIMAL DESIGN OF SANDWICH STRUCTURES PRODUCED BY AM

The main purpose of the work is to develop a validated design procedure for Additive Manufactured Honeycomb Sandwich (AMHS) subjected to flexural loads. Such structures are manufactured using the multi-material deposition method previously investigated. The design procedure leverages a purposely developed Evolutionary Multi-Objective Optimization (EMOO) routine to identify the optimal structure. The analytical formulations used in the optimization process are derived by means of a combined analytical and experimental approach. The experimental results obtained through testing of AMHS specimens, realized through the CFC technology, have been related to structural mechanics principles to develop design equations suited to the purposes of the EMOO.

2.4 NUMERICAL ASSESSMENT OF SANDWICH STRUCTURES PRODUCED BY AM

The main purpose of the work is to assess to which extent Additive Manufactured Honeycomb Sandwich (AMHS) can be applied as primary structural members in navy ships. To achieve such an objective, different AMHS solutions are designed, leveraging the optimal design methods previously developed, to satisfy the structural requirements of an already designed and manufactured steel Fast Patrol Vessel (FPV). Hereafter, such innovative structural solutions are compared against traditional primary structures employed in the FPV midship section. Moreover, this work establishes solid benchmarks w. r. t. minimum material requirements from Classification Societies Rules and current providers of similar structural solutions.

3 STATE OF THE ART

The literature study is reported and discussed in detail in this chapter. It has been conducted concerning the following main topics:

- additive manufacturing technology (section 3.1);
- the potential of the robotic additive manufacturing technology in fulfilling the main needs of the maritime sector (section 3.2);
- design methodologies for sandwich structures (section 3.3);
- optimization procedures for the design of sandwich structures (section 3.4).

Section 3.1 describes the additive manufacturing technology, highlighting the main process features, advantages and drawbacks. Particular attention is given to additive manufacturing processes and composite materials suited to robotics applications.

Section 3.2 highlights the potential of the robotic additive manufacturing technology in fulfilling the main needs of the maritime sector and describes the main research drivers and challenges to integrate the RAM technology in such a sector.

Section 3.3 addresses currently used methodologies for the structural design of traditional sandwich structures.

Section 3.4 gives an insight into the main principles related to optimization procedures for the structural design of sandwich structures.

3.1 ADDITIVE MANUFACTURING TECHNOLOGY

Additive Manufacturing (AM) refers to technologies that build physical objects directly from 3D Computer-Aided Design (CAD) data. AM techniques add layer-by-layer liquid, sheet, wire, or powdered materials to form parts with little (or without) post-processing requirements.

The “American Society of Testing and Materials” (ASTM) has defined Additive Manufacturing as follows:

“Process of joining materials to make objects from 3D model data, usually layer upon layer, as opposed to subtractive manufacturing methodologies, such as traditional machining.”

The Additive Manufacturing processes can be categorized in relation to the methodology employed to construct the layers that form the part geometry. According to ASTM, the additive manufacturing methods may be grouped as:

- *Material jetting*: "process in which droplets of build material are selectively deposited";
- *Vat photopolymerization*: "process in which liquid photopolymer in a vat is selectively cured by light-activated polymerization";
- *Binder jetting*: "process in which a liquid bonding agent is selectively deposited to join powder materials";
- *Material extrusion*: "process in which material is selectively dispensed through a nozzle or orifice";
- *Direct energy deposition*: "process in which focused thermal energy is used to fuse materials by melting as they are being deposited";
- *Sheet lamination*: "process in which sheets of material are bonded to form an object";
- *Powder bed fusion*: "process in which thermal energy selectively fuses regions of a powder bed".

Each group embeds different AM processes characterized by the same deposition methodology. However, techniques in the same group may present various process features and utilize different raw materials.

The above-addressed additive manufacturing methods are illustrated in Figure 1.



Figure 1: Additive Manufacturing processes

The illustrated additive manufacturing methods utilize a common workflow for part production, which can be briefly summarized as follows:

1. component design and 3D CAD modelling;
2. generating suitable file format (e.g., high-resolution STL);
3. slicing and generation of code for the machine (e.g., G-Code);
4. machine preparation and additive manufacturing process;
5. post-processing (e.g., annealing, coating, etc.).

The engineering approach for parts production is reshaped from the design and 3D CAD model development to the final post-processing step. Some process steps are entirely renewed (e.g., design, post-processing) w. r. t. traditional manufacturing operations, enabling relevant advantages. The Additive Manufacturing technology opens up the innovative design paradigm of “manufacturing the design”, which is replacing the traditional “design for manufacturing” [1]. The AM reduces the design constraints concerning conventional manufacturing methods and promotes innovation in the design and optimisation phases [2]. Moreover, additive manufacturing disrupts the traditional supply chain, allowing the resulting products to be produced at the point of use and at the time of need, which limits material waste, inventory costs and lead time [3].

Considering the provided general framework, it is possible to understand why industrial and military sectors are expressing a growing interest in the additive manufacturing technology. The European Defence Agency (EDA) expects to

enhance defence capabilities in mobility, sustainability, effect, and protection [4]. The maritime sector progressively recognises additive manufacturing as a promising solution to meet its needs. Several innovative case studies have been recently developed, assessing the potential applicability of such a technology to marine applications [5]. Moreover, the availability of new materials and AM methods is growing the interest towards the integration of innovative solutions in ship design processes, oriented to achieve optimal structural performances [6]–[8].

Despite the advantages and potential of additive manufacturing, it is necessary to face drawbacks and challenges to fully integrate the AM technology in industrial sectors. The main difficulties concern product mechanical properties, component size and structural design methods.

The main drawbacks of additive manufactured components include inferior and anisotropic mechanical properties, with defects [9]. Such disadvantages are related to the manufacturing strategy, which involves the definition of process parameters, deposition patterns and post-processing solutions. Each approach leads to different outcomes, highly affecting product properties [10]. Additional constraints derive from the deposition process of conventional AM techniques, which is based on horizontal layer fabrication through machines possessing three degrees of freedom (DOF) and often operating in controlled environments. Such a machine setup generates further limitations related to product size, part complexity, deposition rates, need for support structures and usually costs [11]. It is finally worth mentioning that it is impossible to fully exploit the potential of additive manufacturing without using validated structural design methods, which lead to the design of components with optimal performances. The gain in performance may boost the integration of AM technology in industrial fields and the development of design and additive manufacturing standards.

Considering the provided context, the rationale behind formulating the objectives for the PhD thesis becomes evident. As it will be demonstrated, a robotic additive manufacturing solution, combined with a validated optimal design approach, has high potential to overcome current AM limitations and challenges, and thus to produce lightweight components with outstanding performances.

The PhD work is focused on additive manufacturing techniques which utilize Fibre Reinforced Plastics (FRP). Therefore, an overview of current manufacturing processes for FRP is given in the following, dedicating particular attention to their mechanical properties and relevant AM process parameters.

Among the established AM processes, the focus of the present PhD thesis work, and thus of the state-of-the-art study, has been on Fused Deposition Modelling (FDM) based processes. FDM is particularly suited to flexible, low-cost, and sustainable robotic additive manufacturing processes for multi-functional and multi-material marine applications.

Fibre-reinforced plastics can be classified into discontinuous (or chopped) and continuous FRPs. Discontinuous FRPs have been fabricated using four AM techniques, namely Fused Deposition Modelling (FDM) using thermoplastic filaments, Direct Ink Writing (DIW) using thermoset epoxy resin, Selective Laser Sintering (SLS) using plastic powder, and Stereolithography (SLA) using photopolymer resin. Continuous FRPs have been manufactured using three AM techniques, namely FDM, SLA, and LOM (Laminated Object Manufacturing), which uses plastic sheets.

The most popular reinforcing fibres employed are carbon fibre (CF), glass fibre (GF) and Kevlar fibre (KF). Fibres are used in the form of filaments or sheets. The most commonly used matrix materials are Nylon (e.g., PA6 and PA12), polylactic acid (PLA), and acrylonitrile butadiene styrene (ABS). Recent advancements in AM techniques have introduced 3D printers capable of processing advanced matrix materials, such as polyether ether ketone (PEEK), which have better mechanical performance than Nylon, PLA, and ABS.

Due to its simplicity and cost-effectiveness, the FDM technique is well-established for manufacturing discontinuous FRPs. Figure 2 illustrates a typical FDM process scheme. The material filament is deposited layer by layer to create the part geometry. Upon printing one material layer, the build platform shifts downward by one layer thickness, allowing the next layer to be fabricated. The support material filament can be used to create a foundation when necessary. After fabrication, the printed part is removed from the platform, and the support material is dissolved or detached.

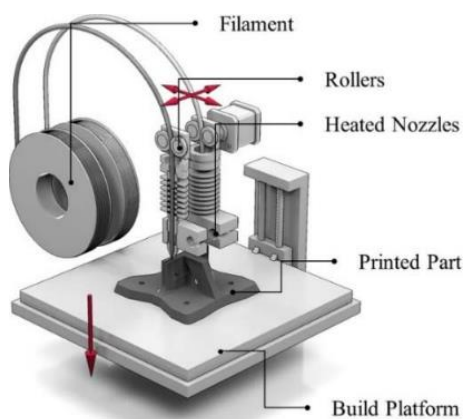


Figure 2: Typical FDM process

Discontinuous fibres used in additive manufacturing (AM) can be categorized based on their length or diameter into three groups: nano-fibres with diameters significantly less than $1\mu\text{m}$, like graphene nanoplates, carbon nano-fibres, multi-walled carbon nanotubes, and carbon black nanoparticles; micro-fibres ranging from $50\mu\text{m}$ to $400\mu\text{m}$ in length; milli-fibres with lengths in the millimetre scale. It is worth mentioning that milli-fibres are currently exclusively suited for successful utilization in the Stereolithography (SLA) process. Despite millimetre-long fibres being applied in the Fused Deposition Modelling (FDM) process, fibre breakage is usually experienced during the intense shear melting and mixing phases, reducing fibres to around $400\mu\text{m}$.

The mechanical properties of discontinuous FRPs vary with the fibre type and treatment of filaments, fibre weight percentage (wt.%), fibre length, matrix, loading direction and printing temperature.

The employment of carbon fibre reinforcements usually leads to the highest mechanical performance. Figure 3 shows that CF/ABS composites manufactured through different AM machines possess higher modulus and strength w. r. t. GF/ABS composites. It is worth noting that even if the same materials are employed, the mechanical properties may vary in relation to employed additive manufacturing process. The mechanical properties of discontinuous FRPs shown in such a figure could be further enhanced by adding a consolidation step when mixing and extruding the reinforced filament [12], [13].

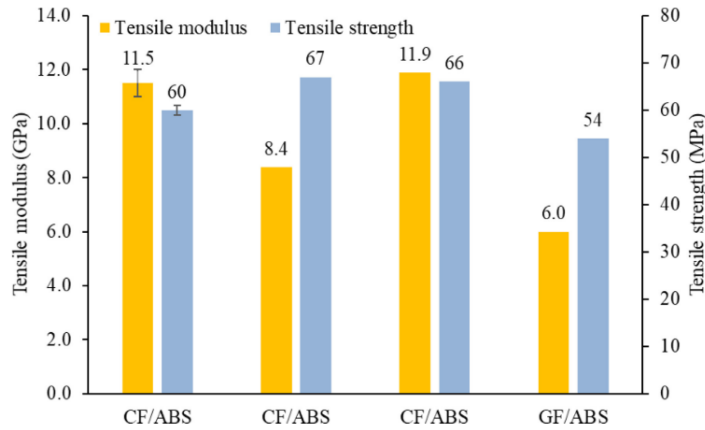


Figure 3: Influence of fibre type on chopped FRP properties (20 wt.%) [14]

The mechanical performances of discontinuous FRPs increase with fibre weight percentage when PA, PLA or ABS is the matrix. As shown in Figure 4, the trend follows the well-known rule of mixtures when a good interfacial bonding between fibres and matrix is obtained. An increase in FRPs mechanical properties may also be achieved by increasing the fibre length and keeping the fibre weight percentage constant. However, as mentioned, fibre breakage may limit the achievable length and, thus, the performance gain.

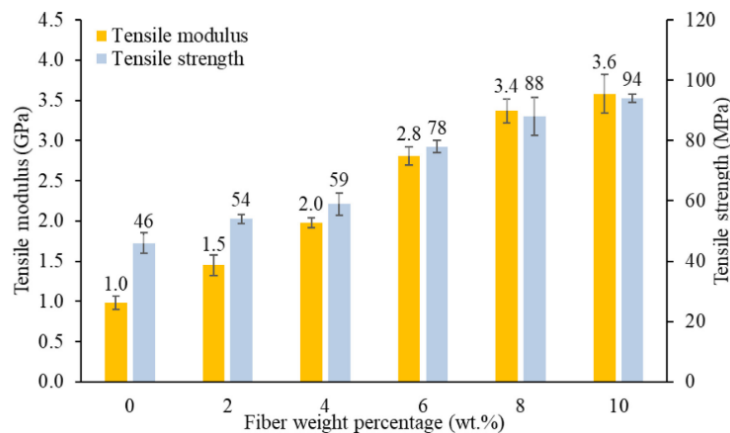


Figure 4: Influence of fibre weight on chopped FRP properties [14]

The combination of fibre and matrix plays an essential role in defining the mechanical properties of FRPs. Composites with PEEK as a matrix have higher tensile strength than the composites using PLA or ABS due to the greater tensile strength of PEEK. However, the tensile modulus of CF/PEEK composite is usually the lower w. r. t. other fibre solutions. This suggests selecting the highest-strength fibre and matrix may not always be the best option.

The tensile properties of discontinuous FRPs are sensitive to the loading direction. The tensile yield strength of CF/PLA composite loaded perpendicularly to the printing direction is only two-thirds of that of CF/PLA composite loaded along the printing direction. A similar result has been found for the CF/ABS material combination. This result is due to the alignment of fibres in the print direction during the extrusion process. Thus, the fibre orientation must be carefully chosen when designing the FRPs components.

The printing temperature is a key parameter to be accounted for the achievement of optimal FRPs mechanical properties. In general, as shown in Figure 5, higher processing temperature increases the tensile properties of PLA and ABS-based composites. However, a decrease in the tensile strength of PA-based composites has been observed when the processing temperature increases. The definition of an optimal processing temperature is indeed relevant to minimize voids and maximize inter-layer and intra-layer bonding, increasing the mechanical properties.

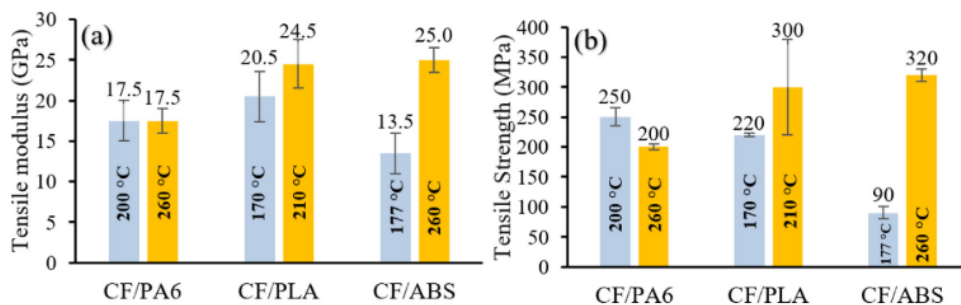


Figure 5: Influence of print temperature on FRP properties [14]

Most continuous fibre-reinforced plastics (CFRPs) are fabricated through FDM due to its simplicity of operation and cost-effectiveness. Current global research approaches for CFRP manufacturing through FDM explore four potential methods, illustrated in Figure 6, to integrate the continuous fibre reinforcement into the thermoplastic matrix (TP) extruded by the 3D printer head:

- fibres are incorporated into the TP filament as a preprocessing step, outside the 3D printer. A continuous fibre-reinforced thermoplastic (CFRTP) filament is thus pre-manufactured and stored. Such a filament is then fed to, processed, and extruded by the 3D printer head (Figure 6 a);
- fibres and TP filament are separately fed to the 3D printer head. The fibres are incorporated into the TP melt inside of the 3D printer head and the resulting CFRTP melt is extruded hereafter (Figure 6 b);

- fibres and TP filament are separately fed to the 3D printer. The fibres are laid down on top of the extruded TP filament (Figure 6 c);
- fibres are impregnated into a high-performance epoxy TS matrix, which is thermally cured as a pre-processing step outside the 3D printer. Such a stabilized filament is fed to the 3D printer head, together with a TP filament. Therefore, the CFRTS filament is embedded into the TP melt inside the 3D printer head and extruded hereafter (Figure 6 d).

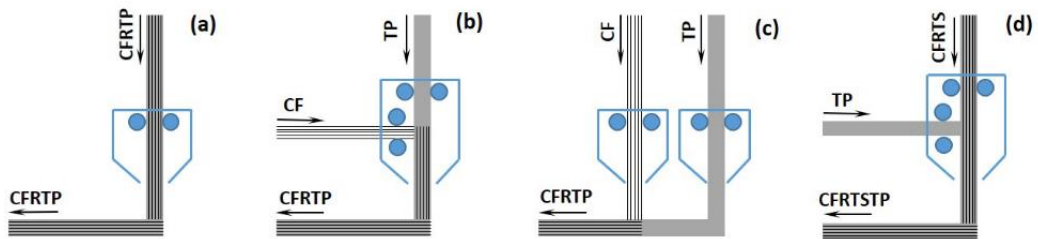


Figure 6: AM of continuous fibre trough FDM [15]

The concept of the TS-TP bi-matrix system was investigated and developed by “Anisoprint Sarl” in conjunction with the idea of CFRP FDM [16]. The main aim was to leverage the process advantages to mitigate the disadvantages associated with additive manufacturing technologies based on TP or TS polymer matrixes.

The TS-TP bi-matrix CFRP FDM method is based on the following:

- the fact that the TS matrix offers the needed processability characteristics (low viscosity for good fibre impregnation) to obtain excellent quality and high-performance CFRTS composite filament;
- the fact that the TP matrix offers the needed processability characteristics for the FDM method: enough viscosity of the melt phase to be extruded by the 3D printer head and optimal solidification time during the cooling down phase to ensure maintenance of the desired shape of the additively manufactured part without self-weight distortions;
- the assumption that the good FDM processability characteristics can be preserved for the multi-material fibre TS-TP composite system;
- the assumption that a good adhesion bond strength can be achieved between the constituents of the multi-material system to ensure the high performance of the 3D printed composite.

The core benefit of the TS-TP bi-matrix CFRP FDM method is the uncoupling of the fibre impregnation and extrusion steps. Impregnation is realized outside the 3D printer as a separate and well-controlled pre-manufacturing step using a high-performance TS polymer matrix (thermo-curable epoxy). As mentioned, the obtained CFRTS filament is fed to the 3D printer head, which embeds the CFRTS filament into the TP melt (co-extrusion), getting a high-performance CFRTSTP composite. This method overcomes one of the main limitations of current CFRP FDM methods and systems, i.e., the poor impregnation of the reinforcing fibres by the high-viscosity TP matrix [15]. Furthermore, owing to the impregnation-extrusion decoupling characteristic, the bi-matrix CFRP FDM can also utilize engineering-grade high-performance TP polymers (e.g., PEEK and PEI), representing another challenge for CFRP additive manufacturing techniques.

The mechanical properties of continuous FRPs vary with fibre type and treatment of fibre filaments, fibre volume fraction, matrix, and external compaction. Figure 7 presents the mechanical test data obtained on “Markforged” composites with approximately 40% of fibre volume fraction (FVF), considering the continuous fibres oriented along the loading direction.

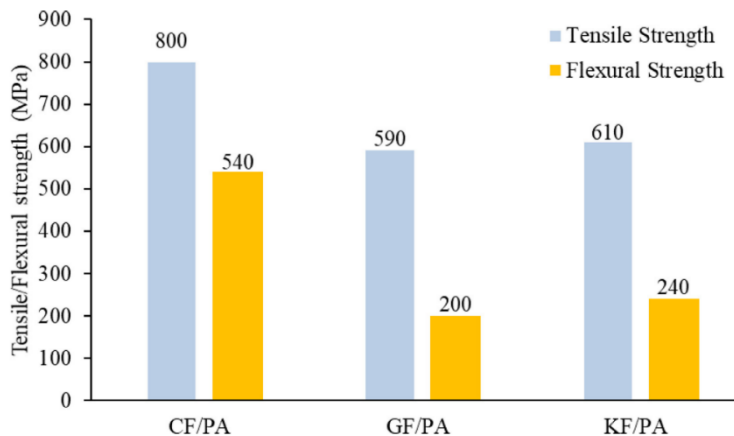


Figure 7: Influence of fibre type on continuous FRP properties [14]

The CF/PA composite has the highest tensile and flexural strengths, followed by KF/PA and GF/PA composites. Notably, the tensile strength of CF/PA composite (800 MPa) is almost ten times the one of composites that embed discontinuous fibres (approximately 80 MPa).

The quality of the fabricated fibre filament affects the bonding between fibres and matrix, influencing the overall properties of continuous FRPs produced by AM. The interfacial bonding between matrix and raw fibres in AM-fabricated composites is usually not particularly good. However, as mentioned, the innovation related to new AM techniques is starting to be successfully oriented to improve the bonding strength between fibres and matrix (bi-matrix 3D printing).

The tensile modulus and strength of the CF/PA composite increase with CF volume fraction, as shown in Figure 8. The mechanical properties of GF and KF-reinforced composites show a similar trend. Moreover, increasing carbon fibre volume fraction in CF/PA composite improved compressive and shear properties.

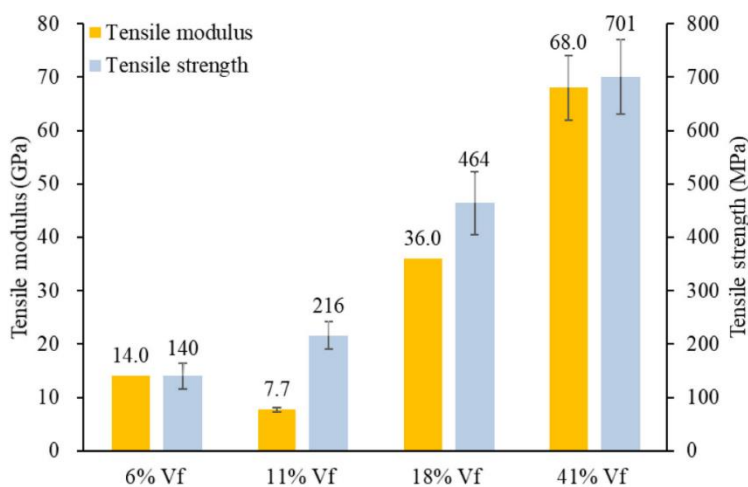


Figure 8: Influence of FVF on continuous FRP properties [14]

The matrix mechanical properties contribute slightly to FRP strength and elastic moduli, as the fibre type and content are the most relevant parameters. However, there are essential features to be considered, such as fibre-matrix interface bonding and matrix-matrix interface bonding, which highly affect the structural response. Moreover, matrix ductility influences the plastic and dynamic response of FRP components.

Compaction during 3D printing has been developed to prevent the formation of a large number of voids in the printing process and to increase the inter and intra-laminar shear strength. Pressure has a significant effect as it greatly enhances the tensile (645 MPa versus 110 MPa) and flexural (401 MPa versus 163 MPa) strengths of CF/PLA composites [13].

3.2 ROBOTIC ADDITIVE MANUFACTURING AND THE MARITIME INDUSTRY

This section describes an innovative solution combining additive manufacturing and robotics to achieve a low-cost, flexible and sustainable manufacturing process, that is not limited to small workspaces or horizontal layer deposition [11].

Robotic Additive Manufacturing (RAM) platforms have the potential to overcome traditional additive manufacturing process constraints and thus to extend the range of applications in industries, such as the maritime one. In the context of the present PhD thesis, RAM means:

“The integration of purposely conceived additive manufacturing techniques into robotic platforms to improve process flexibility, building volumes, deposition rates, material waste and product properties at contained costs.”

The present section reports the potential benefits of employing a robotic additive manufacturing solution, and more generally, the AM technology, in the maritime sector (section 3.2.1). Moreover, the main challenges and research drivers to integrate such technology in industrial fields are addressed (section 3.2.2).

3.2.1 RAM CAPABILITIES FOR THE MARITIME INDUSTRY

Several benefits may be achieved by employing the robotic additive manufacturing technology for shipbuilding. The main ones are illustrated in Figure 9.

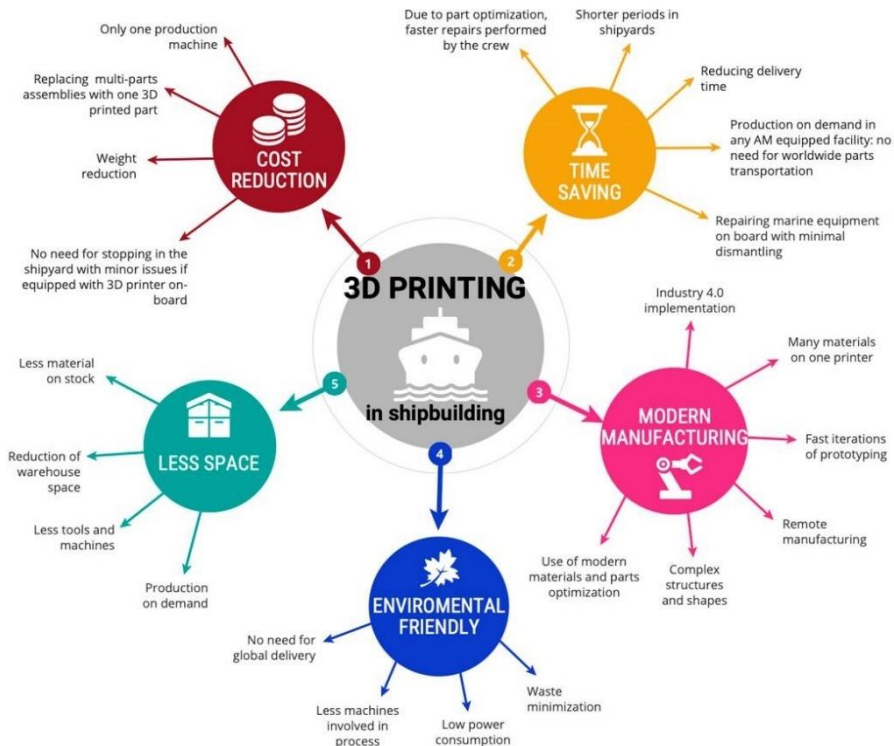


Figure 9: Potential benefits of the AM/RAM technology for shipbuilding

The potential advantages that may result from the integration of RAM technology in the maritime field can be grouped into two big categories:

- *industrial*: which is related to the efficiency of production processes and supply chain;
- *operational*: which is dependent on the intended use of the vessel, but can be translated into the enhancement of performances (e.g., speed increase).

The main industrial advantages are:

- *production flexibility*: one of the main challenges of current naval components manufacturing processes is the production of large-size parts with complex shapes. Nowadays, the manufacturing processes of double-curved hull blocks and components (e.g., propeller, rudder, bulbous bulb, etc.) are expensive and time-consuming [17]. The highly utilized moulds for complex shape parts, metal

casting, or hull construction through lamination are inefficient solutions regarding production flexibility, lead times and costs. Furthermore, modern shipbuilding technologies, such as ship block assembly or hull lamination, are carried out manually, raising concerns about quality control and safety [18]. Considering this framework, using the RAM technology to manufacture large-size and complex parts offers significant advantages over traditional manufacturing methods. Components that are difficult to manufacture or assemble, such as steel plates, can be directly produced as one piece in one process stage, resulting in increased production efficiency and quality [19]. Complex components or structures, such as propellers or boat hulls, usually produced via moulds, are starting to be optimized and manufactured through RAM. Two examples of RAM applications in the maritime sector are given in Figure 10. On the top of such a figure, a hollow propeller blade manufactured through a robotic WAAM process in duplex stainless steel is shown. Process flexibility has been exploited to enhance propeller performances by developing an innovative hollow propeller concept. The hollow blade significantly improves the hydrodynamic and transverse performances: the cavitation is reduced considerably compared to the reference propeller, and the mass is reduced by 23% in air and 36% in water [20]. On the bottom of Figure 10, a boat hull (“MAMBO”) produced through continuous fibre manufacturing technology (patent WO 2017/085649 A1) is shown. Such a robotic process has been exploited to develop an innovative procedure for the production of composite boat hulls, paving the way for optimized designs which minimize material waste;

- *manufacturing efficiency*: the RAM process characteristics imply less use of raw material w. r. t. traditional manufacturing processes and AM methods. The buy-to-fly (BTF) ratios, i.e., the weight of the raw materials divided by the final weight of the final component, may be up to 20:1 in traditional manufacturing processes. In conventional AM processes, material waste is related to post-processing operations and to the need for support structures. This can drastically reduce the BTF ratios, achieving material savings of approximately 60% and time savings of 30% [21]. The additional RAM flexibility can be leveraged to further reduce material waste by eliminating the need for support structures and thus allow the direct production of components with overhangs [22]. This possibility is a great advantage, especially for large and complex components, and represents a challenge towards a sustainable manufacturing process;

- *supply chain efficiency*: one of the ship owners' main concerns is ship downtime. Inactive ship working times result in high costs without profits. Additive manufacturing allows the production of parts where the ship is currently located, reducing lead times, and supplying costs. The AM building platform can be integrated onboard, providing a good solution for ordinary maintenance operations [23]. The physical inventory is only limited to raw materials, as "digital twins" components need to be stored. This is extremely important for old ships, as keeping old parts implies a notable inventory cost. Considering such a context, the RAM technology can meet any demand regarding construction type and lead times. Parallel robotic operations can indeed increase the system deposition rates, and the process flexibility can allow the construction of components with ideally any shape. Moreover, RAM can also be used for repairing damaged components, which sometimes can be more efficient than replacing in terms of costs and lead time.



Figure 10: Examples of RAM for marine applications

The main operational advantages are:

- *design flexibility*: components and structural elements possessing high strength-to-weight and stiffness-to-weight ratios are essential in the maritime sector. One of the main advantages of RAM integration is the improved design freedom, which can be directly translated into a lightweight design concept. Such freedom can be utilized to fully exploit topology optimization techniques and-or lattice structures design to produce more efficient marine structures and components [24], [25]. The possibilities to tune the sandwich lattice structure in relation to the part technical requirements [26], [27] and to orient and place the fibre reinforcement as needed are very attractive solutions to optimize metal or composite ship structures. Moreover, combining RAM technology with biomimetic science could provide innovative and efficient solutions for designing lightweight marine structures [28], [29]. It is finally worth mentioning that wire extrusion-based AM techniques can even be utilized to build multi-functional products [30].
- *prototyping efficiency*: as marine structures are large and complex in shape, it is challenging to conduct testing campaigns on real-scale elements. Therefore, experimental tests are typically carried out in model scale, and proper scaling laws are applied to predict the response of the real structure [31]. Considering this framework, the possibility to accurately build model-scale marine structures with a high degree of complexity through RAM platforms is a significant advantage;
- *integrated manufacturing*: the RAM technology can be successfully utilized to produce complex assemblies and-or structural joints (e.g., welds) on site [32]. This solution can potentially optimize component integration, enhancing their quality and performance.

Considering the provided framework, combining additive manufacturing and robotics can efficiently match the primary demands of the maritime sector. However, there are relevant challenges to integrate such a technology in industrial fields.

3.2.2 RAM MAIN CHALLENGES AND RESEARCH DRIVERS

Considering the framework provided in previous sections, it can be stated that the main challenges and research drivers to be faced to integrate the RAM technology in the maritime sector are the following:

- *product properties and repeatability*: components produced through additive manufacturing techniques can experience variations in geometrical accuracy and mechanical properties in relation to the adopted manufacturing procedure (e.g., process parameters, deposition patterns, etc.). Such problems are even emphasized for complex and large-size structures manufactured in non-controlled environments. Therefore, the achievement of proper accuracy and mechanical properties is one of the main challenges related to the RAM manufacturing process;
- *design workflow*: the RAM technology provides more design freedom concerning component internal and external shapes. This, in turn, allows to fully exploit efficient optimization procedures to enhance part performances. However, a consolidated design procedure that can predict the structural response of the component needs to be developed and validated. Testing campaigns on additive-manufactured specimens can provide useful information, but to which extent it is possible to extend such results to real components is an open question. Moreover, the problem of the correlation of the results between specimens and real elements is emphasized for complex and large-size structures;
- *RAM system control*: the control of the RAM platform represents a challenge as different sub-systems are involved and need to be managed in parallel. While robot flexibility allows for multi-directional or non-planar deposition strategies, current slicing software cannot provide G-code data compatible with the robot language if multi-directional slicing methodologies or non-planar deposition methods are applied. An efficient information flow for the manufacturing process and proper control procedure needs to be developed.

3.3 DESIGN METHODOLOGIES FOR SANDWICH STRUCTURES

The section overviews current design theories for sandwich structures subjected to flexural loads. In particular, the 3-point bending loading condition is used as reference for the study.

A general description of sandwich structures is given in section 3.3.1, highlighting the potential of both traditional and additive manufactured solutions. Hereafter, the bending stresses (section 3.3.2) and flexural deflection (section 3.3.3) are analysed. Finally, the failure modes are addressed (section 3.3.4).

It is worth mentioning that, for simplicity, the theory exposed in this section assumes a beam with unit width.

3.3.1 SANDWICH GENERAL DESCRIPTION

The PhD thesis has focused on sandwich structures, which possess promising structural performances and provide relevant design flexibility. Purposely developed design and manufacturing processes may leverage such features to enable multi-functional and multi-material structures with unprecedented performances.

The American Society for Testing and Materials (ASTM) defines a sandwich structure as follows:

“A structural sandwich is a special form of a laminated composite comprising a combination of different materials that are bonded to each other to utilise the properties of each separate component to the structural advantage of the whole assembly.”

The main constituents of the sandwich structure are reported in Figure 11.

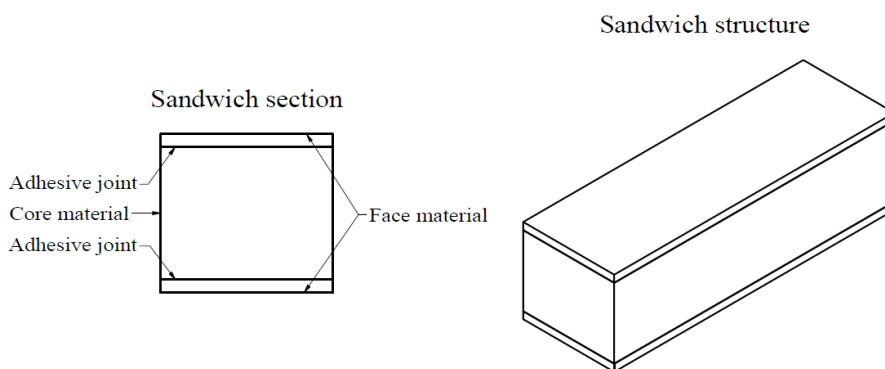


Figure 11: Sandwich structure main constituents

The figure shows two faces (or skins) separated by a core. The faces are usually thin, solid and stiff, while the core is thicker and weaker than the faces. In standard sandwich structures, the faces are adhesively bonded to the core to correctly transfer the load between the components.

The sandwich structure concept is the same as that of an I-beam. The difference is that the core and the faces are usually made of different materials and are located on a continuous support rather than concentrated in a narrow web. The faces counteract the external bending moment, while the core resists shear and stabilises the faces against buckling or wrinkling (local buckling on elastic foundation). The bond between the faces and the core must resist to shear and tensile stresses set up between them.

The sandwich structure is very efficient in withstanding flexural loads. The gain is achievable by employing a sandwich solution w. r. t. a single skin structure is highlighted in Figure 12. Such a figure shows the interesting “sandwich effect” on the structure flexural response.

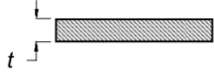
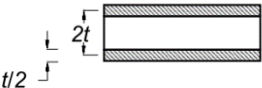
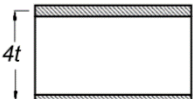
	Weight	Flexural rigidity	Bending strength
	1	1	1
	~1	12	6
	~1	48	12

Figure 12: The “sandwich effect” on flexural response [33]

It is interesting to note that, by utilizing the sandwich concept, the flexural stiffness and strength can be increased compared to a single skin structure, by keeping the weight almost constant. The advantages of sandwich structures may be high stiffness and strength-to-weight ratios, integration of functions such as thermal and acoustic insulation, high energy absorption capability and buoyancy. Therefore, in addition to gains in structural efficiency, the sandwich solution provides relevant functionalities, which may be achieved by adequately selecting the core material among the traditionally fabricated ones.

Employing the key enabling technology of additive manufacturing may further enhance the sandwich capabilities. The design flexibility unlocked by such technology may lead to the development of multi-functional and multi-material structures whose properties and features may be tuned to satisfy advanced structural requirements. The sandwich skins may employ continuous fibre-reinforced plastic materials. The fibre orientation and the choice of the raw materials of the skins (matrix, fibre) are tailored to provide specific functionalities and structural requirements within and through the layers that build up the skin thickness. The sandwich core may employ a composite cellular material. The core topology and its raw materials are selected to fulfil specific structural and functional requirements within and through the layers that build up the core thickness.

Given the above framework, it is clear that using additive manufacturing technology opens up unprecedented possibilities concerning the potential to tune structural and functional requirements within and through the layers that build the whole structure. Moreover, it enlarges the range of employable core cellular topologies and the usable composite materials for the skins and core, which are not limited to the traditionally manufactured and employed ones.

The main geometrical and mechanical parameters of the sandwich structures considered within this thesis work are reported in Figure 13.

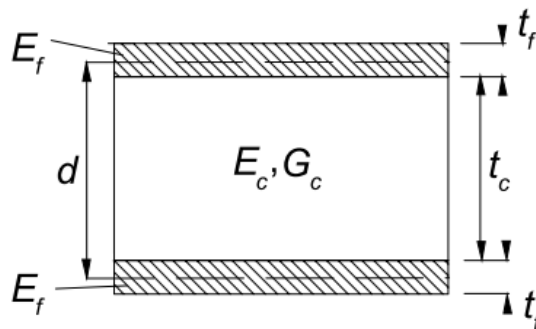


Figure 13: Geometry and properties of sandwich

The figure shows the mechanical properties of the skins and core, together with relevant geometrical parameters to consider for the design process.

The sandwich beam analysed is subjected to a 3-point bending condition. A schematic representation of such a loading condition is reported in Figure 14.

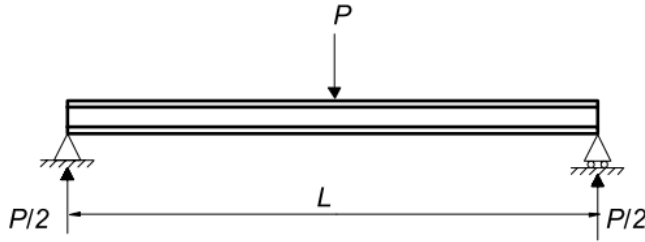


Figure 14: Sandwich beam in 3-point bending

The maximum bending moment and transverse force occurring in the beam are:

$$M_{\max} = \frac{PL}{4} \quad T_{\max} = \frac{P}{2}$$

3.3.2 BENDING AND SHEAR STRESSES

The flexural stiffness D has to be calculated by weighting the contribution of the different materials which constitute the sandwich section. For a sandwich with identical and symmetrical faces, it can be written as follows:

$$D = \int Ez^2 dz = \frac{E_f t_f^3}{6} + \frac{E_f t_f d^2}{2} + \frac{E_c t_c^3}{12} = 2D_f + D_0 + D_c$$

Where $d = t_c + t_f$. The first term corresponds to the flexural stiffness of the faces w. r. t. their neutral axes, the second one represents the stiffness of the faces associated with bending w. r. t. the centroidal axis of the entire sandwich, and the third term is the flexural stiffness of the core.

The bending stresses in the core and skins can be written as follows:

$$\sigma_f = \frac{E_f M_x}{D} z \quad \text{for } \frac{t_c}{2} \leq |z| \leq \frac{t_c}{2} + t_f$$

$$\sigma_c = \frac{E_c M_x}{D} z \quad \text{for } |z| \leq \frac{t_c}{2}$$

The stresses vary linearly within each material constituent, but there is a jump in the stress at the face-core interface due to the difference in the mechanical properties.

The shear stresses can be calculated as follows:

$$\tau = \frac{T_x}{D} \int_z^{(d+t_f)/2} E z dz = \frac{T_x B(z)}{D}$$

Where T_x is the shear load and $B(z)$ is the first moment of the area. The shear stresses in the faces and core can be calculated as follows:

$$\tau_c(z) = \frac{T_x}{D} \left[\frac{E_f t_f d}{2} + \frac{E_c}{2} \left(\frac{t_c^2}{4} - z^2 \right) \right] \text{ for } \frac{t_c}{2} \leq |z| \leq \frac{t_c}{2} + t_f$$

$$\tau_f(z) = \frac{T_x E_f}{D} \left[\frac{t_c^2}{4} + t_c t_f + t_f^2 - z^2 \right] \text{ for } |z| \leq \frac{t_c}{2}$$

The maximum shear stress appears at the neutral axis for $z = 0$:

$$\tau_{c,\max}(z=0) = \frac{T_x}{D} \left(\frac{E_f t_f d}{2} + \frac{E_c t_c^2}{8} \right)$$

The shear stress in the core-skin interface is:

$$\tau_{c,\min} = \tau_{f,\max} = \tau\left(\frac{t_c}{2}\right) = \frac{T_x}{D} \left(\frac{E_f t_f d}{2} \right)$$

Some approximations may be conducted to simplify the analysis. For a sandwich with a weak core $E_c \ll E_f$, the following equations can be written:

$$\sigma_c(z) = 0 \quad \sigma_f(z) = \frac{E_f M_x}{2D_f + D_0} z$$

$$\tau_c(z) = \frac{T_x E_f t_f d}{2(2D_f + D_0)} \quad \tau_f(z) = \frac{T_x}{(2D_f + D_0)} \frac{E_f}{2} \left[\frac{t_c^2}{4} + t_c t_f + t_f^2 - z^2 \right]$$

For a sandwich with a weak core, $E_c \ll E_f$, and thin faces $t_f \ll t_c$, the following further simplifications can be conducted:

$$\sigma_c(z) = 0 \quad \sigma_f(z) = \frac{M_x}{t_f d} \quad \tau_c(z) = \frac{T_x}{d} \quad \tau_f(z) = 0$$

The effect of the approximations mentioned above is reported in Figure 15.

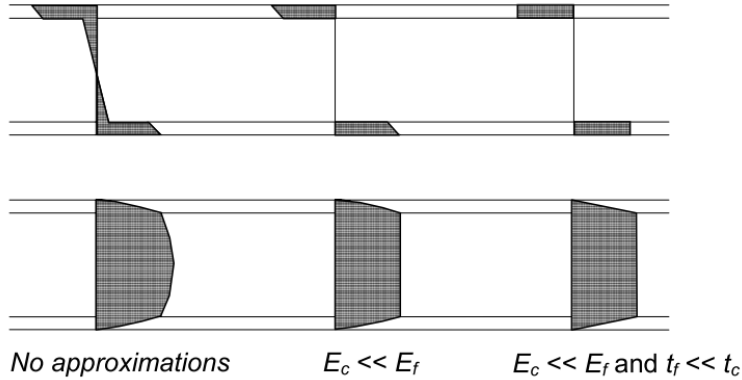


Figure 15: Approximations in sandwich theory [33]

3.3.3 FLEXURAL DEFORMATION

For sandwich beams it is necessary to account for transverse shear deformations. As shown in Figure 16, the total deformation can be divided into bending and shear deformation.

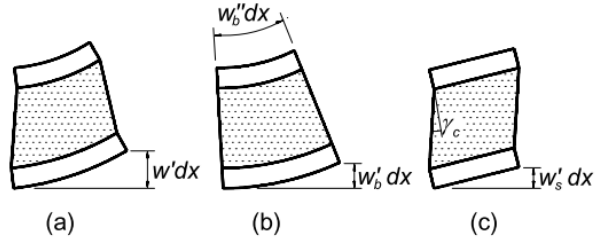


Figure 16: Sandwich total (a), bending (b) and shear deformation (c) [33]

For a sandwich beam subjected to a 3-point bending condition, the total deformation w can be written as follows:

$$w = w_b + w_s = \frac{PL^3}{48D} + \frac{PL}{4S}$$

Where $S = d^2 / t_c$ is the shear stiffness derived from the approximations of weak core and thin faces.

3.3.4 FAILURE MODES

Sandwich structures can fail in several ways. Each one of the failure modes sets a constraint on the structural capacity of the sandwich. Depending on the geometry of the sandwich and the loading condition, a specific failure mode becomes critical. The sandwich failure modes are exhaustively illustrated in Figure 17.

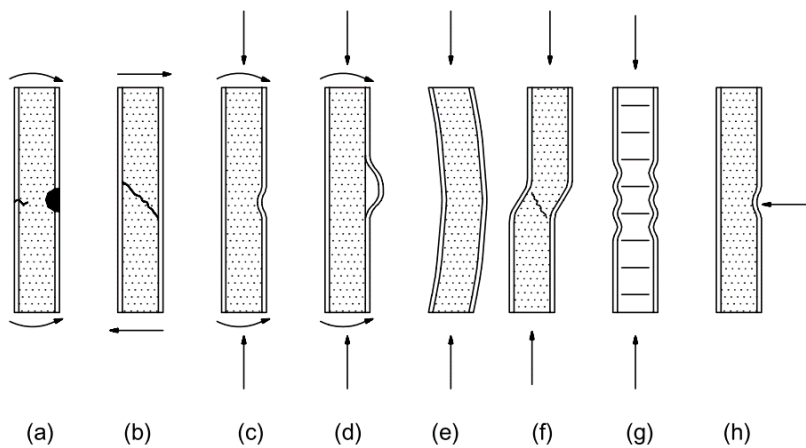


Figure 17: Failure modes in sandwich beams. (a) Face yielding/fracture, (b) core shear failure, (c and d) face wrinkling, (e) general buckling, (f) shear crimping, (g) face dimpling and (h) local indentation [33]

According to Craig et al. [34], among all the possible failure modes, a sandwich beam loaded in bending can collapse in the ones illustrated in Figure 18. It may fail in core shear, skin compression (due to micro-buckling), skin wrinkling or core indentation. According to the literature, the sandwich failure modes are not correlated. Therefore, the sandwich will fail in the mode which has the lower limit load at failure.

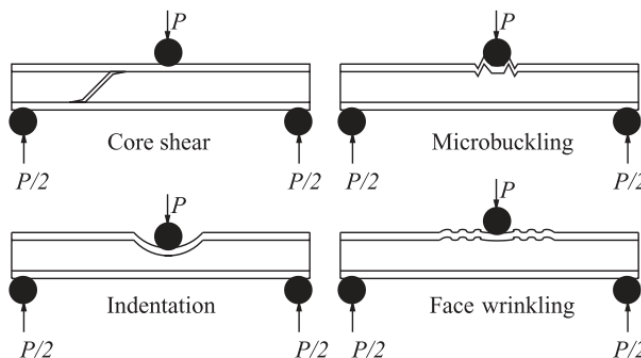


Figure 18: Failure modes for a sandwich beam loaded in bending [34]

It is worth mentioning that the not-mentioned failure modes (shear crimping, global buckling, face dimpling) reported in Figure 17 are more likely to occur under different boundary conditions, such as uniaxial compression. Moreover, the intracell buckling (or dimpling) will hardly occur for the employed layup configuration, which interposes plastic layers as an interface between skins and core (section 6.1). The core indentation failure (induced by localized loads) is not considered in the present study, as the interest is not in localized loads but in the flexural behaviour of the structure. For practical applications, care should be taken to apply the load on an appropriate area that does not reach core yielding in compression.

The micro-buckling criteria prevent the composite sandwich face from failing in compression. To avoid this, the normal stress in the faces must be lower than their micro-buckling strength. Interesting studies have been performed by Waas and Schultheisz [35], [36], dealing with theories for compressive failure of composite specimens, which are based on the properties of their constituent materials. These theories can be used to predict the strength of unidirectional composites and can be integrated into models to predict the behaviour of more complicated laminated structures. Such studies have highlighted the dependency of the micro-buckling stress on the matrix and fibre properties, specimen thickness, and geometrical imperfections (e.g., fibre waviness), proposing analytical formulations to account for such parameters.

The main difference between compressive and wrinkling failure is that the wrinkling limit stress depends on the core properties, which is not the case for the micro-buckling stress. According to Fagerberg [37], there is a transition between wrinkling failure and micro-buckling failure, occurring at a specific core density value. Such a density value will lead to the inception of compressive failure due to micro-buckling, because it will occur at a lower limit load w. r. t. wrinkling failure. It is suggested that the wrinkling failure has to be avoided to exploit the skins to their maximum capacity.

The wrinkling failure is skin-localized buckling on elastic foundation, represented by the core. A well-established formulation in literature is the following:

$$\sigma_w = 0.5\sqrt[3]{E_{fx}E_{cz}G_{cxz}}$$

Where:

- $E_{fx}[MPa]$ is the Young's modulus of the faces in the longitudinal direction;
- $E_{cz}[MPa]$ is the Young's modulus of the core in the out-of-plane direction;
- $G_{cxz}[MPa]$ is the shear modulus of the core in the out-of-plane direction.

As the present PhD study deals with additive-manufactured honeycomb sandwich structures, it is necessary to specialize the above-reported equation to analyse the application. To account for the dependency of the above-reported elastic moduli from the honeycomb geometry, the following closed-form equations based on structural mechanics have been selected from the Gibson and Ashby theory [38]:

$$E_{cz} = E_{cs} \frac{\rho_c}{\rho_s} \quad G_{cxz} = 0.577G_{cs} \frac{t_h}{l_h}$$

Where:

- $E_{cs}, G_{cs}[MPa]$ are the Young's and shear moduli of the core base material, assuming isotropic behaviour;
- $t_h, l_h[mm]$ are the thickness and side length of the honeycomb cell;
- $\frac{\rho_c}{\rho_s} = \frac{2}{\sqrt{3}} \frac{t_h}{l_h}$ is the relative density of the core as the ratio between the core density and the density of the solid material by which the core is made.

Extensive experimental work has concluded that the above formula gives good and conservative predictions. Therefore, despite the formulation being rather vague, it is usually correct, and it is suggested as design criteria for traditional sandwich applications [37], [39], [40].

The failure can occur in two ways: a wrinkle that becomes unstable, causing an indentation in the core, if the compressive strength of the core is lower than the tensile strength of the core and of the adhesive joint, or the wrinkle-causing a tensile fracture, if the tensile strength of the core (or the adhesive joint) is lower than the

compressive strength of the core. Whichever case applies does not affect the actual wrinkling stress. Still, a poor adhesive joint or geometrical imperfection (e.g., fibre waviness) will undoubtedly reduce the wrinkling stress.

The core is subjected to shear and carries the entire transverse force. In the hypothesis of weak core and thin faces, the core shear failure occurs when the shear stress in the core exceeds the core shear limit. The shear strength can be again estimated using the Gibson and Ashby theory [38] for traditionally manufactured honeycomb cores.

The core strength of a traditional regular hexagonal honeycomb core (with double walls) under out-of-plane shear load can be calculated as follows:

$$\tau_{xz} = 1.7 \left(\frac{\rho_c}{\rho_s} \right)^3 E_{cz}$$

Where:

- ρ_c / ρ_s is the relative density of the honeycomb core;
- E_{cz} [MPa] is the Young's modulus of the core in the out-of-plane direction.

It is worth mentioning that the exposed analytical formulations are valid for traditionally manufactured sandwich structures and honeycomb cores. Specific assumptions have been placed to develop current sandwich design theories. The main ones are core isotropy and the perfect bond between skin and core.

3.4 OPTIMIZATION PROCEDURES FOR SANDWICH STRUCTURES

This section overviews optimization methods, as fundamental tools employed across various disciplines to enhance decision-making and streamline processes. Particular attention is dedicated to multi-objective optimization and evolutionary algorithms as they represent flexible and efficient procedures for various optimization problems.

In general terms, the main goal of optimization is to find the best solution from a set of feasible options while fulfilling specific constraints. The aim is to achieve the maximum benefit, or the highest level of performance, within a given context.

Multi-objective optimization takes optimization further by addressing scenarios where multiple conflicting objectives must be simultaneously considered. Unlike single-objective optimization, which aims to identify a single optimal solution, such procedure covers a range of solutions representing different trade-offs between competing objectives.

Multi-objective optimization involves the simultaneous optimization of multiple objectives. This effort is notable when the objectives conflict, yielding distinct optimal solutions for each objective function. Addressing such challenges, whether with or without constraints, gives rise to a collection of trade-off optimal solutions known as Pareto-optimal solutions. Evolutionary algorithms (EA), or evolutionary optimization (EO), have emerged as particularly suited approaches to face these problems. The evolutionary optimization has the following main advantages: w. r. t. classical optimization methodologies [41]:

- *no reliance on gradient information*: an EO procedure does not usually use gradient information in its search process. They are thus classified as direct search procedures and can be applied to a wide variety of optimization problems;
- *population-based approach*: an EO procedure uses more than one solution (population approach) in an iteration, unlike most classical optimization algorithms, which update one solution in each iteration (point approach). The population-based approach provides a parallel processing power that lowers the overall computational time; better performance in finding multiple optimal solutions, solving multi-objective and multi-modal (possessing multiple local optima) problems in an efficient way; the ability to normalize decision variables (as well as objective and constraint functions) within an evolving population;

- *stochastic operators*: an EO procedure uses stochastic operators, unlike most classical optimization methods, which use deterministic operators. The operators tend to achieve a desired effect by using higher probabilities towards desirable outcomes, instead of predetermined and fixed transition rules. This allows an EO algorithm to explore multiple optima and other complexities better and provides a global perspective in their search.

An evolutionary optimization (EO) explores the design space generating a random population within predefined lower and upper bounds for each design variable. Subsequently, the EO procedure starts an iterative process, aiming to refine the current population and generate a new one. This iterative process relies on four primary operators: selection, crossover, mutation, and elite preservation. The key features of such operators are the following:

- *selection*: to determine which solutions from the current population will be carried forward to the next generation, based on their fitness values. This mechanism has the aim to favour solutions that are more fit and adaptive to the requirements of the problem;
- *crossover*: to pick two or more solutions (parents) and create one or more solutions (child) by exchanging information among the parent solutions. This operator introduces diversity and combines favourable traits of different solutions, potentially leading to improved solutions;
- *mutation*: to introduce small random changes to individual child solutions created by the crossover operator, contributing to exploration, and preventing premature convergence to suboptimal solutions. It enhances the ability of the algorithm to escape local optima;
- *elite preservation*: to ensure that the best-performing solutions from the current population are carried over to the next generation without modification. This strategy safeguards the conservation of highly fit solutions.

The above-described iterative process continues until one or more pre-specified termination criteria are fulfilled. Termination criteria can include a maximum number of iterations, achieving a certain level of convergence, or reaching a satisfactory solution quality. By adhering to these termination criteria, the EO procedure efficiently balances exploration and exploitation, identifying high-quality solutions within the given problem space.

A multi-objective optimization problem involves different objective functions ($f_m(x)$) that must be minimized or maximized. The multi-objective optimization problem may contain various constraints ($g_j(x), h_k(x)$), which any feasible solution (x_i) must satisfy.

A multi-objective optimization problem can be stated as follows:

$$\left. \begin{array}{ll} f_m(x) & m = 1, 2, \dots, M \\ g_j(x) \geq 0 & j = 1, 2, \dots, J \\ h_k(x) = 0 & k = 1, 2, \dots, K \\ x_i^L \leq x_i \leq x_i^U & i = 1, 2, \dots, n \end{array} \right\}$$

A solution is a vector $\vec{x} = (x_1, x_2, \dots, x_n)^T$ of n decision variables which satisfies the imposed constraints and variable bounds (lower and upper), constituting a feasible decision variable space. The objective functions constitute a multi-dimensional space, in addition to the decision variable space, which is called the objective space. Therefore, for each solution \vec{x} in the decision variable space, a point in the objective space exists, denoted by $\vec{z} = (z_1, z_2, \dots, z_M)^T$.

All the optimal solutions in a multi-objective optimization problem are the non-dominated ones, constituting the Pareto-optimal frontier. The domination and the Pareto front concepts are clarified in the following.

A solution \vec{x}_1 is said to dominate the other solution \vec{x}_2 , if both the following conditions are true:

- the solution \vec{x}_1 is no worse than \vec{x}_2 in all objectives. Thus, the solutions are compared based on their objective function values or location of the corresponding points (\vec{z}_1 and \vec{z}_2) on the objective space;
- the solution \vec{x}_1 is strictly better than \vec{x}_2 in at least one objective.

The concept of non-dominated solutions is illustrated in Figure 19. For the set of the solutions shown in figure, they are represented by points 3, 5, and 6. One property of such points is that a gain in an objective from one point to the other happens only due to a sacrifice in at least one other objective. These points constitute a front when viewed together in the objective space.

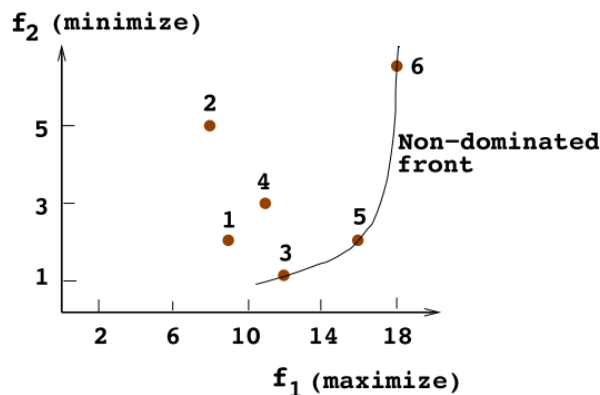


Figure 19: Example of non-dominated solution set [41]

Considering the above framework, the Pareto-optimal solution concept definition in a multi-objective optimization problem is straightforward. By definition, the points on the non-dominated front shown in figure are non-dominated by any other point in the objective space. They are thus classified as Pareto-optimal points (together, they constitute the Pareto-optimal front). The corresponding decision variable vectors are called Pareto-optimal solutions.

Finding representative Pareto-optimal solutions using an EMO procedure is only part of the optimization problem. Choosing a single preferred optimal solution from the obtained set is equally important.

To select the preferred solution from the optimal solution set, the following main approaches can be used:

- *a-priori approach*: preference information of a decision-maker (DM) is used to focus the search effort on part of the Pareto-optimal front instead of the entire frontier;
- *a-posteriori approach*: preference information is used after a set of representative Pareto-optimal solutions are found by an EMO procedure. A multiple criteria decision-making (MCDM) approach, including reference point method, weighted score method, etc. can be employed;
- *interactive approach*: DM's preference information is integrated into an EMO algorithm during the optimization run. In the progressively interactive EMO approach, the DM is called and asked to rank the solutions according to preference between the iterations of the algorithm. The information is then processed through an optimization task to capture DM's preference using a utility function. This utility function is then used to drive the search till the procedure is repeated in the next DM call.

3.5 DISCUSSION

The driving vision of the study emerges from the state-of-the-art analysis. The development of flexible robotic additive manufacturing process and validated optimal design methodologies paves the way for the integration of promising structural solutions and materials, such as multi-functional and multi-material sandwich structures, in the maritime sector.

The robotic additive manufacturing technology represents a key enabling technology to achieve the integration of continuously emerging new materials and advanced structural solutions in the maritime sector. The state-of-the-art analysis revealed that the combination of additive manufacturing and robotics has the potential to match the primary demands of the maritime sector and to achieve efficient and innovative structural solutions. Particular attention needs to be dedicated to product properties, process repeatability and to the development of a validated workflow for efficient component design, as they represent the main challenges to fully integrate the RAM technology in industrial fields.

The fused deposition modelling-based processes deserve particular attention for RAM applications, as they are suited to produce sustainable and multi-functional composite structures. Such a simple, flexible, low-cost process can manufacture thermoplastic polymers reinforced with different fillers (e.g., chopped and continuous fibres). Product properties and repeatability are one of the main challenges, as different process parameters and materials may lead to highly different mechanical performances. The research in such a field has been oriented to develop deposition methods that overcome process drawbacks. The co-extrusion process deserves particular attention, as it attempts to overcome one of the main limitations of current AM techniques for composite manufacturing, i.e., the poor interfacial bond between matrix and fibres.

Traditional sandwich structures possess consolidated design methods, supported by extensive experimental work. The total deformation and the wrinkling failure are sensitive to the core mechanical properties, which depend on core topology, material, and geometrical features. Particular attention should be dedicated to identify a method to estimate the core properties in relation to its features. Different failure modes may occur for a sandwich subjected to flexural loads, in relation to the mechanical properties of its constituents and to the geometrical features of the structure. The expected failure is the one which appears at the lower load. The modes are not correlated and can thus be monitored separately. Such consolidated design

methods are valid under specific assumptions (e.g., core isotropy, perfect bond between skins and core). Moreover, the presence of geometrical and manufacturing imperfections (e.g., fibre waviness, voids), which are likely to occur in additive manufacturing, may affect the expected structural response. Therefore, the validity of such methodologies should be verified and adapted to the new materials and technology.

The design framework for sandwich structures can be classified as a multi-objective optimization problem. The optimal sandwich geometrical features must be determined considering different competing objectives (e.g., minimising weight, cost, total thickness, etc.) and fulfilling specific structural and additive manufacturing constraints. Multi-objective evolutionary algorithms have emerged to be effective tools to identify the set of Pareto-optimal solutions. An efficient solution to an MO problem may be to couple such algorithms with an a-posteriori MCDM approach. This approach finds the preferred solution among a pre-identified optimal set according to specific DM preferences, oriented to fulfil the required specifications.

4 CONCEPT DESIGN OF A RAM PLATFORM FOR MARINE APPLICATIONS

This chapter provides the conceptual, or functional, design of a robotic additive manufacturing platform suited to marine applications. Moreover, key research areas to be addressed to fully integrate RAM technology in the maritime sector are highlighted.

The study is driven by the findings of the state-of-the-art analysis (see section 3.5), which stated that the manufacturing processes should be oriented at enhancing the mechanical properties of the components to be produced, while guaranteeing repeatability. Moreover, particular attention needs to be dedicated in developing a validated workflow for efficient component design.

To achieve the objective, the work has been organized in the following phases:

- *phase I*: identification of AM techniques tailored to robotic applications for the maritime sector, according to specific indicators (section 4.1). Two techniques have been selected in relation to the material utilized for the deposition process. One technique is finally chosen as a reference for the RAM platform concept design development;
- *phase II*: the concept design of a robotic additive manufacturing platform for marine applications is provided (section 4.2). Such a design is given in terms of design and manufacturing workflow description.

4.1 PHASE I: ADDITIVE MANUFACTURING TECHNIQUES FOR RAM

The most promising AM techniques for RAM applications have been identified, accounting for the need for large-scale manufacturing of complex structures and repair solutions at high deposition rates and low costs. Such features have been selected to satisfy the primary needs of the maritime sector (see section 3.2.1).

A systematic investigation has been conducted to identify the additive manufacturing techniques. The following indicators support such an analysis:

- system flexibility;
- environmental impact;
- need for a controlled environment;
- deposition rate;
- range of printable materials;
- cost of investment and operational costs.

The Fused Deposition Modelling (FDM) and the Wire Arc Additive Manufacturing (WAAM) processes have been selected for composite and metal applications. The main reasons that drove the selection are the following:

- *system flexibility*: both techniques use a feedstock material in the form of filament instead of powders. This enormously simplifies material handling. A single RAM platform has the potential to switch from metal to composite deposition by changing the extrusion system. The same platform can even be built as a hybrid system, which combines additive and subtractive manufacturing methods for multi-purpose applications;
- *environmental impact*: a process that melts filaments instead of powders is safer for human health and the environment. Such an indicator applies to both technologies. In addition, as far as composites are concerned, it is expected a rapid growth related to the “green challenge” that will facilitate the introduction of bio-compatible materials;
- *need for a controlled environment*: the deposition can potentially occur for both techniques in a non-controlled environment, even if a closed chamber, or an inert gas shield, can be beneficial to control the process outcome better;
- *deposition rate*: both techniques are characterized by high deposition rates [42], [43]. Typical deposition rates are given in Table 1;

- *range of printable materials*: the selected techniques can print a vast range of materials. Different materials can be even combined by simply melting two filaments, or different types of fillers (e.g., fibres) can be applied. This enables the production of multi-functional structures;
- *costs*: the investment cost is limited for both techniques, and the filaments cost less than powders. The estimated initial investment for a WAAM system, which is the highest, is around 130k € [44].

Table 1: Typical RAM deposition rates

Technique	Deposition rate (cm^3/h)
FDM	1250
WAAM	625

The FDM technology is expected to be significantly enhanced, mainly because of the continuous development of novel composite materials. For this reason, the RAM platform functional design focuses on the deposition of Continuous Fibre Reinforced Plastic (FRP) materials, considered one of the most promising research developments. To highlight their potential, typical mechanical properties of additively manufactured composites, which embed short and continuous fibre reinforcements, are reported in Table 2 [45]. One attractive property of FRP is that their mechanical properties do not depend only on the filament characteristics. The combination of fibre volume ratio, fibre location and orientation in the component can lead to highly different mechanical performances, achieving properties comparable or superior to aluminium alloys [46].

Table 2: Fibre-reinforced plastic material properties

Mechanical Property	Short Fibres	Continuous Fibres
Tensile Strength	33.5 MPa	968 MPa
Tensile Modulus	1.85 GPa	62.5 GPa

The mechanical properties of FRP produced through AM are nowadays lower w. r. t. composites manufactured through traditional methods. This seems to be due to the presence of process drawbacks and challenges that may currently limit industrial applications [47]. Therefore, further investigation is needed to understand such limitations and thus to enhance the current state of the art related to materials and manufacturing solutions.

To improve the FDM process capabilities, the robotic arm flexibility may be exploited to apply the fibre reinforcement most efficiently, and only at the point of need, to satisfy component requirements and to produce marine structures with enhanced performances. Moreover, efficient deposition strategies can be implemented. They are not limited to the conventional planar layer-by-layer procedure and aim at low waste production by eliminating, or drastically reducing, the need for support structures. Finally, the proper spatial deposition of matrix and fibres with specific properties and of polymers containing different fillers has a high potential to unlock the production of multi-functional and sustainable marine structures with unprecedented performances.

4.2 PHASE II: RAM PLATFORM DESIGN

This section provides the functional design of a hybrid robotic additive manufacturing platform for marine applications, whose general layout is shown in Figure 20. The figure shows two cranes equipped with multi-purpose robots that can translate on linear guides and perform parallel operations. The deposition occurs on a building plate, which can be oriented in space to cope with process requirements. Such a platform layout aims to increase the building volume, building rate and process flexibility.

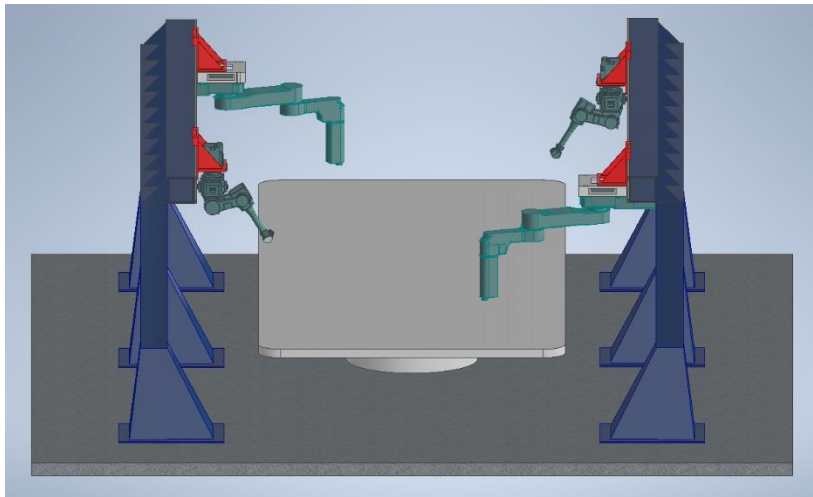


Figure 20: RAM platform general layout

The proposed preliminary process workflow represents a smart manufacturing process that aims to overcome the challenges related to RAM technology implementation (see section 3.2.2).

The RAM workflow is reported in Figure 21, where the algorithm to produce continuous fibre-reinforced structures is illustrated. With reference to such a figure, the main process areas are described below through interrelated functional blocks. The grey-coloured blocks represent the process parts needing particular research attention to unlock the full potential of the RAM technology.

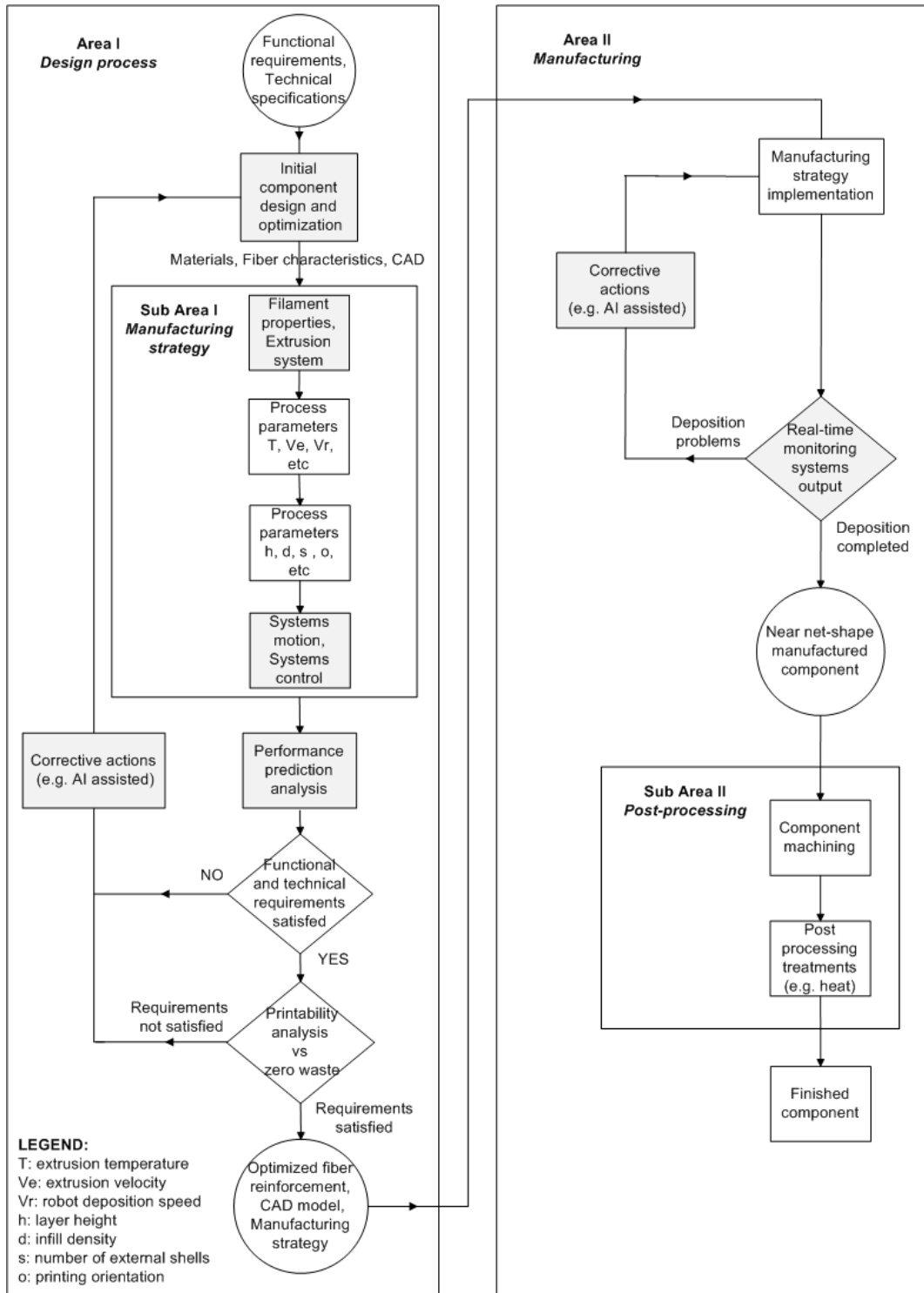


Figure 21: RAM process workflow

The main process areas are:

- *Area I*: it regards the design process. The main objective is to design and optimise the component in relation to its technical specifications. The component requirements are utilized to perform the initial design and optimization processes. The fibre and matrix raw materials are thus selected and the optimization is performed (e.g., through numerical techniques). The aim is to identify the optimal component shape and to define the best orientation of the fibre reinforcement, the fibre volume ratio and the location to maximize performance. These data are the input for the sub-area I, which establishes the manufacturing strategy to build the component in relation to such inputs. Once such a strategy is defined, the design of the component is verified using performance prediction models, which can predict its strength and failure modes in relation to design loads and to the manufacturing strategy. Such models can integrate extensive experimental testing and-or numerical techniques [48]. If the component requirements are not satisfied, proper corrective actions will be conducted, and the design and manufacturing processes will be optimized to ensure compliance. Hereafter, the suitability of such optimized design and manufacturing procedures to a zero-waste production process is verified (e.g., the need for support structures). Multi-directional slicing algorithms or non-planar deposition patterns will be evaluated and optimized to achieve a specific process waste requirement. The output of area I are the optimized component design and the related manufacturing strategy that are compliant with technical specifications and process waste requirements;
 - *Sub Area I*: this sub-area is related to the manufacturing procedure. The inputs are raw materials, component CAD model and fibre characteristics. The first block identifies the filament properties and the extrusion procedure for the selected raw materials. Proper extrusion system characteristics and deposition techniques, suited to the identified filament, must be chosen to enhance component mechanical properties and ensure compliance with the CAD model. The following two blocks define the process parameters. Some depend on the filament to be processed and on extruder characteristics, i.e., temperature, robot deposition speed, extrusion speed (wire speed), etc. Other parameters can be chosen in relation to the application to achieve a good compromise between material

consumption, printing time and product properties, i.e., layer height, infill density, number of shells, printing orientation, etc. The last block defines systems motion and control procedures in relation to the sub-area input and to the defined manufacturing parameters. This comprises the definition and correlation of robot patterns, process parameters, printing bed motion, in-process operations, and process control techniques. Such data must be interfaced with the robot programming language and verified through robotic platform Off-Line Programming (OLP) simulations.

- *Area II*: it regards the manufacturing process. As mentioned, the process takes place on a printing bed, which can be oriented in space to increase manufacturing efficiency and flexibility. Different monitoring systems inspect the deposition quality in real-time to provide data for process parameter tuning and to take actions for fixing deposition issues. Corrective actions are conducted to guarantee good component mechanical properties and avoid re-manufacturing, which is not time and cost-effective, especially for large-size components. Due to the process complexity and lower robot accuracy w. r. t. conventional AM machines, a hybrid manufacturing approach may be needed (e.g., additive and subtractive manufacturing);
 - *Sub Area II*: this sub-area deals with the final manufacturing step, i.e., component post-processing. The first operation is component machining to achieve full compliance with the CAD model, if needed. This solution may overcome RAM accuracy limitations. The second step regards post-processing operations, to enhance component mechanical properties (e.g., thermal treatments) or to provide additional functionalities (e.g., hydrophobic coating).

4.3 DISCUSSION

The concept design of a hybrid RAM platform has been provided in the present chapter, highlighting the process workflow and the most promising research areas. Such a smart process aims to leverage the RAM flexibility to develop efficient and sustainable design and manufacturing methodologies that, in turn, will facilitate the integration of optimized multi-functional and sustainable lightweight structures in the maritime sector. Moreover, Fused Deposition Modelling (FDM) based techniques have been identified as the most promising additive manufacturing techniques for the production of continuous fibre-reinforced composite structures.

The enhanced process capabilities provided by the RAM technology can be summarized as follows:

- *process flexibility*, that allows the utilization of efficient deposition strategies to achieve an optimized and zero-waste production process. The given workflow enables the placement of fibre reinforcements most efficiently to enhance component performances, satisfying technical and functional requirements. Moreover, this approach paves the way for the utilization of matrix and fibres with different properties and of polymers containing different types of fillers for the production of multi-functional and sustainable marine structures;
- *integrated design process*, that leverages performance prediction models, printability analysis and corrective methods to efficiently optimize the component design and manufacturing, in relation to technical requirements, materials, manufacturing strategy and suitability to a zero-waste process;
- *manufacturing control*, that exploits the output of real-time monitoring systems to optimize the deposition parameters, or to take proper actions to solve deposition issues. Such a closed control loop aims to ensure good component mechanical properties and to avoid the costly and time-consuming re-manufacturing;
- *hybrid manufacturing*, that combines additive and subtractive production methods to overcome RAM accuracy limitations and shape a facility suited to multi-purpose applications.

The key research areas for the successful integration of the RAM technology are:

- development of a design procedure to perform component optimization and derive the best fibre orientation, fibre volume ratio and location. The optimization should be applied for component external and internal shapes to fully exploit the process flexibility;
- definition of raw materials properties and related extrusion methodology that aim to enhance product mechanical characteristics. An interesting research area is related to the utilization of natural fillers as reinforcement material to reduce the environmental impact of the product;
- definition of systems motion and control. Particular attention needs to be dedicated to the development of efficient deposition techniques to achieve an optimized and zero-waste manufacturing process and to the definition of an efficient procedure for systems parallel control;
- development of performance prediction models that aim to predict additive manufactured composite strength and failure modes, in relation to the implemented design and manufacturing procedures;
- definition of real-time monitoring systems characteristics to perform in situ process control and thus provide valuable data to be used for ensuring good component properties (e.g., mechanical properties, compliance to CAD model, etc.);
- definition of proper corrective actions to optimise the design and manufacturing processes. An efficient and smart manufacturing process can exploit artificial intelligence, which utilizes the data obtained through extensive experimental testing to perform, or suggest, such actions.

Among the above-listed key research areas, the one related to the definition of raw materials properties and related extrusion methodology deserves particular attention. The development of the RAM platform technical features and control procedures has to be indeed shaped on a well-defined deposition method, which aims to enhance the structural performances of the composite components to be manufactured and to guarantee repeatability.

Another relevant key research area regards the development of optimal design procedures and performance prediction models for composite components. Utilizing such procedures can indeed lead to an appropriate improvement in performance, enhancing the capabilities of the vessel and, in turn, boosting the integration of

innovative technologies and processes in the maritime field. Moreover, identifying key design parameters is of unprecedented importance to guide the development of materials and additive manufacturing processes.

Given the above framework, the study has been oriented to identify the capabilities of current AM processes for composite materials production and, in particular, to define their main limitations and weaknesses (Chapter 5). Moreover, extensive work has been carried out to develop optimal design methodologies for composite sandwich structures (Chapter 6), with the dual aim of providing innovative structural solutions with enhanced performances and of establishing guidance for raw materials and additive manufacturing process developments.

The research findings mentioned above will be utilized in future developments to deploy an innovative RAM platform, which leverages a purposely conceived deposition method, to provide naval components with enhanced capabilities.

5 EXPERIMENTAL ASSESSMENT OF COMPOSITES PRODUCED BY AM

The present chapter highlights the potential of multi-material deposition methodologies for the production of composite structures. In particular, the focus is on Fibre Reinforced Plastics (FRP) produced by Fused Deposition Modelling (FDM) based additive manufacturing techniques. Such methods have been indeed identified particularly suited to flexible, low-cost, and sustainable RAM processes for multi-functional marine applications (see section 4.1).

To achieve this objective, the promising “Anisoprint CFC technology” has been selected as a case study to investigate its capability in overcoming one of the main limitations of current continuous fibre-reinforced FDM methods and systems, i.e., the poor impregnation of the reinforcing fibres by the matrix (see section 3.1). Such an AM process, described in section 5.1, has been analysed by investigating the tensile response of FRP specimens through a systematic testing campaign, which accounts for the main AM process variables and constraints (section 5.2).

The potential applicability of the analysed materials to marine structures has been evaluated by considering the minimum material requirements imposed by the Classification Society Rules and by performing a comparative analysis concerning traditional composite structures (section 5.3).

The main objectives of the work are the following:

- the evaluation of the influence of different carbon fibre reinforcements on the mechanical response of fibre-reinforced thermoplastics, produced by additive manufacturing;
- the evaluation of the influence of the deposition methodology (deposition path) on the mechanical response of fibre-reinforced thermoplastics produced by additive manufacturing;
- the assessment of the impact of thermal post-manufacturing treatment (annealing) on the mechanical response of fibre-reinforced thermoplastics produced by additive manufacturing;
- the correlation of the mechanical performances and failure modes of fibre-reinforced thermoplastics with the additive manufacturing methodology;
- the evaluation of the potential applicability of different carbon-fibre-reinforced thermoplastics to marine structures.

5.1 CFC ADDITIVE MANUFACTURING PROCESS

The AM technique chosen as a case study is the patented Anisoprint CFC (“Continuous Fibre Co-Extrusion”) technology. The machine Composer A3, which leverages the mentioned technique, has been used to manufacture the specimens. Such a technology produces a bi-matrix fibre-reinforced composite. The main feature is the co-extrusion of a continuous fibre filament, pre-impregnated and cured within a thermoset matrix, with a thermoplastic filament [15]. The printhead is composed by two different extrusion systems. One deals with the deposition of thermoplastic materials (or chopped reinforced thermoplastics) through a classical fused deposition modelling (FDM) technique. In contrast, the other one deals with the mentioned co-extrusion process.

All the specimens have been designed using the 3D CAD software Autodesk Inventor, while the printing profiles have been developed through the slicing software Aura. Figure 22 shows the deposition process of chopped and continuous FRP specimens.

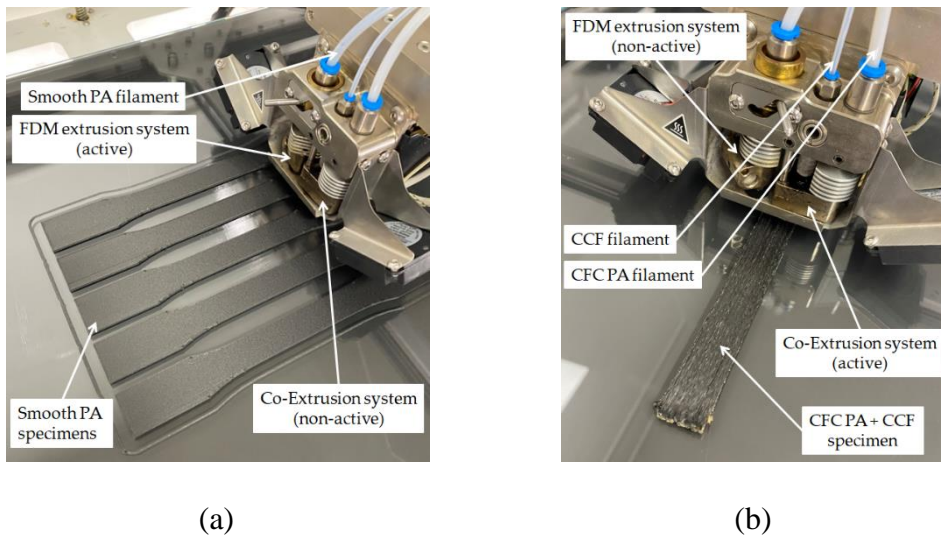


Figure 22: (a) AM of Chopped FRP; (b) AM of Continuous FRP

Figure 23 shows one set of additively manufactured chopped and continuous fibre-reinforced plastic specimens oriented at 0° .

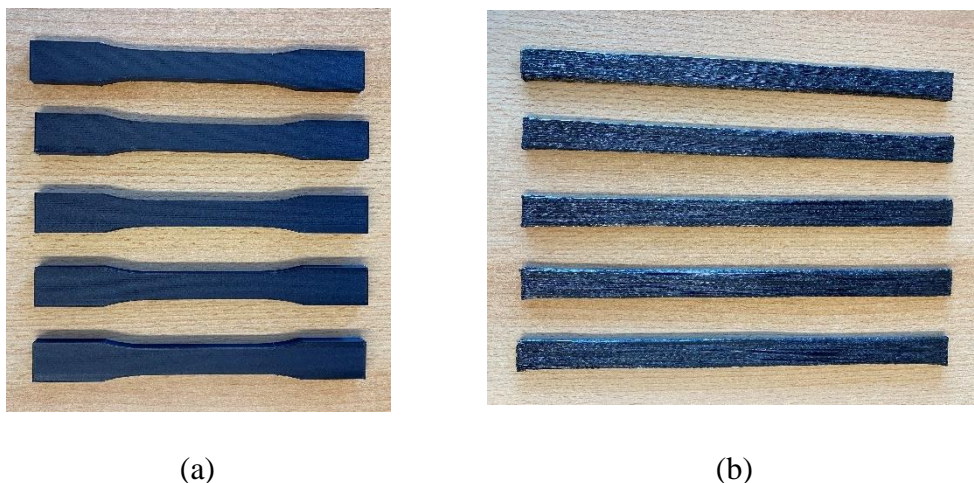


Figure 23: (a) Additively manufactured chopped FRP specimens, 0° ; (b) additively manufactured continuous FRP specimens, 0°

According to the manufacturer's specifications, all plastic filaments have been dried before printing to eliminate moisture. The additively manufactured specimens have been sealed in a vacuum box until testing.

5.2 MECHANICAL CHARACTERIZATION

This section describes the methodology to investigate the structural performances of fibre-reinforced thermoplastics produced by additive manufacturing for marine applications.

The tensile behaviour of chopped and continuous carbon-fibre-reinforced thermoplastics has been investigated, considering the anisotropy induced by the additive manufacturing methodology and the influence of thermal post-manufacturing treatments (annealing) on the mechanical properties. Moreover, non-destructive techniques (e.g., optical microscopy and flash thermography) have been applied to achieve in-depth knowledge of the relation among the AM methodology, the mechanical performances and the failure modes of the analysed materials. Test setups have been developed accounting for the requirements of the Classification Society Rules [49].

Tensile tests have been conducted on additively manufactured FRP specimens with the following main objectives:

- to analyse the influence of different reinforcement types on the tensile performances and failure modes. This is achieved by testing different sets of specimens with two types of carbon fibre reinforcements (chopped and continuous) on a thermoplastic nylon matrix;
- to investigate the impact of the deposition pattern on the mechanical properties and failure modes of thermoplastic materials reinforced with different fibre types. Plenty of printing settings need to be considered to achieve an optimal deposition process (e.g., print temperature, speed, cooling rate, etc.), and each of them influences the structural behaviour of the component. However, it can be stated that once the optimal settings are developed, the deposition pattern is one of the critical parameters to be taken into account to achieve optimal structural performances;
- to analyse the influence of the thermal post-manufacturing treatment (annealing) on the mechanical performances of additively manufactured FRP. This is achieved by applying an annealing treatment to a set of FRP specimens and by comparing the results with a non-annealed set;
- to evaluate the potential applicability of additively manufactured FRP to marine structures. This is achieved by comparing the mechanical properties of such materials to traditionally manufactured FRP and the minimum material structural requirements imposed by the Classification Society Rules.

The tensile tests have been conducted using an Instron 8854 universal testing machine (Instron, Norwood, MA, USA), with a load cell of 250 kN and a maximum torque of 2 kNm. Suitable grip pressure and testing speed have been applied to the tested specimens, and the reference standard has been considered.

Optical microscopy and flash thermography have been used to gain in-depth knowledge of the relations between the additive manufacturing methodology, the mechanical performances, and the failure modes of the specimens. In particular, the following equipment has been used: Leica microsystem DVM5000 digital microscope (Leica, Wetzlar, Germany), Leica microsystem M165C stereomicroscope and Flir systems X8400sc thermal camera (Teledyne FLIR, Wilsonville, OR, USA).

The analysis of chopped fibre-reinforced specimens is reported in section 5.2.1, while the one of continuous fibre-reinforced specimens is given in section 5.2.2. The potential of the technology is highlighted in section 5.3.

5.2.1 CHOPPED FIBRE-REINFORCED PLASTIC

The used material is “Smooth PA,” a thermo-plastic nylon (PA12) reinforced by chopped carbon fibres at 10%. All specimens have been printed with a layer height of 0.2 mm, an extrusion temperature of 265 °C, and a constant speed of 40 mm/s. The used bed temperature is 60 °C, and the fan speed for cooling is 20%.

Chopped fibre-reinforced plastic specimens have been manufactured and evaluated according to ASTM D638 and concerning the test plan reported in Table 3. The standard follows the Classification Society Rules for materials manufacture, testing, and certification [49]. The annealing treatment has been performed, exposing the specimens at 80 °C for 6 hours in a drying oven, according to manufacturer specifications. Heating has been applied according to a trapezoidal profile, where the steady state is reached after approximately 15 min.

Table 3: Chopped FRP specimens test plan

Material	Printing Path	Annealing	Specimen Number
Smooth PA	0°	YES	5
Smooth PA	90°	YES	5
Smooth PA	0°	NO	5

Figure 24 compares the planned deposition path for chopped fibre-reinforced plastic specimens oriented at 0° and 90°.

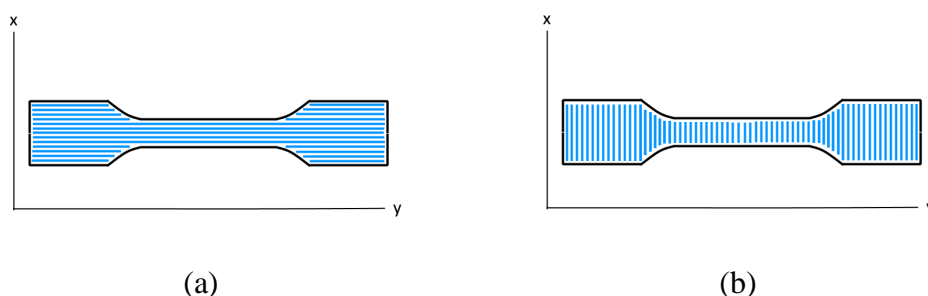


Figure 24: (a) Planned printing path for chopped FRP, 0°; (b) planned printing path for chopped FRP, 90°

The specimens have been designed and manufactured according to the dimensions provided in the standard for the Type I specimen. The constant test speed is 5 mm/min, and the applied grip pressure is 5 bar. The failure modes of the specimens have been analysed using optical microscopy.

Figure 25 compares the stress-strain relationships obtained through the tensile tests on chopped FRP with different deposition patterns (0° – 90°). The mean values for tensile strength (σ_u), Young’s modulus (E), deformation at the break (ϵ_r), and their standard deviation are reported in Table 4.

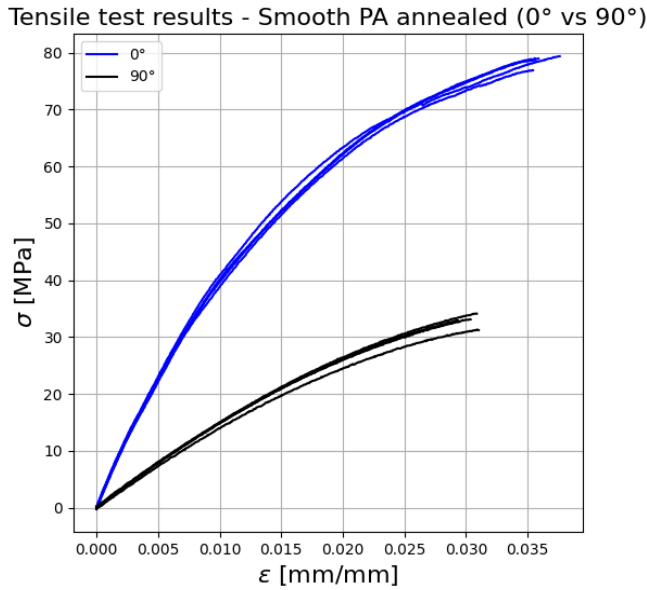


Figure 25: Stress-strain relationship of chopped FRP with different deposition patterns

Table 4: Tensile test results — Chopped FRP

Material	Printing Path	Annealing	σ_u [MPa]	E [MPa]	ϵ_r [%]
Smooth PA	0°	YES	78.57 ± 0.84	5168.21 ± 160.15	3.60 ± 0.08
Smooth PA	90°	YES	32.74 ± 1.05	1597.35 ± 128.53	2.98 ± 0.13
Smooth PA	0°	NO	68.05 ± 0.52	4578.77 ± 67.24	5.26 ± 0.29

The deposition pattern significantly influences the tensile response of chopped FRP. In particular, the tensile strength of FRP printed at 0° orientation is more than twice that of FRP printed at 90° orientation, while Young's modulus is more than three times higher. The deformation at break follows the same trend. It is approximately 17% higher for the FRP specimens oriented at 0° . This behaviour can be explained by analysing the extrusion process. The chopped fibres are forced to align in the deposition direction when passing through the nozzle. As the fibres exhibit higher mechanical performances when loaded in the direction of their axis, the maximum tensile properties are encountered when the deposition pattern is aligned with the load direction. The optical microscopy analysis confirms this assumption.

Figure 26 shows the influence of the annealing treatment on the tensile response of chopped FRP oriented at 0° .

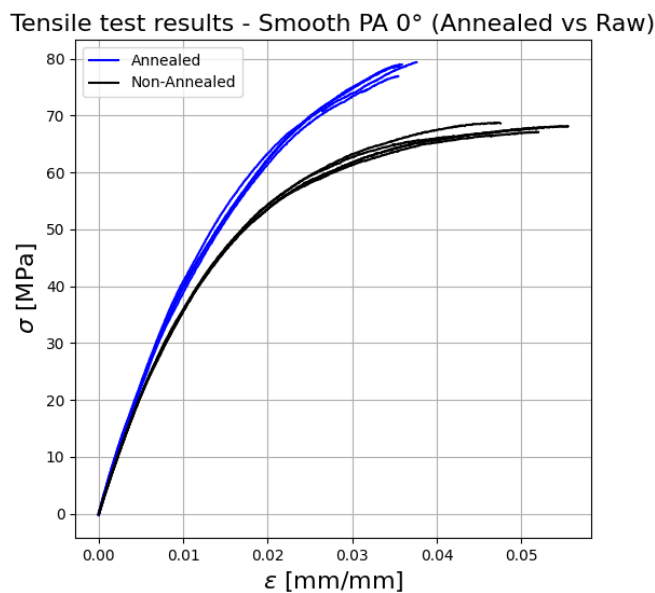


Figure 26: Stress-strain relationship of annealed and non-annealed chopped FRP (0°)

It can be seen that the thermally treated specimens show a tensile strength and Young's modulus, which is approx. 12% higher than the one of the non-treated (raw) specimens. A reversed trend is shown for the strain at the break, which is approx. 32% higher for the raw specimens. This behaviour can be explained by the increase in crystallinity in the polymer, which leads to better inter-layer bonding and to the reduction in residual stresses and gaps between layers (porosity) caused by the material re-flow when heated above its glass transition temperature [50].

Figure 27 shows an overview of the tensile failure modes for chopped fibre-reinforced specimens oriented at 0° and 90° .



Figure 27: (a) Failure modes under tensile load for chopped FRP- 0° ; (b) failure modes under tensile load for chopped FRP- 90°

From the visual inspection of the fracture surfaces and by analysing the graphs, it can be noticed that the FRP specimens oriented at 0° show a more ductile behaviour than those oriented at 90° . The fracture surfaces of annealed chopped FRP oriented at 0° and 90° , analysed through optical microscopy, are shown in Figure 28.

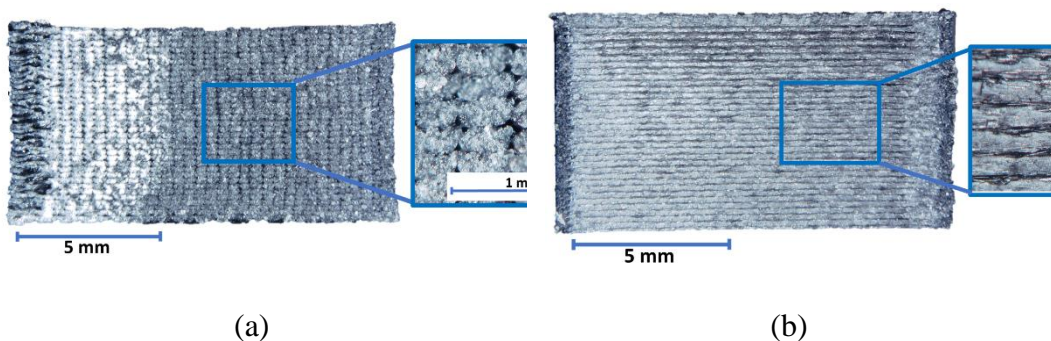


Figure 28: (a) Fracture surface of annealed chopped FRP- 0° ; (b) fracture surface of annealed chopped FRP- 90°

It is interesting to note the layered structure of additively manufactured specimens from different perspectives (0° – 90°). Such a structure is indeed related to the employed manufacturing method. The presence of gaps between extrusion lines is observed. Moreover, the chopped fibres (in white) alignment in the deposition direction is visible in both cases (0° – 90°). As mentioned, the superior mechanical

performances of the chopped FRP oriented at 0° are due to the alignment of the chopped fibres in the load direction. For the specimens oriented at 90° , the mechanical strength relies only on the bonding among the extrusion lines, whose contact surface is reduced by gaps. In this case, lower mechanical performances are indeed encountered. Regarding the deformation behaviour, intact extrusion lines are visible on the fractured surface of chopped FRP oriented at 90° , which appears smooth and thus less deformed than the surface of the FRP specimens oriented at 0° . Finally, the analyses highlighted that the raw chopped FRP specimens oriented at 0° exhibit a less homogeneous structure than the annealed ones, as shown in Figure 29.

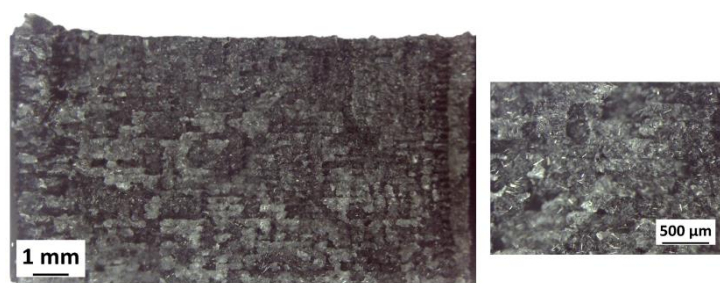


Figure 29: Fracture surface of raw chopped FRP, 0°

5.2.2 CONTINUOUS FIBRE-REINFORCED PLASTIC

The used material is “CFC PA+CCF,” a thermoplastic nylon (PA12) reinforced by continuous carbon fibre. The theoretical fibre volume fraction (FVF) is approx. 25%. All the specimens have been printed with a layer height of 0.34 mm and an extrusion temperature of 250°C . The used bed temperature is 60°C , and the fan speed for cooling is 50%. A fibre deposition algorithm controls the printing speed, while the maximum speed is 10 mm/s.

Continuous fibre-reinforced plastic specimens have been manufactured and evaluated according to ASTM D3039 and concerning the test plan reported in Table 5. The standard suggested by the Classification Societies (ASTM D638) has been modified to better suit the continuous reinforcement in place and for comparison purposes with specimens manufactured by different AM techniques, evaluated according to the chosen standard. The annealing treatment has been performed, exposing the specimens at 80°C for 6 hours in a drying oven, according to the manufacturer’s specifications. Heating has been applied according to a trapezoidal profile, where the steady state is reached after approximately 15 min.

Table 5: Continuous FRP specimens test plan

Material	Printing Path	Annealing	Specimen Number
CFC PA + CCF	0°	NO	5
CFC PA + CCF	90°	NO	5
CFC PA + CCF	0°	YES	5

Figure 30 compares the planned deposition path for continuous fibre-reinforced plastic specimens oriented at 0° and 90°.

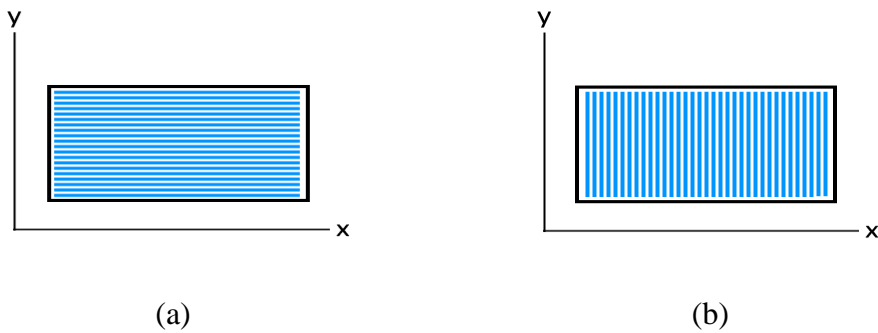


Figure 30: (a) Planned printing path for continuous FRP-0°; (b) planned printing path for continuous FRP-90°

The width and length of the specimens have been designed and manufactured according to the dimensions provided in the standard, and the thickness used is 2 mm. The constant test speed is 2 mm/min, and the applied grip pressure is 30 bar. The failure modes of the specimens have been analysed using optical microscopy.

In addition, thermography has been used to highlight the preferential failure path in the specimens. The infrared camera used to perform the flash thermography tests is equipped with a cooled indium antimonide (InSb) focal plane array detector, having a spatial resolution of 1280×1024 pixels. The frame rate of the acquired thermograms was set to 130 Hz by sub-windowing at 640×720 pixels. The integration time was 362 μ s, with a temperature range of $5 \div 90^\circ\text{C}$. The lens was an MW 28 mm ($38^\circ \times 31^\circ$) 2.0 HD. The camera was mounted on a tripod at a distance of 45 mm from the specimens, and the flash was placed alongside the camera.

Figure 31 shows the setup for analysing the continuous FRP specimens oriented at 0° . The thermograms were post-processed by ResearchIR Max software by applying image subtraction.

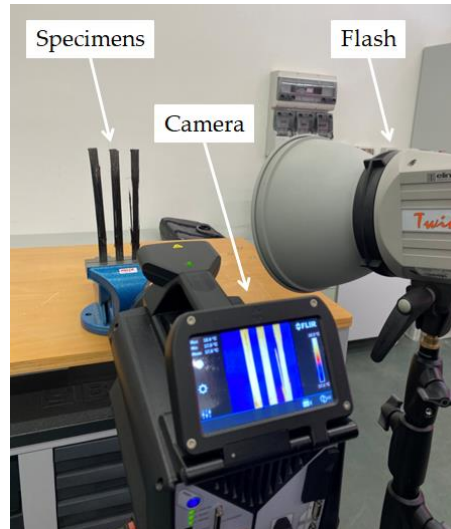


Figure 31: Flash thermography setup

Figure 32 compares the stress-strain relationships obtained through the tensile tests conducted on continuous FRP with different deposition patterns (0° – 90°). The mean values for tensile strength (σ_u), Young's modulus (E), deformation at the break (ϵ_r), and their standard deviation are reported in Table 6.

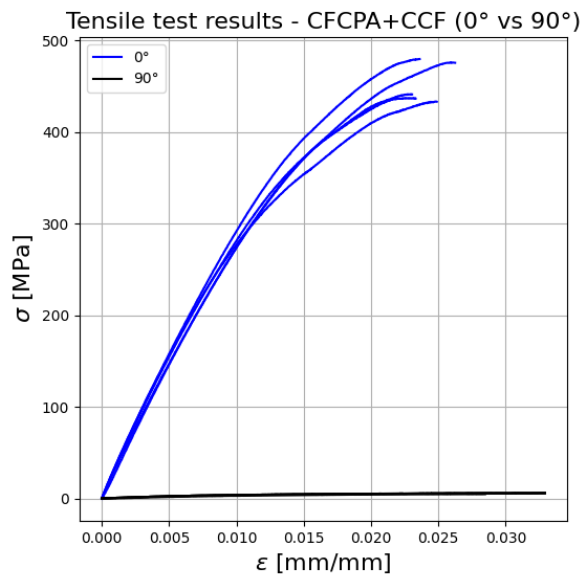


Figure 32: Stress-strain relationship of continuous FRP with different deposition patterns

Table 6: Tensile test results — Continuous FRP

Material	Printing Path	Annealing	σ_u [MPa]	E [MPa]	ϵ_r [%]
CFCPA + CCF	0°	NO	453.65 ± 20.1	34,203.35 ± 4075.23	2.42 ± 0.11
CFCPA + CCF	90°	NO	5.47 ± 0.54	444.81 ± 169.39	3.11 ± 0.21
CFCPA + CCF	0°	YES	493.66 ± 11.25	37,066.79 ± 297.34	2.09 ± 0.09

As expected, the deposition pattern greatly influences the tensile response of continuous FRP. In particular, the tensile strength and Young's modulus of FRP printed at 0° orientation are far higher than those of continuous FRP printed at 90° orientation, which exhibits lower properties. The deformation at break has a different trend. It is approximately 22% higher for the FRP specimens oriented at 90°. Such a tensile behaviour is due to the continuous fibre not contributing to the tensile response when it is oriented at 90° concerning the load direction. Therefore, the properties measured for the specimens oriented at 90° are related only to the pure nylon and represent the bonding strength between adjacent continuous fibre filaments (extrusion lines).

Figure 33 shows the influence of the annealing treatment on the tensile response of continuous FRP oriented at 0° .

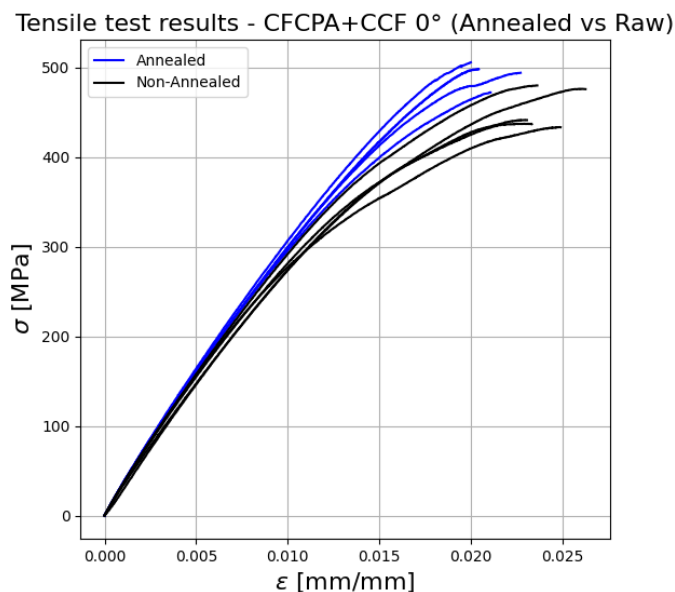


Figure 33: Stress-strain relationship of annealed vs non-annealed continuous FRP (0°)

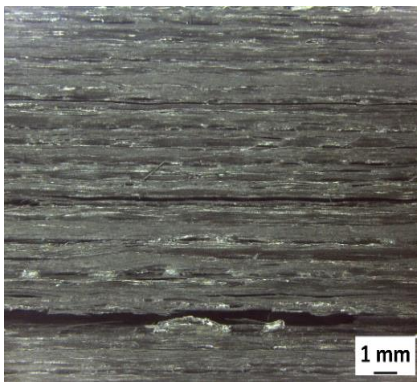
The thermally treated specimens show a tensile strength and Young's modulus of approximately 8% higher than the non-treated (raw) ones. A reversed trend is shown for the strain at the break, about 14% higher for the raw specimens. These results agree with the ones obtained for chopped FRP specimens and can be related to the above-stated reasons. Such assumptions are validated by the statistical analysis, which shows that the annealing treatment lowers the standard deviations of the measured properties. This trend can be related to decreased manufacturing defect concentration in the specimens.

Figure 34 shows an overview of the tensile failure modes encountered for continuous fibre specimens oriented at 0° and 90° .

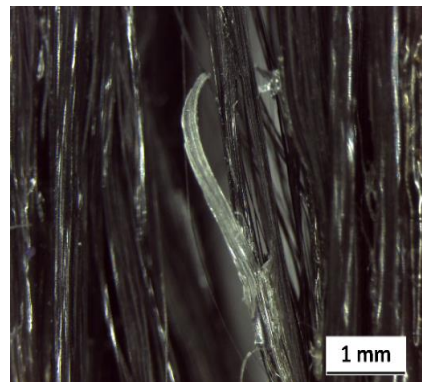


Figure 34: Tensile failure modes of continuous FRP, 0° (left); tensile failure modes of continuous FRP, 90° (right)

From the visual observation of the fracture surfaces of continuous FRP, both brittle fibre failure and fibre-matrix debonding can be seen. The fracture surfaces of continuous raw FRP oriented at 0° and 90° , analysed through optical microscopy, are shown in Figure 35.



(a)



(b)

Figure 35: (a) Fracture surface of continuous raw FRP, 0° ; (b) fracture surface of raw continuous FRP, 90°

Interestingly, continuous FRP specimens oriented at 0° show preferential failure paths propagating among the extrusion lines, with brittle fibre failure and fibre-matrix debonding. Such a finding suggests low bonding strength between adjacent continuous fibre filaments. The assumption is confirmed by the deficient properties encountered for the continuous FRP specimens oriented at 90° , which may affect the load transmission capacity of the matrix, lowering the mechanical properties. The continuous FRP specimens oriented at 90° experience fibre-matrix debonding failure. The image shows the intact fibre, which separates from the thermoplastic matrix. As mentioned, the measured mechanical performances of such specimens are related to the bonding strength between adjacent continuous fibre filaments (extrusion lines).

Figure 36 shows the results of the thermography analysis conducted on annealed and raw continuous FRP specimens oriented at 0° .

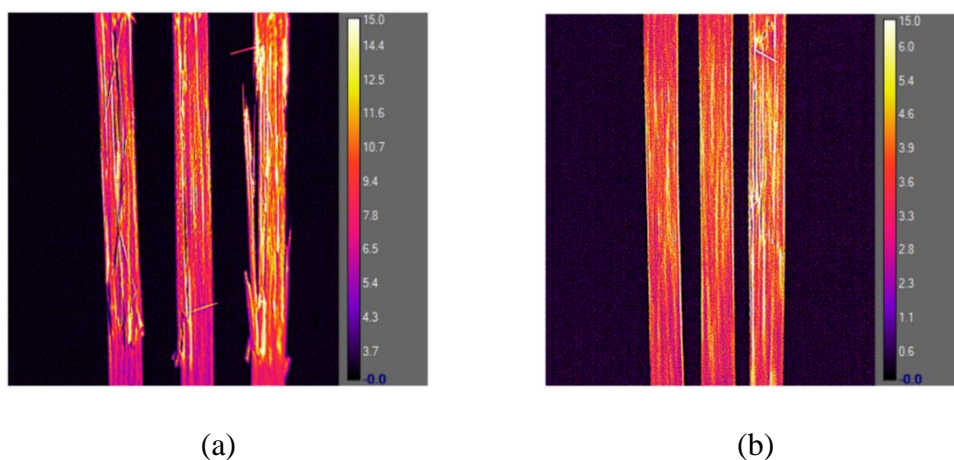


Figure 36: (a) Damaged specimens—annealed continuous FRP, 0° ; (b) damaged specimens—raw continuous FRP, 0°

The analysis highlights, in a straightforward way, that the preferential failure paths are aligned with the load direction and propagate along the extrusion lines. Fibre brittle failure can also be observed. The annealed specimens show a more brittle behaviour than the raw ones. This is confirmed by the fracture surface analysis, which offers a higher fibre brittle failure concentration for such specimens. Moreover, the fracture damage is more severe for the annealed specimens, where the failure, parallel to the direction of the fibre, is associated with fibre splitting. Such a mechanism requires higher energy than the one related to the tensile failure of the matrix [51] and may explain the higher mechanical properties encountered.

5.3 DISCUSSION

The main findings of the experimental work are given in the present section. The main results of the work can be grouped into the following categories:

- comparison of the tensile response of additively manufactured chopped and continuous FRP;
- comparison of the tensile test results obtained for additively manufactured continuous FRP with typical mechanical properties of unidirectional continuous FRP manufactured through traditional techniques;
- comparison of the additively manufactured continuous FRP mechanical properties with the minimum requirements imposed by the Classification Society Rules.

Figure 37 compares the tensile stress-strain relationships of the annealed chopped and continuous FRP oriented at 0° .

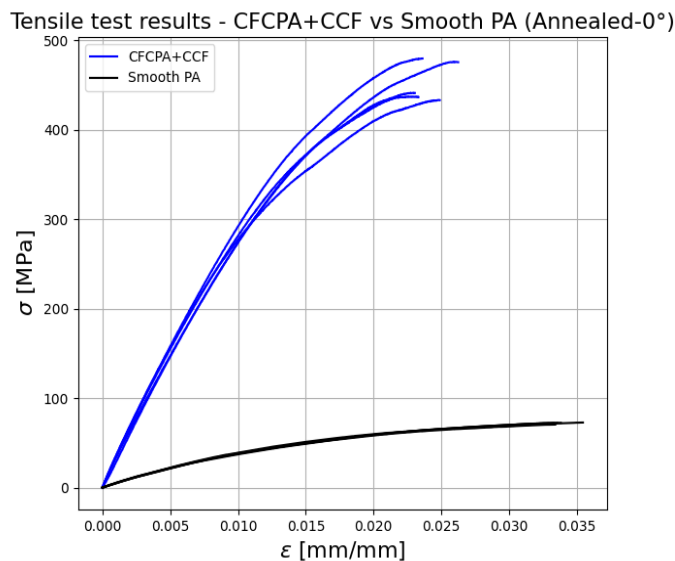


Figure 37: Stress-strain relationship of chopped and continuous FRP oriented at 0°

The use of the continuous fibre reinforcement leads to a significant improvement in mechanical performance. In particular, the tensile strength and modulus of continuous FRP are approximately seven times higher than the ones of chopped FRP. The strain at break shows a different trend. It is 40% higher for the chopped FRP specimens, showing a more ductile behaviour.

It is worth mentioning that the analysed additive manufacturing process has good repeatability. If the same specimen set is considered, this is confirmed by the low standard deviations and by the high similarity of the results.

A summary of the mechanical properties (ultimate strength and Young's modulus) of traditionally manufactured unidirectional continuous FRP is given in Table 7 [52].

Table 7: Properties of traditionally manufactured unidirectional continuous FRP (0°)

Material–Fibre Orientation	E [GPa]	σ_u [MPa]
Boron–Epoxy—0°	207	1585
AS Carbon–Epoxy—0°	127.5	1447.5
T-300–Epoxy—0°	138	1447.5
HMS Carbon–Epoxy—0°	207	827
GY-70–Epoxy—0°	276	586
Kevlar 49–Epoxy—0°	76	1379
E-Glass–Epoxy—0°	39	1103
S-Glass–Epoxy—0°	43	1214

Comparing Table 6 and Table 7, it can be stated that additive manufacturing continuous FRP presents lower strength and Young's modulus than composite structures manufactured through traditional methods. However, promising results have been achieved. In particular, the tensile strength of additively manufactured continuous FRP at 0° orientation is comparable to that of the GY-70–Epoxy. At the same time, it is twice or more times lower if other traditionally manufactured composites are considered. The Young's modulus is comparable to the glass-reinforced plastic composites (E-Glass, S-Glass), while it is twice or more times lower if other traditionally manufactured composites are considered. Figure 38 compares the tensile response of the additively manufactured FRP and the minimum mechanical properties requirements for composite laminates imposed by the RINA rules for Fast Patrol Vessels FPV [49].

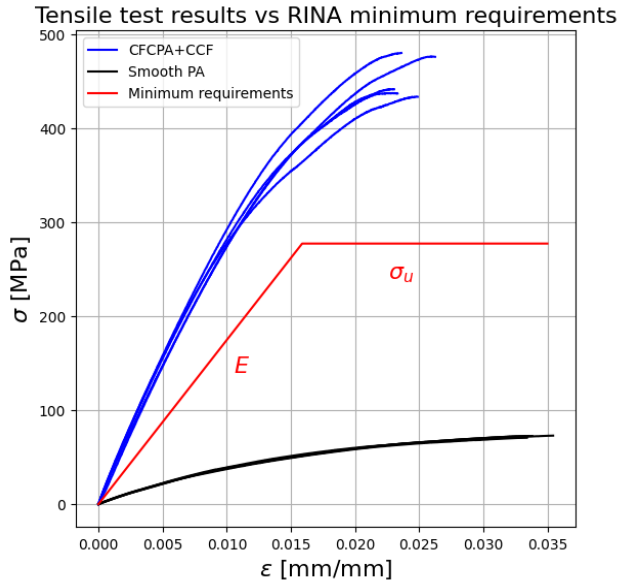


Figure 38: Tensile test results vs RINA minimum requirements

The figure emphasises that the continuous carbon-fibre-reinforced thermoplastics can be a promising solution for marine structural applications. In particular, the minimum requirements on the mechanical properties imposed by the standard are matched if the continuous fibre reinforcement is employed. In contrast, the chopped fibre reinforcement leads to non-satisfying mechanical properties. The chopped carbon fibre reinforcement does not significantly increment strength w. r. t. matrix-only specimens, possessing modest properties in all directions. In contrast, continuous fibre reinforcement significantly increases component mechanical properties when the load is aligned with the fibre direction.

The minimum ultimate tensile strength and Young's modulus have been calculated according to the following equations, derived from the RINA rules for FPV [49]:

$$\sigma_u = 1278G_c^2 - 510G_c + 123 = 277 \text{ [MPa]}$$

$$E = (37G_c - 4.75)10^3 = 17.4 \text{ [GPa]}$$

The results are calculated considering a glass fraction by weight $G_c = 0.6$, the value that “is to be used” for manufacturing glass-reinforced unidirectional specimens for mechanical properties testing.

The Classification Society requirement for the minimum fibre volume fraction content to be used for the mechanical testing of the specimens does not match the one achievable by the additively manufactured continuous FRP, suggesting that a technological limit currently exists. The reinforcement content that “is to be used” for unidirectional carbon fibre specimen preparation is 41%, while the maximum achievable by the considered AM technology is approximately 25%. The mentioned drawbacks relate to the raw materials used and to the additive manufacturing process. The thermoplastic–thermoset matrix lowers the global fibre volume fraction in the component and, thus, its mechanical properties. Moreover, lower properties may also be due to the absence of a compacting stage and thermal control in the manufacturing process.

The main findings of this study are the following:

- continuous carbon-fibre-reinforced thermoplastics possess mechanical properties approximately seven times higher than chopped carbon-fibre-reinforced thermoplastics;
- the additive manufacturing deposition pattern significantly influences the mechanical response. In particular, the mechanical properties are more than doubled if such a path is aligned with the load direction. This suggests that the design process should be carefully developed to fully leverage the process flexibility and thus achieve optimal structural performances;
- the annealing post-manufacturing treatment enhances the mechanical properties by approximately 10%, decreasing material ductility and manufacturing defects. Such a finding suggests that a thermal control on the AM process would benefit structural performance;
- the analysis based on the Classification Society Rules related to composite materials testing indicates that there is currently a technological limit on the maximum achievable fibre volume fraction, as it does not match the one imposed by the rules for the production of the specimens;
- continuous fibre-reinforced thermoplastics produced by AM match the minimum structural requirements imposed by the Classification Society Rules. Moreover, their mechanical properties are comparable to some of the traditionally manufactured composites;

- the mechanical properties of additively manufactured continuous FRP are currently lower than the ones of composites manufactured with traditional methods.

The provided framework revealed that continuous fibre-reinforced thermoplastics produced by AM have a high potential to be used as light-weight structural solutions for marine applications, as far as the tensile performances are concerned. However, to fully assess the potential of such materials, their complete mechanical response (e.g., flexural response, interlaminar shear strength, etc.) needs to be analysed, considering water absorption properties. Moreover, the work results suggest that the AM technology needs further developments to fully comply with Classification Society Rules and structural performances comparable, or superior, to traditionally manufactured composites.

An efficient approach to assess routes for enhancing the capabilities of current AM processes is to leverage a validated design process to guide the development of raw materials and manufacturing procedures. Such a design process may indeed be used, among others, to identify structural weaknesses and to set the material requirements in relation to the technical specifications of the application. The Chapter 6 is indeed oriented to develop optimal design methodologies for composite sandwich structures, which integrate the analysed FRP as base materials (core and skins).

6 OPTIMAL DESIGN OF SANDWICH STRUCTURES PRODUCED BY AM

This chapter describes the development of a validated optimal design procedure for Additive Manufactured Honeycomb Sandwich structures subjected to flexural loads. The core of the design procedure is a purposely developed Evolutionary Multi-Objective Optimization (EMOO) routine.

The analytical formulations utilized in the optimization process have been derived using a combined analytical and experimental approach. Such formulations, and thus the developed design procedure, rely strongly on the experimental testing campaign reported in section 6.3. The methodology followed to develop the analytical formulations for the EMOO routine is reported in section 6.2, while the multi-objective optimization framework for the design of additive manufactured honeycomb sandwich structures is addressed in section 6.4.

The design procedure provides the optimal scantling of additive-manufactured honeycomb sandwich structures subjected to quasi-static flexural loads. In particular, the 3-point bending condition is considered as reference, and the “Anisoprint CFC technology”, analysed in Chapter 5, has been utilized to produce the specimens. Details related to the modelling and additive manufacturing of the analysed structural solutions are given in section 6.1.

6.1 MODELLING AND ADDITIVE MANUFACTURING

This section highlights the key features of additive-manufactured honeycomb sandwiches, providing information on the additive manufacturing process employed for producing the specimens to be analysed according to the experimental testing campaign reported in section 6.3.

Two different types of sandwich structures have been modelled and manufactured. The first is the additive manufactured honeycomb sandwich raw (AMHSR) structure, which presents visible continuous fibre-reinforced skins and chopped fibre-reinforced honeycomb core. The second one has the core and the skins embedded in a chopped fibre-reinforced thermoplastic shell (AMHS). A comparison between the two structural solutions is shown in Figure 39.

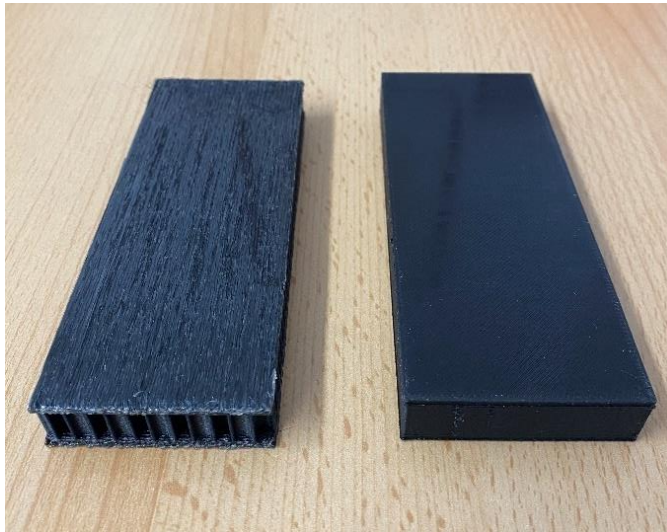


Figure 39: AMHSR (left) vs AMHS (right)

The 3D CAD model of AMHS and AMHSR structures has been developed using the software Autodesk Inventor. The model is fully parametric, i.e., it takes in input the geometrical dimensions of the structure and specific AM process parameters to update the sandwich geometry accordingly. The structures have been modelled accounting for the selected additive manufacturing process features, which implies the modelled geometries are optimized for the 3D printing profile generation.

A three-quarter section of the CAD model of AMHSR is shown in Figure 40 to highlight its main constituents.

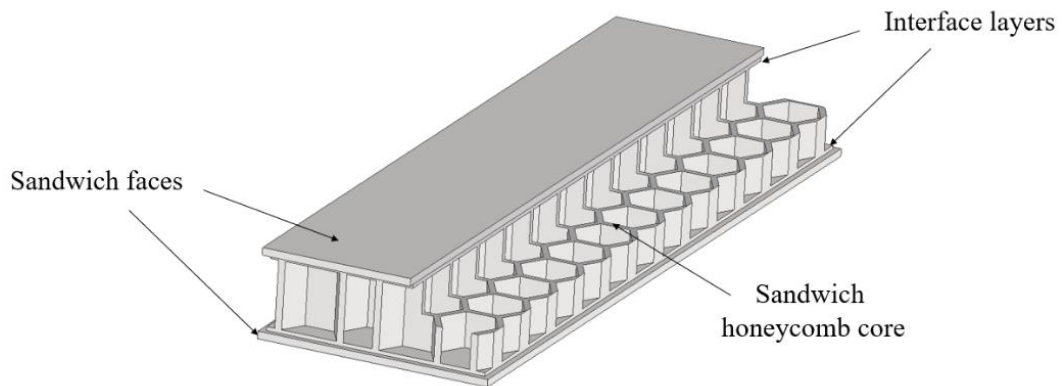


Figure 40: 3D CAD Model of AMHSR

The AMHSR structure comprises two faces (continuous fibre-reinforced thermoplastic) and a regular honeycomb core (chopped fibre-reinforced thermoplastic). These two elements are interfaced by fully chopped fibre-reinforced thermoplastic layers, which aim to maximize the core-skin bonding and achieve good continuous fibre deposition. The bonding between skins and core relies on the interlayer bonding strength, which depends on the employed AM technique and materials. Therefore, no adhesive has been used, and the above structure is the output of one single AM process.

The AMHS structure embeds, as mentioned, the above-addressed constituents in a chopped fibre-reinforced thermoplastic shell. Therefore, plastic perimeters and top and bottom layers are purposely added to the CAD model to achieve such a solution.

The additive manufacturing process of AMHSR is shown in Figure 41 for different honeycomb cell dimensions. The key features of the employed AM process and materials are reported in Chapter 5.



Figure 41: Additive manufacturing process of AMHSR

The first layers, which lie on the build plate, are made of continuous fibre-reinforced thermoplastic material, and the interface between core and skins is made of chopped fibre-reinforced thermoplastic layers. On the top of such an interface, the honeycomb core geometry is visible, whose geometrical features (honeycomb thickness and cell size) can be purposely adapted to structural requirements.

The used material for the core is “Smooth PA,” a thermo-plastic nylon (PA12) reinforced by chopped carbon fibres at 10%. The core has been printed with a layer height of 0.2 mm, an extrusion temperature of 265 °C, and a constant speed of 40 mm/s. The used bed temperature is 60 °C, and the fan speed for cooling is 20%.

The used material for the skins is “CFC PA+CCF”, a thermoplastic nylon (PA12) reinforced by continuous carbon fibre. The theoretical fibre volume fraction (FVF) is approximately 25%. The skins have been printed with a layer height of 0.34 mm and an extrusion temperature of 250 °C. The used bed temperature is 60 °C, and the fan speed for cooling is 50%. A fibre deposition algorithm controls the printing speed, while the maximum speed is 10 mm/s.

The utilized skins and core materials have been selected to account for the influence of different fillers on the thermoplastic matrix. In contrast, the core topology has been chosen as the honeycomb design method has a high potential to be generalised to any cellular structure [38]. Moreover, the current employment of honeycomb sandwich in industrial sectors can facilitate the integration process of additive-manufactured honeycomb sandwich structures in the maritime field.

The two proposed structural solutions have been developed with specific purposes. The AMHSR structure has been designed to simplify the investigation of the structural response (e.g., failure modes) and to identify geometrical and manufacturing imperfections. The AMHS has been designed to increase the geometrical accuracy, minimize surface roughness, enhance the load carrying capability and to provide a better appearance.

For the above reasons, the AMHS structure is the best candidate to be utilized as a structural element. However, the present PhD work is focused on the raw structure (AMHSR). This choice is due to the fact that the AMHSR solution is more suited to the development of an in-depth knowledge of the structural behaviour. Identifying sources of problems and routes of improvement on such a raw structure is indeed more straightforward, as the inspection of the constituents can be carried out visually. This is a relevant need to achieve the development of a purposely conceived manufacturing technique, tailored to improve the structural response. Moreover, following the proposed approach, the design procedure can be straightforwardly developed for AMHS.

6.2 ANALYTICAL FORMULATIONS FOR DESIGN

The present section provides the analytical formulations for the design of AMHSR subjected to the 3-point bending condition and it describes the experimentally-based methodology followed to develop them. The equations that have required particular attention to be integrated into the EMOO routine have been classified as displacement, failure modes, weight and cost.

The formulation to predict the sandwich displacement under load has been critically selected from state-of-the-art and calibrated on experimental data. Conversely, the equations related to the failure modes are based on purposely developed failure criteria. The weight and cost equation have been developed on the basis of the utilized materials and additive manufacturing technology.

The objectives of the study have been pursued according to the following main steps:

- identification of potentially suited analytical formulations from the current state-of-the-art to model the structural response of AMHSR. Such equations predict the sandwich displacement under load and the maximum load at failure, together with the expected failure mode;
- systematic experimental testing to compare the two developed design solutions. The flexural response of AMHSR and AMHS is analysed to assess the benefits of embedding the raw structure within a thermoplastic shell;
- systematic experimental testing to calibrate the identified analytical equations, or to develop new design theories, for AMHSR design;
- calibration of the analytical equations for the design of AMHSR, or development of new design theories, based on a careful observation and analysis of the experimental results;
- integration of the developed formulations in the EMOO design routine.

All the analytical formulations related to displacement, failure modes, weight and cost are described in the following sections, highlighting their dependency on the design variables, i.e., the geometrical features of AMHSR.

6.2.1 DISPLACEMENT

The bending and shear stiffness of the AMHSR structure are calculated as follows:

$$D_s = \frac{E_f b_s t_f (t_c + t_f)^2}{2}$$

$$S_s = \frac{b_s G_c (t_c + t_f)^2}{t_c}$$

Where:

- $D_s [Nmm^2]$ is the flexural stiffness;
- $S_s [N]$ is the shear stiffness;
- $E_f [MPa]$ is the tensile Young's modulus of the faces, assuming the elastic moduli in tension and compression are equal. It is derived from the tensile test on the face base material according to ASTM D3039, or ASTM D638;
- $b_s [mm]$ is the sandwich beam breadth;
- $t_f [mm]$ is the thickness of the skin;
- $t_c [mm]$ is the thickness of the core;
- $G_c [MPa]$ is the shear modulus of the core. As mentioned in section 3.3, to account for the dependency of such a parameter from the honeycomb geometry, the following closed-form equation based on structural mechanics has been selected from the Gibson and Ashby theory [38]:

$$G_c = 0.577 G_{cs} \frac{t_h}{l_h}$$

The shear modulus of the core base material G_{cs} is taken as G_{csxz} , which is the lowest shear modulus. It is derived from a short beam test according to ISO 14130. $t_h [mm]$ and $l_h [mm]$ are the thickness and side length of the honeycomb cell.

The displacement at midspan is calculated as follows:

$$w = \frac{Pl_s^3}{48k_{Ds}Ds} + \frac{Pl_s}{4k_{Ss}Ss}$$

Where:

- $w[mm]$ is the total displacement at midspan;
- $P[N]$ is the load applied at midspan, depending on structural requirements;
- $l_s[mm]$ is the length between the supports;
- $k_{Ds} = 0.95$ is the correction factor for the flexural stiffness. It accounts for geometrical deviations in sandwich and not perfect load transmission between skins and core due to poor bonding or manufacturing imperfections (e.g., voids);
- $k_{Ss} = 0.75$ is the correction factor for the shear stiffness. It accounts for geometrical deviations in a sandwich, not perfect estimation of the core shear modulus G_{cs} , due to imperfect material extrusion (e.g., voids), and geometrical deviations in the honeycomb geometry (l_h, t_h).

The correction factor values employed in the displacement equation have been identified according to the experimental results reported in section 6.3. The values of these factors have been defined for each experimental test, taking the average value among them as a representative to calibrate the equation.

An example of the calibration conducted on the displacement equation, for one of the analysed specimens, is shown in Figure 42. The figure compares the calibrated and non-calibrated equations against experimental results.

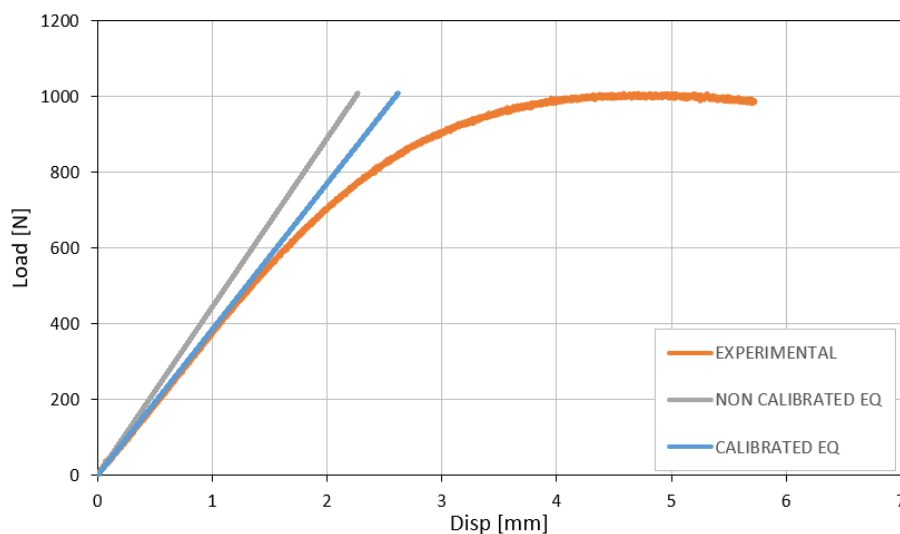


Figure 42: Example of displacement equation calibration

The displacement equation is linear instead of the real AMHSR response, which is non-linear. Therefore, such an equation cannot reproduce the displacement up to structural failure. However, as far as the design is concerned, this is unnecessary. The structure will be designed with a safety coefficient of 2 on the load at failure. This means the AMHSR will never be exploited up to its maximum load capacity, containing the error on the predicted displacement. In particular, the maximum load acting on the structure will always be half the load at failure. This means the maximum error on the displacement will occur at such a load value, which can be seen (in Figure 42) to be low (below 5%).

The calibration procedure was conducted according to the following steps:

1. the correction factor values have been defined for each acquired data point to minimize the error $e = (x_{ex} - x_{eq})^2$, as the squared difference between the experimental data and the equation value in a portion of the linear region. The calculation has been conducted in excel through a purposely developed macro;
2. for each specimen, the average value of the correction factors, among all the analysed data points, has been taken as representative;

3. for each specimen, the quality of the calibration has been verified, ensuring a suited value for the coefficient of determination ($R^2 > 0.9$) and for the angular coefficient ($m > 0.9$) representing the relation between the experimental data and the equation value in the analysed region;
4. the final values of the correction factors, to be used in the displacement equation, have been taken as the average among all the tested specimens;
5. the accuracy of the calibration has been verified by analysing the deviation between the displacement equation and the experimental data when the load is half of the maximum. This ensures low deviation in the design range. The registered error is less than 10% for all the specimens, which has been considered a good result.

6.2.2 FAILURE MODES

The developed equations for the structural failure prediction are based on a stress approach. Therefore, the controlling variables are the normal and shear stresses acting in the structure. The normal stresses acting in the skins and the shear stresses acting in the core are illustrated in Figure 43. It has been considered that the bending stress varies linearly in the skins and it is null in the core, while the shear stress is constant in the core and null in the skins.

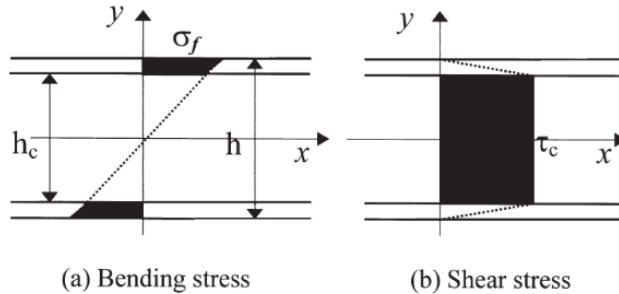


Figure 43: Stresses in a sandwich beam under 3-point bending

The normal and shear stresses in the skins and the core are calculated as follows:

$$\sigma_f [MPa] = \frac{E_f \frac{Pl_s}{4} \left(\frac{t_c}{2} + t_f \right)}{D_s} \quad \tau_c [MPa] = \frac{\frac{P}{2}}{b_s(t_c + t_f)}$$

The failure modes which have been considered in this study are the following:

- *skin failure in compression*: this would be the desirable failure type to exploit the skins up to their maximum capacity. However, it has been found that compression failure does not occur as high initial imperfections (e.g., fibre waviness) and poor bonding between layers incept different modes;
- *skin wrinkling-delamination failure*: this is the experimentally observed failure mode. A purposely conceived failure criterion has been developed to predict this failure. The full capacity of the skins is not fully exploited because such a combined failure mode occurs before compression failure;
- *core interlaminar shear failure*: this is the experimentally observed failure mode for $l_s / b_s < 3$. Current state-of-the-art failure theories on honeycomb core shear strength (see section 3.3.4) cannot predict such a failure. Therefore, a purposely conceived failure criterion has been developed.

6.2.2.1 SKIN FAILURE

The failure criteria for the skin failure are the following:

$$\sigma_f = \sigma_{cf}$$

$$\left(k_\sigma \frac{\sigma_f}{\sigma_w} \right)^{n_\sigma} + \left(k_\tau \frac{\tau_c}{\tau_{lf}} \right)^{n_\tau} = FI \quad (FI = 1 \text{ at failure})$$

Where:

- $\sigma_{cf}[MPa]$ is the compression strength of the skins, derived from compression testing according to ASTM D6641. Failure occurs when the acting stress σ_f reaches the compression strength. No correction is required as this value is directly derived from the testing of the skin base material;
- $\sigma_w[MPa] = 0.5\sqrt[3]{E_c E_f G_c}$ is the skin wrinkling stress limit. Such limit stress has been used as the experimental results (section 6.3) have shown that the stress at failure depends on the relative density. Moreover, this choice is numerically justified as the error in the calibration procedure is lower when this stress is considered instead of a fixed one (e.g., σ_{cf}).

Where:

- $E_c [MPa] = E_{csz} \frac{\rho_c}{\rho_s}$ is the Young's modulus of the core in the out-of-plane (z-printer) direction. The Gibson and Ashby theory [38] is again employed to account for the dependency of such a parameter from the honeycomb geometry;
- $E_{csz} [MPa]$ is the core base material Young's modulus in the out-of-plane direction (z printer), derived from tensile test according to ASTM D638;
- $\frac{\rho_c}{\rho_s} = \frac{2}{\sqrt{3}} \frac{t_h}{l_h}$ is the relative density of the honeycomb core;
- $\tau_{if} [MPa]$ is the interlaminar shear strength of the skins, taken equal to the interlaminar shear strength of the nylon matrix co-extruded with the continuous fibre. This limit stress has been used as the experimental results (section 6.3) show that skin delamination occurs before failure. Moreover, this choice is numerically justified as the error in the calibration procedure is lower when this stress is considered instead of a variable one (e.g., dependent on the core density). τ_c is the acting shear stress, taken as the maximum shear stress acting in the skin. This is the stress acting at the interface between skins and core;
- $k_\sigma = 1.0, k_\tau = 1.0, n_\sigma = 0.62, n_\tau = 0.2$ are linear and exponential correction factors for the normal stress and shear stress terms in the combined failure mode equation. Their values have been identified according to the experimental results reported in section 6.3 to get a failure index (FI) equal to 1 (at failure) for all the tested specimens.

The calibration of the correction factors is conducted, leveraging multi-objective optimization techniques to identify their values. In particular, a multi-objective problem framework has been built with the following key features:

- the objective functions are represented by the wrinkling-delamination failure criteria equations, which are wrote for each tested specimen. All the objective functions have to be maximized;
- the objective functions have been purposely constrained to yield a value between 0.97 and 1.03;
- the decision variables are represented by the correction factors, the linear coefficients lower and upper bounds are 1 and 3, while the exponential factors lower and upper bounds are 0.2 and 1.

The solution of the above-addressed multi-objective optimization problem yields the optimal values of the correction coefficients, which generate the collapse of the structure at a failure index (FI) approximately equal to 1. The optimal solution has been selected leveraging the weighted score method, considering the same weighting factor for all the objective functions.

The wrinkling-delamination failure criterion has been purposely developed because the criteria found in the literature (see section 3.3.4) could not accurately predict the load at failure. From the analysis of the experiments, it has been found that the limit stress at failure depends on the density of the core, which is in agreement with the wrinkling equation. However, such an equation could not explain the limit stress dependency on other AMHSR geometrical parameters. Moreover, the compressive stress limit of the skins was not reached.

The wrinkling-delamination failure criteria for the AMHSR skins are shown in Figure 44 for all the tested specimens. The figure shows the dependency of the normal stress ratio to the shear stress ratio for different values of the failure index. The points related to the tested specimens have been highlighted. Moreover, the “safe points” have been plotted. Such safe points have been identified considering half of the stress values (normal and shear) at failure.

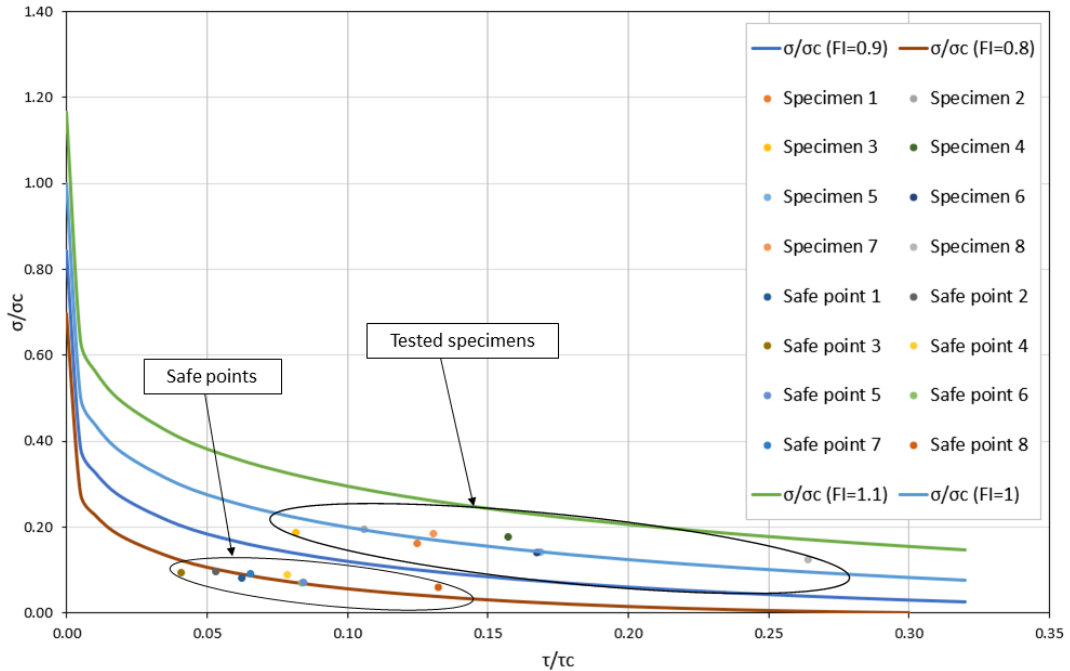


Figure 44: Wrinkling-delamination failure criteria for AMHSR skins

The region below the considered FI curve is the safe zone, while the region above is the failure zone. For all the tested specimens, failure occurs for $0.97 < FI < 1.03$, the corresponding points lie indeed in the proximity of the $FI = 1$ curve.

For design purposes, the main objective is to identify the curve corresponding to a safety coefficient equal to or higher than 2. It can be seen that lowering the failure index increases the safety coefficient on the analysed combined skin failure. All the safe points lie in the proximity of the curve corresponding to $FI = 0.8$, which means such a failure index provides the required safety. Therefore, a $FI = 0.8$ has been considered in this study for design purposes.

The graph clearly shows that to exploit the maximum capacity of the skins, and thus to increase the normal stress in the skins at failure, two main options can be

implemented. The first one is to increase the interlaminar shear strength of the skins, the second one is to increase the wrinkling stress limit.

The main reason which leads to the inception of the wrinkling-delamination failure mode is the presence of the following structural weaknesses:

- initial imperfections in the skins, seen as fibre in plane and out of plane waviness;
- poor inter-layer bonding in the skins and in the core;
- manufacturing imperfections (e.g., voids) in the skins and in the core.

The mentioned structural weaknesses need to be addressed to optimize the structural performances of AMHSR, as they are the main responsible for the low wrinkling and interlaminar shear limit stresses.

6.2.2.2 CORE FAILURE

The failure criterion for the core is the following:

$$\tau_c = \tau_{lc}$$

Where:

- $\tau_{lc} [MPa] = k_{\tau c} \frac{\rho_c}{\rho_s} \tau_{lcs}$ is the core interlaminar shear strength. Where the variables have the following meanings:
 - $\tau_{lcs} [MPa]$ is the core base material interlaminar shear strength. It is derived from a short beam test according to ISO 14130. Failure occurs when the acting stress τ_c is equal to the developed limit stress;
 - $k_{\tau c} = 0.96$ is a correction factor that accounts for geometrical deviations and not perfect material extrusion during the honeycomb deposition. The value of $k_{\tau c}$ has been calibrated on the basis of experimental results.

This criterion has been purposely developed to account for AMHSR core shear strength, which is a relevant parameter to be considered for the design if $l_s / b_s < 3$.

In fact, this failure mainly occurs in panels, instead of beams ($l_s / b_s > 3$).

It is worth mentioning that the developed core failure criterion allows to assess the core performances and thus to carry out a comparison among currently employed structures and Classification Rules requirements (section 7.2).

6.2.3 WEIGHT

The utilized equation for the sandwich weight calculation is the following:

$$W_s = w_c + w_f$$

$$w_c = \rho_c \{ \rho_r k_c [b_s (l_s + l_{sn}) (t_c - t_p)] + b_s t_p (l_s + l_{sn}) \}$$

$$w_f = \rho_f k_f (l_s + l_{sn}) b_s 2t_f$$

Where:

- $W_s [g]$ is the total weight;
- $w_c [g]$ is the core weight;
- $w_f [g]$ is the skins weight;
- $l_{sn} [mm]$ is the unsupported length;
- $\rho_c [g / mm^3]$ is the density of the core base material;
- $t_p [mm]$ is the total thickness of the solid plastic layers placed between core and skin;
- k_c is the correction factor to account for the chosen core print settings and for the incorrect estimation of the relative density (e.g., due to the layup employed);
- $\rho_f [g / mm^3]$ is the density of the skin, which considers the fibre and the matrix to be co-extruded with;
- k_f is the correction factor to account for the chosen skin print settings.

It is worth mentioning that the sandwich structure weight is sensitive to 3D printing settings (e.g., flow rate, extrusion width, extrusion speed, etc.). Therefore, the optimal settings have been first identified and then the values of the corrective factors have been selected to calibrate the equation. The weight equation needs to be

introduced in the EMOO algorithm to perform the optimization. However, in standard applications the weight of the structure is known from the slicing software (e.g., Aura) utilized to generate the G-code for the machine. Such software properly accounts for the influence of 3D printing settings on the weight of the structure.

The weight equation has been calibrated using weight output data from the slicing software. In particular, AMHSR reference geometries have been selected for data generation by systematically varying the geometrical parameters of the sandwich structure. In particular, three weight-data have been obtained by varying each variable individually ($l_s, b_s, t_c, t_f, t_h, l_h$), while keeping the others constant.

The calibration has been performed by identifying the values of the correction factors that minimize the error between the slicing software data and the equation value for each data. Hereafter, the average among all the data analysed has been taken as representative. The quality of the calibration has been verified by ensuring a suited value for the coefficient of determination ($R^2 > 0.9$) and for the angular coefficient ($m > 0.9$) representing the relation between the slicing software data and the equation value.

It is worth mentioning that the weight utilized is ideal, which may differ from the real weight for the presence of manufacturing imperfections (e.g., geometry deviations and voids). This is not a problem for the optimization, as this is a constant deviation, as far as the print settings and post-manufacturing treatments are not changed. However, if the real structural weight has to be known, the weight equation should be further calibrated, considering both slicer output and real weight measurements.

6.2.4 COST

The utilized equation for the sandwich cost calculation is the following:

$$C_T = C_M + C_L + O$$

$$C_M = w_c c_c + 2c_f k_{CE} (l_s + l_{sn}) \frac{b_s t_f}{e_w l_f}$$

$$C_L = P_T L_R$$

$$O = 0.3(C_M + C_L)$$

Where:

- C_T [€] is the total cost of the sandwich structure;
- C_M [€] is the material cost;
- C_L [€] is the labour cost;
- O [€] are the overheads;
- c_c [€/g] is the core base material cost;
- c_f [€/mm] is the fibre cost;
- k_{CE} is a correction factor to account for the cost of the plastic material which is co-extruded with the fibre and for the print settings, which may vary the extruded fibre length;
- e_w [mm] is the fibre extrusion width;
- l_f [mm] is the fibre layer height;
- P_T [h] is the print time;
- L_R [€] is the labour rate of the operator involved in the design and manufacturing process.

The print time equation has been developed using a multi-variable polynomial regression, using the sandwich geometrical parameters as variables, according to the following steps:

- the print time has been obtained from the slicing software (Aura) in a systematic way. In particular, three time-data have been obtained by varying individually each variable ($l_s, b_s, t_c, t_f, t_h, l_h$) while keeping the others constant;
- a multivariable polynomial regression has been developed for the print time considering all the variables as follows: $a_i + b_i x_i + c_i x_i^2 + d_i x_i^3$, where x_i is the generic variable and a_i, b_i, c_i, d_i are the coefficients of the polynomial;
- the coefficients have been calculated, for each data, by minimizing the error $e = (x_r - x_p)^2$ between the real-time (from Aura slicer) and the predicted time. Hereafter, the average among all the data analysed has been taken as representative;
- the quality of the calibration has been verified, ensuring a suited value for the coefficient of determination ($R^2 > 0.9$) and for the angular coefficient ($m > 0.9$) representing the relation between the experimental data and the equation value. Moreover, the quality of the predicted time-variable relationship has been verified by assessing the influence of each variable is well represented;
- lower and upper bounds have been plotted to verify the level of confidence in real-time time-data;
- the upper bound level of confidence has been conservatively taken as representative.

6.3 EXPERIMENTAL TESTING

This section describes the experimental tests conducted to assess the potential of the proposed design solutions and to develop, and finally validate, the AMHSR optimal design methodology. A detailed analysis of the experimental results has been conducted, illustrating the key features of the structural response and highlighting its correlation with the design method.

The following experimental test blocks have been executed:

- 3-point bending tests, to compare the two developed design solutions (AMHSR and AMHS), with the main aim to evaluate the benefits of embedding the raw structure within a chopped thermoplastic shell;
- 3-point bending testing campaign, to feed the design models with a proper amount of data and to perform their final validation.

The 3-point bending test set-up is shown in Figure 45. The actuated element is the cylinder acting at the midspan of the specimen, while the support cylinders are fixed and attached to a load cell of 25kN. Such cylinders are placed at pre-defined distances, according to the systematic test plan developed. The tests have been conducted following the specifications of ASTM C393.

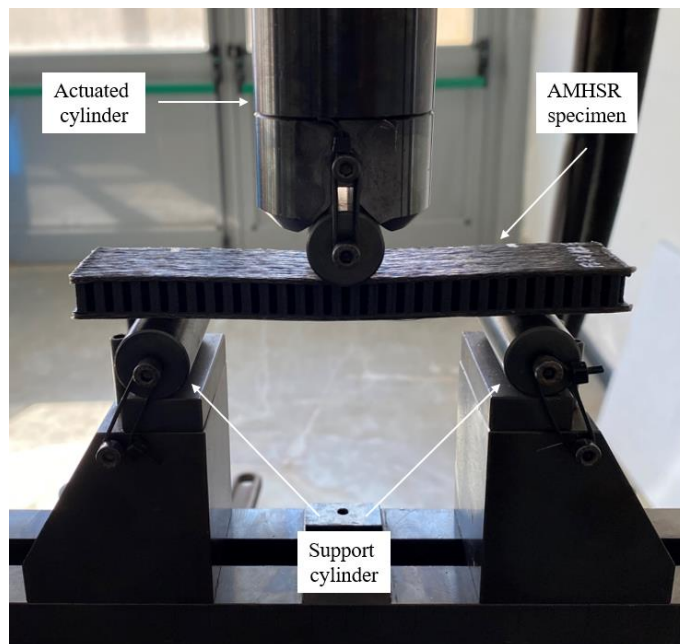


Figure 45: Experimental test set-up for 3-point bending

The actuated cylinder moves downwards with a constant speed of 1mm/min. The load (measured by the load cell) and the displacement of the middle cylinder are registered. The tests have been recorded with a video-camera to carefully inspect the structural response in time and thus accurately evaluate the structural behaviour. An NBR sheet of 1mm has been placed between the specimen and the middle cylinder to limit skin indentation, containing the error on the registered displacement.

The details related to the modelling and to the production through AM of the additive-manufactured honeycomb sandwich specimens are given in section 6.1.

6.3.1 DESIGN SOLUTION COMPARISON: AMHS VS AMHSR

The main objective of the experimental testing reported and discussed in this section has been to compare the structural behaviour of AMHSR and AMHS to assess the capabilities of different design solutions.

The main dimensions of the tested specimens are reported in Table 8.

Table 8: Main dimensions of the specimens – Design solution comparison

Specimen	l_s	b_s	t_c	t_f	t_s	t_h	l_h
AMHS-H5-L100	101.6	31.6	10	1	0.5	1.2	5
AMHSR-H5-L100	100	30	10	1	0	1.2	5

It is worth mentioning that the external dimensions of AMHS are slightly increased w. r. t. AMHSR. In particular, the length and the breadth are increased by 1.6mm, while the total thickness ($t_c + 2t_f + 2t_s$) of the structure is increased by 1mm. This is due to the inclusion of the chopped thermoplastic shell.

The flexural response of the specimens is shown in Figure 46 in terms of load-displacement relationship.

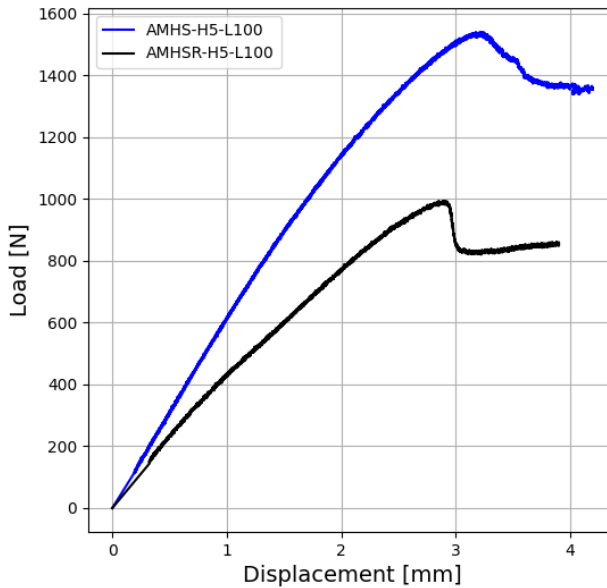


Figure 46: Flexural response – AMHS vs AMHSR

Interestingly, embedding the raw structure in the chopped thermoplastic shell increases the load carrying capability of the structure and its stiffness. In particular, the load at failure and the load-displacement ratio are approximately 50% higher. This is an outstanding result, as it means that the flexural response of such structures may be significantly enhanced by purposely developed design solutions, while keeping almost the same geometry, constituent materials and mechanical properties.

The failure modes of the specimens are shown in Figure 47. The AMHS specimen is at the top part of the figure, while the AMHSR specimen is at the bottom.

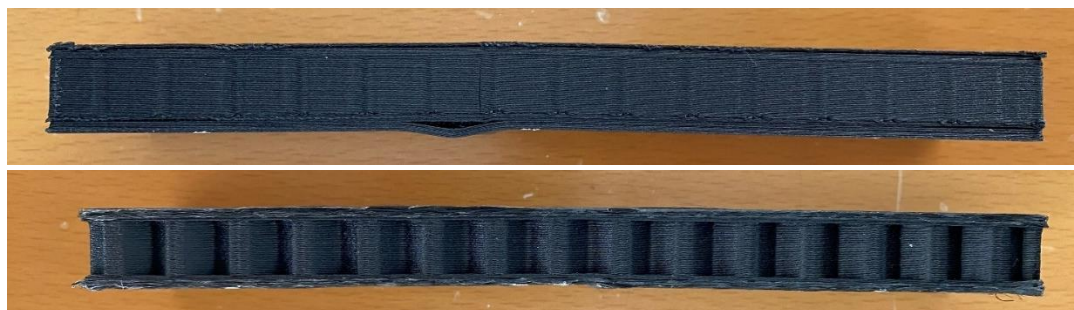


Figure 47: Specimens failure modes - AMHS vs AMHSR

Using the failure modes equations presented in section 6.1, it is possible to estimate the load at failure and the expected failure mode for AMHSR with a reasonable accuracy. The predicted failure mode is wrinkling-delamination failure. Such a failure mode is more evident on the AMHS specimen, while the AMHSR experiences a less visible failure. In the AMHS specimen is indeed clearly visible the wrinkle of the compressed skin, whose formation has been accompanied by delamination. This statement is further clarified in the following section.

The wrinkling-delamination failure is promoted by initial imperfections (fibre in the plane and out-of-plane waviness), poor inter-layer bonding and defects (e.g., voids) due to the additive manufacturing technique.

It is worth mentioning that the load at failure is higher for AMHS because the plastic layers placed on top of the continuous fibre skins prevent their local buckling and delamination in the out-of-plane direction. Utilizing AMHS with a suitable number of thermoplastic layers above the skin, may thus be a way to increase the skin structural capacity.

6.3.2 RESULTS OF THE 3-POINT BENDING TESTING CAMPAIGN

The main objective of the experimental testing reported and discussed in this section have been the following:

- to evaluate the influence of AMHSR geometrical parameters (e.g., length, thickness, core density) on the flexural response;
- to feed the experimental data in the design models for calibration purposes;
- to validate the developed failure criteria.

The main dimensions of the tested specimens are reported in Table 9.

Table 9: Main dimensions of the specimens – 3-point bending testing campaign

Specimen	l_s	b_s	t_c	t_f	t_h	l_h
AMHSR-L50-T1.7-H5	50	30	10	1.7	1.2	5
AMHSR-L90-T1.7-H5	90	30	10	1.7	1.2	5
AMHSR-L120-T1.7-H5	120	30	10	1.7	1.2	5
AMHSR-L150-T1.7-H5	150	30	10	1.7	1.2	5
AMHSR-L120-T1-H5	120	30	10	1	1.2	5
AMHSR-L120-T2.4-H5	120	30	10	2.4	1.2	5
AMHSR-L120-T1-H3	120	30	10	1	1.2	3
AMHSR-L120-T1-H7	120	30	10	1	1.2	7

The influence of the length between the supports on the flexural response of AMHSR is shown in Figure 48. The experimental data are plotted up to the maximum load for clarity reasons.

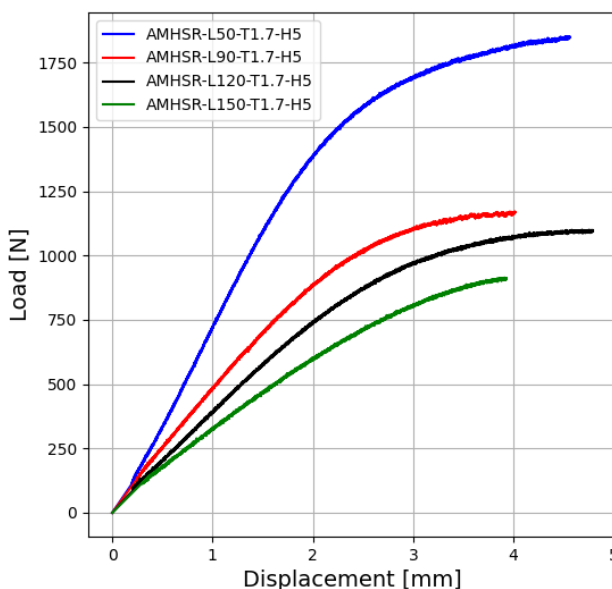


Figure 48: Influence of specimen length on AMHSR flexural response

As expected, decreasing the length between supports, the strength and the stiffness of the specimen are increased. However, this increase is lower than expected if current state-of-the-art failure theories would have been used. This is due to the fact that failure occurs when a specific combination of normal and shear stresses in the skin reaches a particular failure index (wrinkling-delamination failure criteria). This finding means that the normal stress in the skins is not the only parameter that governs the failure, but the shear stress plays also a role. Therefore, even if the normal stress is decreased up to 40% from $l_s = 150$ to $l_s = 90$, the increment in the load at failure is limited.

The above-addressed structural behaviour, which is due to the inception of the wrinkling-delamination failure, is mainly due to the poor interlaminar shear strength of the skins. Such a feature promotes delamination, that, in turn, induces the localized buckling of the skin on the core foundation (wrinkling).

The developed wrinkling-delamination failure criteria predicts the failure of all the AMHSR specimens analysed with reasonable accuracy, as shown in Figure 49. Such a figure reports the curves corresponding to the failure criteria for different values of the failure index, highlighting the points related to the tested specimens at failure. Moreover, the “safe points” are reported in the graph, calculated by considering half of the normal and shear stresses acting at failure.

All the tested specimens lie in the proximity of the $FI = 1$ curve, assessing the accuracy of the developed criterion. Moreover, all the safe points lie in the proximity of the $FI = 0.8$ curve. This means a safety coefficient of 2 on the load at failure is obtained if the criterion sets a maximum $FI = 0.8$ instead of $FI = 1$.

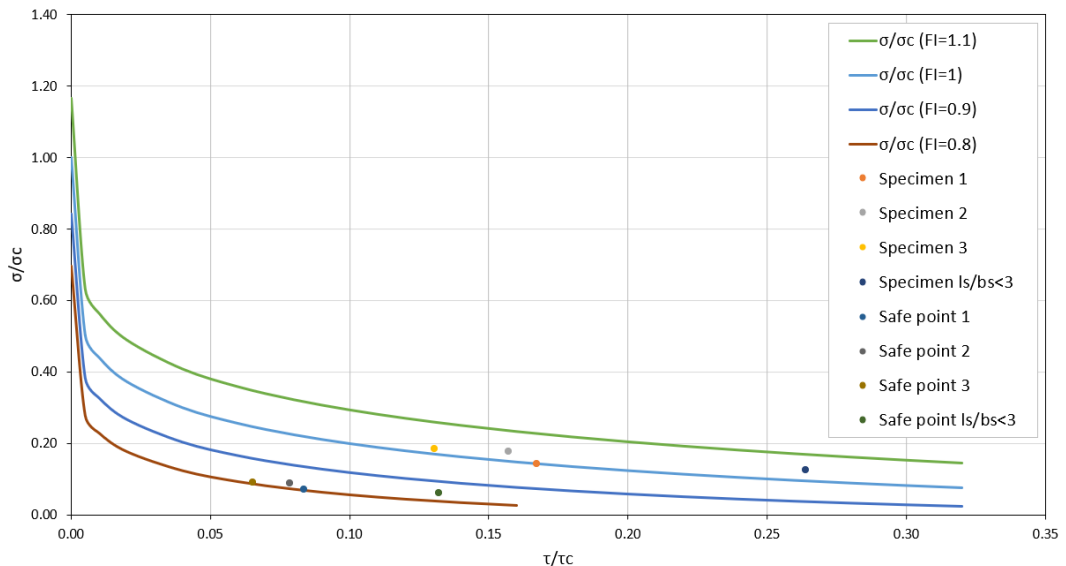


Figure 49: Wrinkling-delamination failure criteria – Length

It is evident from both Figure 48 and Figure 49 that, the specimen with $l_s = 50$ ($l_s / b < 3$) encounters failure at a load which is 50% or more higher than the other tested specimens. This is due to the fact that for this specimen $l_s / b_s = 1.67$, while the others are characterized by $l_s / b_s \geq 3$. Such a short length highly reduces the normal stress in the skin, triggering the skin failure mode at a higher load. Moreover, the core interlaminar shear failure occurs for such a short specimen. Therefore, skin failure (wrinkling-delamination) and core shear failure are observed for the specimen with the lowest length. This finding suggests that controlling different failure modes in parallel is necessary for design purposes.

The combined failure (core and skin failure) is shown in Figure 50 for the AMHSR specimen with the lowest length ($l_s = 50$). It is indeed possible to observe a crack in the core and a wrinkle on the left side of the cylinder zone.

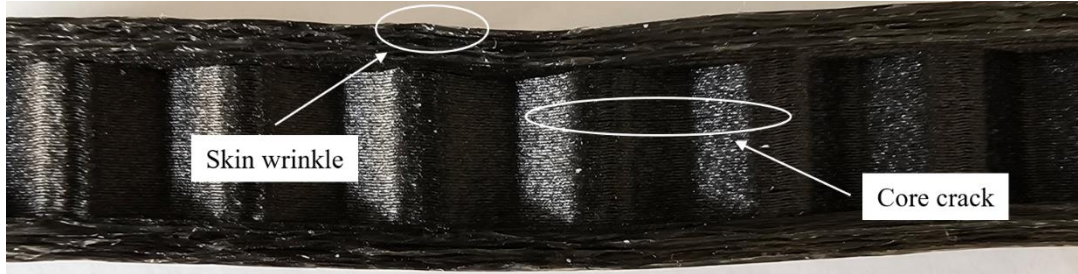


Figure 50: Combined failure modes for $l_s=50$ – Core and skin failure

It is worth mentioning that the specimen with $l_s = 50$ is the only one which failed by core shear. All the other specimens have experienced only failure in the skins. This is due to the shorter length, which lowers the normal stresses in the skins and raises the shear stresses to the core shear failure limit.

The failure mode encountered by the specimens with $l_s / b_s \geq 3$ is skin wrinkling-delamination. Figure 51 shows the wrinkles which are typically present on the compressed skin outer surface. It is indeed possible to observe two wrinkles on the left and right sides of the cylinder zones in all the tested specimens.



Figure 51: Skin wrinkling - $l_s/b_s > 3$

Skin delamination is also present in all the specimens. The video-camera records have shown that delamination is progressively developed until it promotes the above-illustrated skin wrinkling. However, it is difficult to observe it on the unloaded specimen, as unloading it closes the gaps in between the skin layers, reducing also the wrinkle amplitude.

The progressive delamination in the compressed skin is clearly shown in Figure 52. Such a figure shows three progressive time instants of the test, upon which the cracks in the skin became more evident, promoting the wrinkling of the skin.

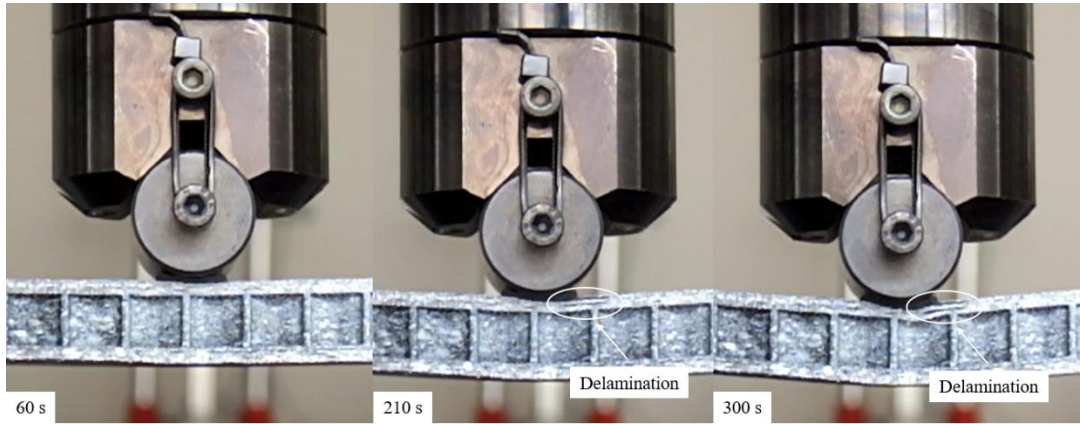


Figure 52: Skin delamination progression - $l_s/b_s > 3$

The influence of the thickness on the flexural response of AMHSR is shown in Figure 53. The test data are plotted up to the maximum load for clarity reasons.

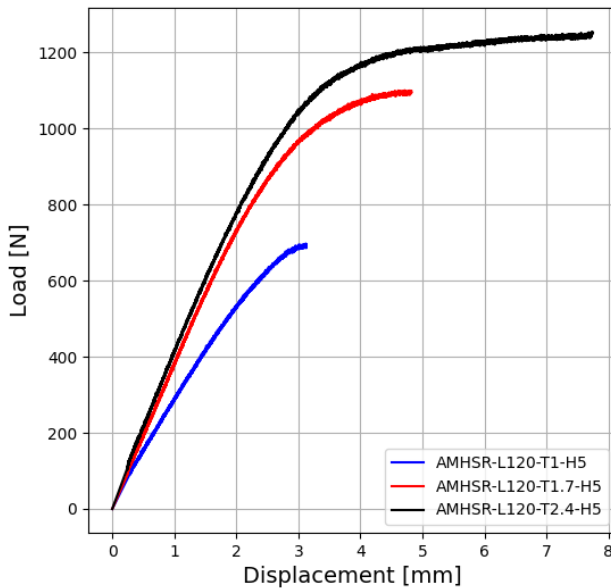


Figure 53: Influence of skin thickness on AMHSR flexural response

As expected, by increasing the thickness of the skins, the strength and the stiffness of the specimen are increased. However, such increment is again lower than expected, if current state-of-the-art failure theories would have been used. In particular, they are drastically reduced between $t_f = 1.7$ and $t_f = 2.4$. The stiffness

increase is believed to be limited because the thicker specimen encountered pronounced indentation, as shown in Figure 54.



Figure 54: Specimen indentation for $t_f=2.4$

Regarding the low difference encountered for the load at failure, it can be stated that, as already discussed, it is limited by the fact the ratio between acting normal stress and normal critical stress and the ratio between acting shear stress and shear critical stress must adhere to a specific equation. The failure is indeed in agreement with the purposely developed wrinkling-delamination failure criterion, as shown in Figure 55.

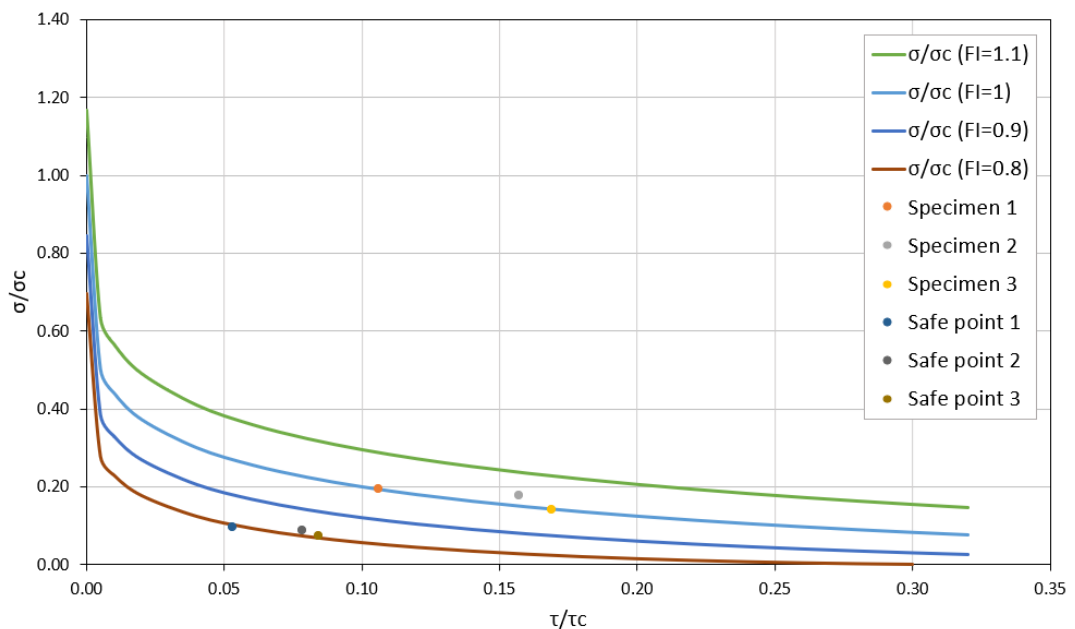


Figure 55: Wrinkling-delamination failure criteria – Skin thickness

The same considerations stated above can be drawn regarding the accuracy of the failure criteria and the safety coefficients achievable selecting the desired curve.

The influence of the honeycomb density on the flexural response of AMHSR is shown in Figure 56. The experimental data are plotted up to the maximum load for clarity reasons.

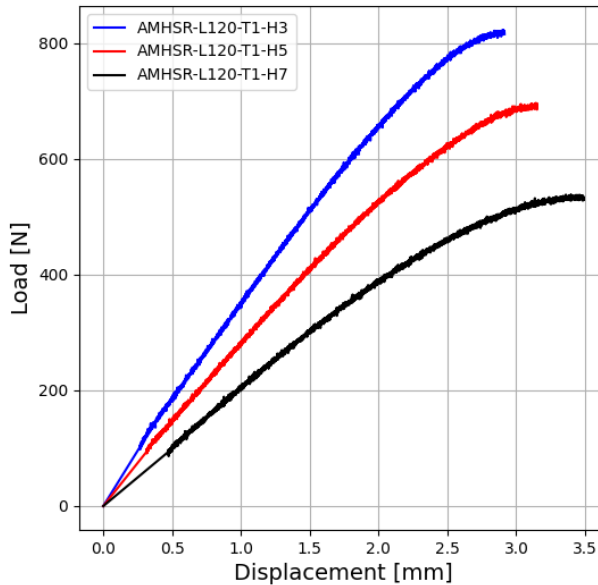


Figure 56: Influence of core density on AMHSR flexural response

As expected, increasing the honeycomb density, i.e., decreasing the cell size, the strength and the stiffness of the specimen are increased. The stiffness increases because the total deformation is extremely sensitive to the shear stiffness. Increasing the density means increasing the shear modulus of the core (on which the shear stiffness linearly depends). The load at failure is higher because the wrinkling limit load increases by increasing the stiffness of core. The phenomenon is indeed localized skin buckling on an elastic foundation, which occurs at a higher load if the stiffness on the foundation (core material) is increased.

Despite the structural behaviour being qualitatively well reproduced, the value of the load at failure does not agree with the current state-of-the-art wrinkling criterion. This is due to the fact the delamination induced by the shear stresses needs to be accounted for. The load at failure is indeed well predicted by the developed wrinkling-delamination criterion, as shown in Figure 57.

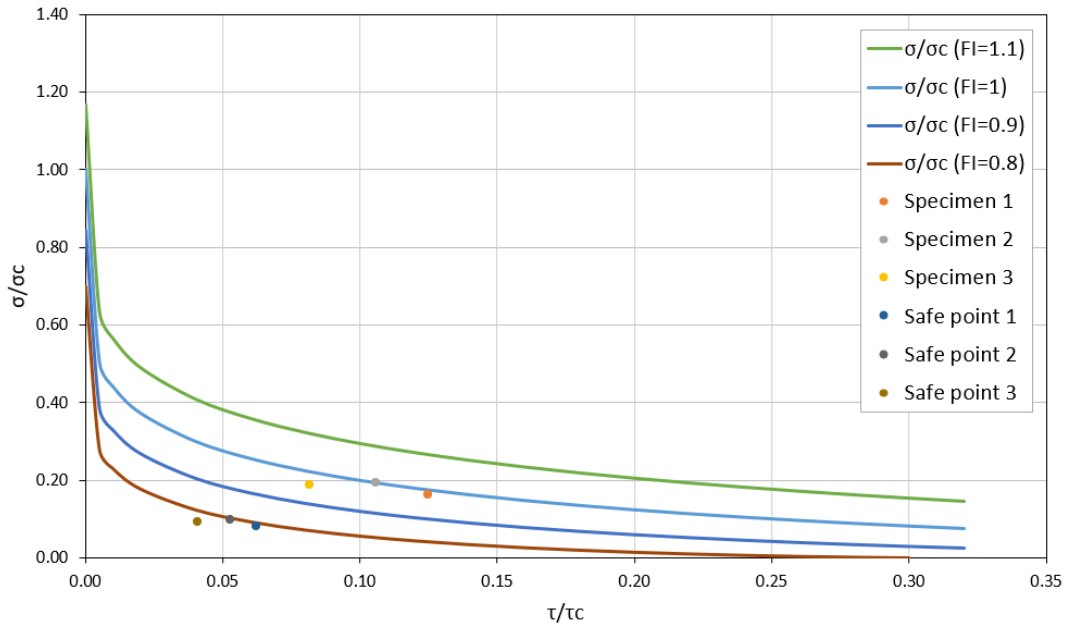


Figure 57: Wrinkling-delamination failure criteria – Core density

The same considerations stated above can be drawn regarding the accuracy of the failure criteria and the safety coefficients achievable selecting the desired curve.

6.4 OPTIMAL SANDWICH DESIGN

The design formulations developed for AMHSR have been integrated into a purposely developed Evolutionary Multi-objective Optimization (EMOO) routine, with the aim to achieve the optimal structural design according to a specific framework. Such a routine leverages the NSGA-II algorithm [53].

The multi-objective optimization framework is highlighted in the present section. To set up the problem, the user must define the mechanical properties of the core base material and of the skins, parameters related to the additive manufacturing technique and the load at midspan (according to structural requirements).

The design variables, varying between upper and lower bounds, are the following:

$$l_{s,low} \leq l_s \leq l_{s,up}$$

$$b_{s,low} \leq b_s \leq b_{s,up}$$

$$t_{c,low} \leq t_c \leq t_{c,up}$$

$$t_{f,low} \leq t_f \leq t_{f,up}$$

$$t_{h,low} \leq t_h \leq t_{h,up}$$

$$l_{h,low} \leq l_h \leq l_{h,up}$$

A solution vector $\vec{x} = (l_s, b_s, t_c, t_f, t_h, l_h)^T$ is formed by the geometrical parameters of the AMHSR structure. The lower and upper bounds (“low” and “up” subscripts) are user inputs which must be carefully chosen in relation to the application.

The objective functions to be minimized are the following:

$$f_1 : \min[w] = \min\left[\frac{Pl_s^3}{48k_{Ds}Ds} + \frac{Pl_s}{4k_{Ss}Ss}\right]$$

$$f_2 : \min[W_s] = \min[w_c + w_f]$$

$$f_3 : \min[C_T] = \min[C_M + C_L + O]$$

$$f_4 : \min[h] = \min[2t_f + t_c]$$

The objective functions are displacement, weight, cost and sandwich total height.

The constraints on the geometrical dimensions are the following:

$$g_1 : \frac{t_h}{l_h} < 0.25$$

$$g_2 : \frac{l_s}{b_s} > 3$$

$$g_3 : \frac{l_s}{S_c + t_h} > 3$$

$$g_4 : \frac{b_s}{S_c + t_h} > 3$$

The constraint g_1 is applied to limit the relative density to conventional values. The constraint g_2 is posed to obtain a beam-type structure, compliant with traditional beam geometries employed in ships. The constraints g_3 and g_4 impose at least three honeycomb cells through the main dimensions of the sandwich (S_c is the cell size), which ensure consistent stress paths in the core.

The constraints dependent on the additive manufacturing process are the following:

$$h_1 : \frac{t_c}{h_c} = \text{int} \quad h_2 : \frac{t_f}{h_f} = \text{int} \quad h_3 : \frac{t_h}{n_D} = \text{int}$$

The equality constraints reported above are dependent on the 3D printing settings and hardware. The constraints state that the skin and core thicknesses have to be a multiple of the layer height, while the honeycomb thickness must be a multiple of the nozzle diameter. They are set to ensure maximum geometrical accuracy and feasible geometries. The layer height of the core (h_c) and of the skins (h_f) are dependent on the print settings employed, while the nozzle diameter (n_D) is dependent on the chosen nozzle hardware.

The constraints on the failure modes are the following:

$$g_5 : \left(k_\sigma \frac{\sigma_f}{\sigma_w} \right)^{n_\sigma} + \left(k_\tau \frac{\tau_c}{\tau_{lf}} \right)^{n_\tau} < 0.8$$

$$g_6 : \frac{\sigma_{cf}}{\sigma_f} > 2$$

$$g_7 : \frac{\tau_{lc}}{\tau_c} > 2$$

The failure modes of the sandwich structure are considered separately as structural constraints. Two failure modes are considered for the skins, while one is considered for the core. The failure index of 0.8 on the combined wrinkling-delamination skin failure corresponds to a safety coefficient of 2 on both normal and shear stresses.

The NSGA-II algorithm is coupled with an a-posteriori MCDM approach to find the preferred solution among the pre-identified optimal set. Such a choice is oriented to fulfil specific structural specifications and user preferences. In particular, the weighted score method has been utilized as an MCDM approach.

The selection of the optimal solution is performed as follows:

$$\vec{x}_{opt} : \min[\sum w_i f_i]$$

where:

- w_i are the weights assigned to the objective functions, which are user inputs;
- f_i are the values of the objective functions associated with each design solution.

6.5 DISCUSSION

This chapter provides a multi-objective design procedure for raw Additive Manufactured Honeycomb Sandwich (AMHSR) subjected to flexural loads (3-point bending condition). The analytical and experimental approach for developing the design formulations has been addressed. Hereafter, the multi-objective optimization framework, which leverages the developed formulations, has been highlighted. Moreover, a comparison between different design solutions has been conducted to highlight the potential of the design over materials and manufacturing developments.

The main findings of the activities are the following:

- development of analytical formulations to predict the load-displacement relation of AMHSR subjected to the 3-point bending condition. The maximum error between the predicted displacement and the experimental one is below 10% in the design range;
- development of analytical formulations to predict the load at failure and the expected failure mode. Specific failure criteria have been developed for the skin and core failures. The skin fails in a combined failure mode which considers delamination as a promoter of wrinkling, while the core fails by interlaminar shear;
- development of an EMOO routine which integrates the above-stated formulations for the optimal design of AMHSR according to specific objectives and constraints;
- the flexural response of AMHS is superior to AMHSR. In particular, the strength and the stiffness are enhanced by approximately 50%. Moreover, such a design solution increases the geometrical accuracy, reduces the surface roughness and provides a better exterior aspect. Therefore, AMHS is the best candidate to be employed as a structural element.

The in-depth investigation carried out, which combines experimental findings with design equations based on structural mechanics, has allowed to identify improvement routes to enhance the structural response of AMHSR.

To increase AMHSR beams structural capacity, two main options can be implemented: the first is to increase the interlaminar shear strength of the skins, the second is to increase the wrinkling stress limit. This would lead to exploit the maximum capacity of the skins, i.e., the skin compression failure will be incepted instead of the skin wrinkling-delamination failure. Moreover, mitigating the identified structural weaknesses is expected to enhance the skins compressive strength, increasing the overall AMHSR performance.

The most relevant structural weaknesses which cause the low wrinkling stress and the low interlaminar shear strength of the skins are:

- initial imperfections in the skins, seen as fibre in-plane and out-of-plane waviness, which are due to the additive manufacturing methodology employed for the skins;
- poor inter-layer bonding in the skins and in the core, due to the employed materials and to FDM based AM techniques;
- manufacturing imperfections (e.g., voids) in the skins and in the core.

Considering the provided findings, it emerges that the development of tailored design solutions, as well as of AM techniques and base materials, has to be oriented to address specific structural weaknesses. Such weaknesses, together with materials requirements, can be identified using a validated design methodology. Therefore, such a design method has to be considered a relevant tool to orient design solutions, manufacturing techniques and material developments towards the enhancement of structural performances. The multi-objective optimization framework developed will be indeed used in Chapter 7 to perform the optimal design of AMHSR beams to be employed as primary structural elements in navy vessels. Moreover, such a design method will be used to identify materials specification that provide outstanding structural performances.

7 NUMERICAL ASSESSMENT OF SANDWICH STRUCTURES PRODUCED BY AM

The present chapter addresses to which extent Additive Manufactured Honeycomb Sandwich (AMHS) can be applied as primary structural elements in navy ships (section 7.1). Moreover, the work conducted establishes solid benchmarks w. r. t. traditionally employed structures and to Classification Society Rules (section 7.2).

The long-term objective is to develop design and manufacturing methodologies to integrate innovative structural solutions in the midship section, and even in the whole ship structure, of different types of vessels. Such integration is oriented to obtain the improvement of performances (e.g., reduction of weight, carbon emissions) and the reduction of overall costs in comparison to traditional structures.

The above-stated vision has been adopted in the present PhD work and in previous studies [6], [54]. The objective of such studies has been to optimize the design of the midship section of a bulk carrier by using Aluminium Honeycomb Sandwich (AHS). Such an innovative structural solution is employed to replace the steel plates of the inner side shell of the cargo hold, creating a hybrid structure, together with the supporting longitudinal reinforcements, as illustrated in Figure 58.

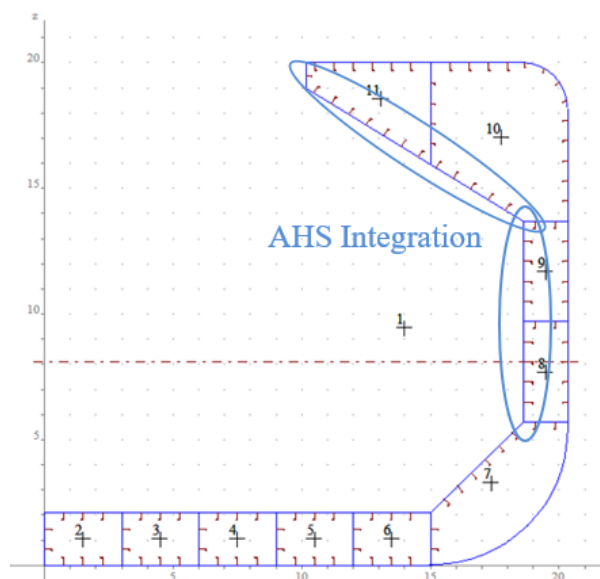


Figure 58: Integration of AHS in the midship section of a bulk carrier

The structural design has been performed leveraging multi-objective design methods. The optimal structural solution has been identified by setting a specific multi-objective optimization problem, aimed at maximizing the ultimate hull strength and the annual cargo and at minimizing the ship cost, lightship weight and transportation cost, while satisfying the imposed structural constraints on steel and AHS structures. The main benefit of using the proposed hybrid solution for the ship structural design, instead of the full steel design solution, is a significant decrease of the lightweight (approx. 13 %) and the ship cost (approx. 11 %). Additionally, it was proven that aluminium sandwich structures provide less energy consumption and carbon footprint, especially if aluminium from secondary production is utilized for ship manufacturing. In this case, a potential 57% of energy savings and 71% of carbon footprint reductions were found in the material production process, compared to the full steel solution.

It is worth mentioning that the present work employs a procedure similar to the above-stated one to assess the potential of the structural solutions developed within the PhD thesis framework. A Fast Patrol Vessel (FPV) is taken as reference for the analysis to be conducted. Therefore, the results presented in section 7.1 have to be related to the demanding structural requirements of such a navy ship. However, the same procedure can be applied to assess the potential of AMHS w. r. t. different types of vessels, such as pleasure yachts, to assess their range of applicability.

7.1 ASSESSMENT OF AMHSR FOR FPV MIDSHIP SECTION DESIGN

This section addresses to which extent AMHSR can be employed as primary structural members in navy ships. Moreover, it will address the capabilities of the developed design methodology.

The activities conducted have dealt with the optimal design of AMHSR according to Fast Patrol Vessels (FPV) structural requirements from the Lloyd Register. The requirements for the analysis have been identified according to an FPV design benchmark. In particular, reference has been made to an already designed and manufactured fast patrol vessel, which has been realized in steel [55].

From the analysis of the traditional FPV midship design, it has emerged that it is currently impossible to employ AMHSR structures directly. The maximum compressive stress acting at the bottom (in hogging condition) is indeed 120 MPa, which is beyond the maximum capacity of AMHSR skins. Therefore, the whole midship section should be re-designed to lower such stresses to the suited AMHSR structural limit. Since this is not the goal of this study, a different approach has been followed.

To demonstrate the capabilities of AMHSR, a currently employed steel primary stiffener and its associated steel plate are extracted from the midship section to be replaced by an AMHSR primary stiffener. The analysis aims to identify the optimal AMHSR structure that can resist to a specific design load, with the same safety coefficient applied for the steel primary member design. Hereafter, the steel primary stiffener and the replacing AMHSR structure are compared to evaluate the potential of the AMHSR solution.

The FPV midship section, taken as a reference [55], comprises shell plating reinforced by secondary and primary frames. A standard bulb profile is used as a secondary member, while fabricated T profiles are employed as primary members. The fabricated T profiles, employed as primary members in the FPV midship section, have been taken as a reference for the analysis. In particular, the structural replacement to be conducted is highlighted in Figure 59.

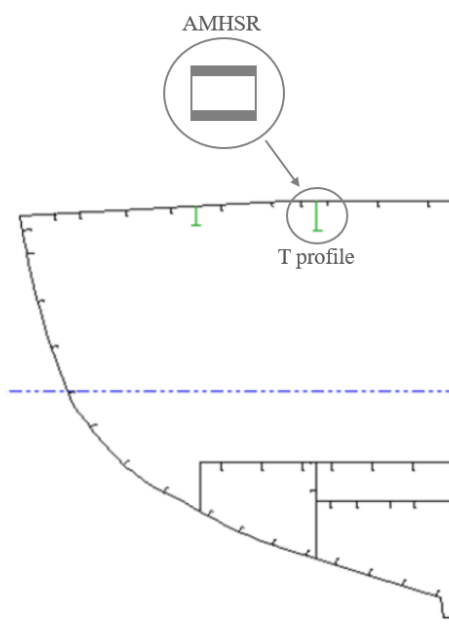


Figure 59: Replacement of T profile primary stiffener with AMHSR primary stiffener

The comparison is conducted by considering two different design solutions:

1. the optimal AMHSR structure is designed considering the current base materials properties. Regarding the EMOO framework, the value of the length design variable has been fixed within 5% of the longitudinal frame spacing for comparison purposes;
2. the optimal AMHSR structure is designed considering the base materials mechanical properties as design variables. Regarding the EMOO framework, the values of the length, breadth and total sandwich thickness have been fixed within 5% of those of the steel primary member for comparison purposes.

The design load considered for the design of AMHSR is the one which generates in the steel primary stiffener (and associated plate), loaded in 3-point bending, the maximum stresses registered in the midship section of the FPV (120 MPa). It has been calculated according to the following formula:

$$P = \frac{4\sigma_{\max} I_{ps}}{(h + H + t - y_c)L_f}$$

Where:

- $P[N]$ load to be applied at sandwich midspan;
- $\sigma_{\max}[MPa]$ is the maximum normal stress at the bottom in sagging condition, taken as 120 MPa;
- $I_{ps}[mm^4]$ is the moment of inertia of the steel T profile w. r. t. the neutral axis, accounting for the associated steel plate;
- $y_c[mm]$ is the distance from the T profile base from the neutral axis, accounting for the associated steel plate;
- $H[mm]$ is the height of the web;
- $h[mm]$ is the thickness of the flange;
- $t[mm]$ is the thickness of the associated plate made of steel;
- $L_f[mm]$ is the longitudinal frame spacing, taken as 1m.

Utilizing the additive manufacturing technology is expected to imply a new design paradigm for the midship section. Therefore, the T profile and its associated plate have been replaced by an AMHSR primary stiffener without an associated plate. The plate effect on the flexural stiffness and on the total weight is indeed considered only for the T primary member.

The design load has been calculated for all the primary members employed in the midship section of the steel FPV. Their geometry, neutral axis, inertia and the corresponding load at midspan (to be used for AMHSR design) are reported in Table 10. The most prominent structural member (number 5), i.e., the most critical in relation to the loading condition, has been considered for the analysis.

A comparison between the T primary member and the replacing AMHSR structure is illustrated in Figure 60, which highlights their main geometrical features.

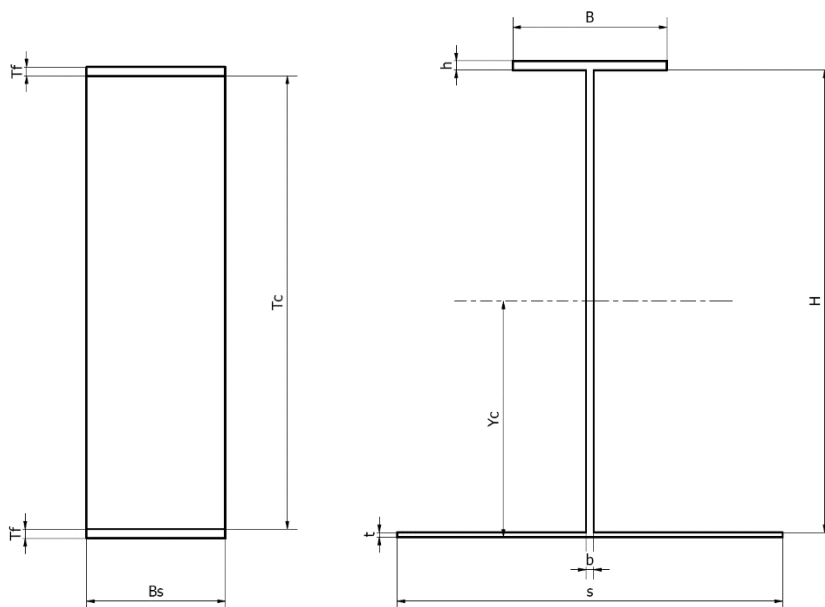


Figure 60: AMHSR (left) vs T primary stiffener (right)

Table 10: T primary stiffeners specifications - Steel FPV

Primary stiffener	B [mm]	h [mm]	H [mm]	b [mm]	L [mm]	Yc [mm]	Ix [mm ⁴]	Design Load [N]
1	70	6	100	5	1000	40.67	3646652	25432
2	70	4	200	4	1000	72.57	12769511	45425
3	100	6	200	4	1000	91.53	17767738	72294
4	100	6	250	4	1000	114.72	28628799	94915
5	100	6	300	5	1000	139.72	44883123	126896

The multi-objective optimization design has been conducted for AMHSR using the maximum load from the above table (member 5), with reference to the framework provided in section 6.4. The optimal design procedure for AMHSR utilizes the same safety coefficient applied for the steel primary member design. Such a coefficient equals approximately two, as the steel yield strength is 235 MPa and the acting normal stress is 120 MPa. Moreover, it has been verified that the AMHSR primary stiffener has a flexural modulus equal to or higher than the steel primary member, to guarantee compliance with Classification Society Rules.

The results of the optimization process are shown in Figure 61, Figure 62 and Figure 63 in terms of pareto frontier for all the combinations of the objective functions with the weight objective function, which is considered one of the most relevant from a design perspective.

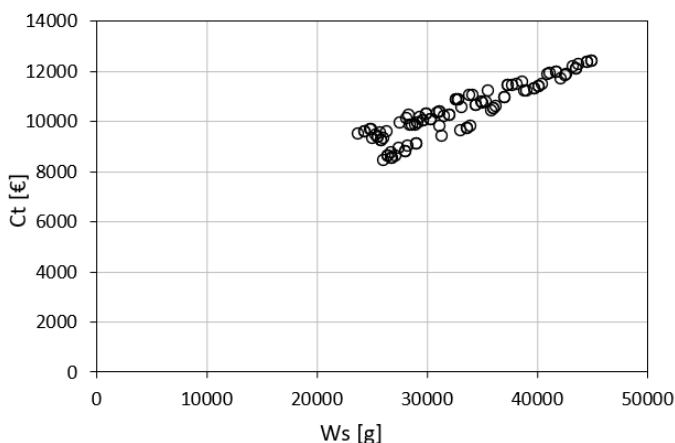


Figure 61: Pareto frontier – Cost vs Weight

Figure 61 shows that, as expected, the relationship between the cost and the weight is almost linear. Therefore, reducing the weight of the structure usually leads to a cost reduction, despite the combination of design variables.

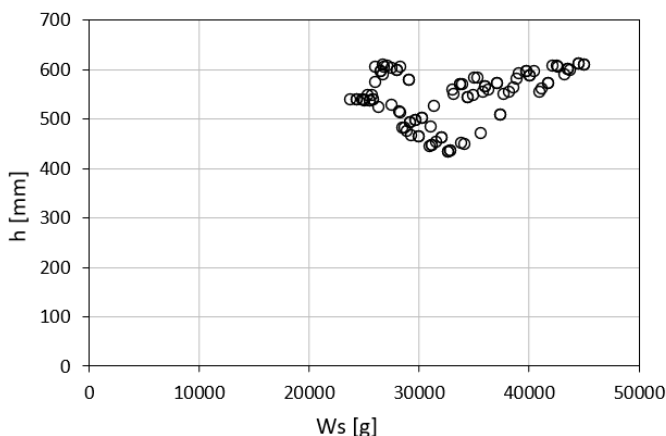


Figure 62: Pareto frontier – Total thickness vs Weight

Figure 62 shows that the total thickness is not extremely sensitive to the weight variations, as for different weight values, different optimal solutions are obtained for a given total thickness. However, it is interesting to note that a few design variable combinations reduce the total height of the structure.

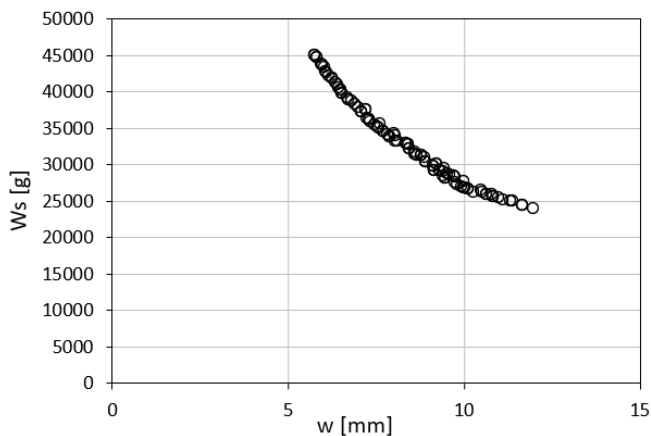


Figure 63: Pareto frontier – Displacement vs Weight

Figure 63 shows that, as expected, the weight is inversely proportional to the displacement. This means increasing the weight of the structure leads to a decrease of the displacement at midspan, despite the combination of design variables.

The AMHSR structure, to be used for comparison purposes, has been chosen among all the optimal solutions (on the Pareto front) leveraging the weighted score method as a multi-criteria decision-making approach. The coefficients utilized for the selection are: 0.1 as the weight factor for the displacement and cost functions and 0.4 as the weight factor for the total thickness and weight functions.

The comparison between the optimally designed AMHSR primary stiffener and the steel primary member is reported in Table 11. The base materials mechanical properties which constitute the two explored design solutions are given in Table 12.

Table 11: Structural solutions for FPV primary stiffener – AMHSR vs T steel profile

	Length [mm]	Breadth [mm]	Height [mm]	Displacement [mm]	Weight [kg]	Cost [€]
AMHSR 1	953	287	537 ($t_f = 6.4$)	12	23.8	9486
AMHSR 2	950	105	314 ($t_f = 6.4$)	10	8	3378
T profile	1000	100	306	0.26	23.2	15

Table 12: Structural solutions comparison – AMHSR mechanical properties

	σ_{yf} [MPa]	τ_{fs} [MPa]	E_f [MPa]	G_{cs} [MPa]	E_{cs3} [MPa]	τ_{cs} [MPa]
AMHSR 1	100	10	35000	270	1000	10
AMHSR 2	388	40	140000	1000	4000	29

The main considerations are the following:

- the AMHSR 1 design solution is worse than the steel primary member in all aspects. To achieve a compliant solution, the breadth and total thickness must be increased by almost three and twice, respectively. Moreover, the weight and the displacement are higher for AMHSR and the cost is not comparable;
- the AMHSR 2 design solution achieves outstanding results. If the optimal values of the mechanical properties (Table 12) are matched, the weight of the structure would be three times lower by keeping the encumbrances within the 5% w. r. t. the traditional solution. The displacement is two orders of magnitude higher, while the cost is again not comparable. The displacement is higher for the AMHSR structure, even if its flexural modulus is higher than the steel member, because AMHSR is more sensitive to the shear load. To

decrease the displacement at midspan, the shear modulus of the core base material has to be enhanced. The difference in costs is explained below;

- despite the cost being far higher w. r. t. the traditional structure for both the AMHSR design solutions, it is worth noting that for the AMHSR 2 the cost is three times lower than AMHSR 1. Therefore, it can be stated that employing optimal mechanical properties leads to great benefits in both weight and cost.

The cost analysis has been conducted considering only the cost of the material employed. The steel cost is 0.9 €/kg, referred to shipbuilding steel sheets of AH32 AH36 AH40. The cost of the structures is not comparable, and the AMHSR cost is two orders of magnitude higher w. r. t. the steel primary stiffener currently employed. This difference is mainly due to the fact that the hardware considered for the analysis (desktop 3D printer) is not suited to manufacture full-scale AMHSR structures. Moreover, the prices of the raw materials are not aligned with large-structure manufacturing.

Considering the provided framework, it can be concluded that Additive Manufactured Honeycomb Sandwich are very promising structural solutions when performance (weight) gains are the design priority, and the cost is less important. This may be the case for navy ships, where the increase of vessels capabilities in relation to the mission profile is a relevant design objective. Moreover, another scenario may be when the weight saving leads to less fuel consumption or more payload. Therefore, the initial investment reaches the breakeven point in a reasonable amount of years.

It is finally worth mentioning that to unlock the full potential of Additive Manufactured Honeycomb Sandwich structures, the following main developments need to be conducted:

- to develop base materials that satisfy the requirements of specific applications (e.g., mechanical properties, functionalities), which can be identified leveraging validated and optimal design methods;
- to develop efficient deposition methodologies tailored to mitigate the identified AMHS structural weakness and that fully achieve the base material requirements.

7.2 COMPARISON AGAINST RINA RULES AND TRADITIONAL STRUCTURES

This section has the main objective of evaluating the compliance of AMHSR structures w. r. t. minimum materials requirements from Classification Societies Rules and to compare their structural response against traditional honeycomb structures. This work will thus establish a benchmark to be taken as a reference for future developments.

The minimum requirements from RINA rules for FPV [49], [56] have been verified for the sandwich bending strength and for the core shear response. Since minimum requirements on the shear response of the honeycomb material are not present [49], the comparison is carried out considering the requirements imposed for typically employed core materials.

The comparison against traditionally employed honeycomb materials is conducted considering the shear performances, as these are the only available data from the main honeycomb providers (e.g., Hexcel).

According to RINA requirements for FPV [56], the minimum breaking strength of the sandwich loaded in bending must be equal to the one obtained using the following formula. Such a formula has been derived considering the maximum thickness among the tested ones ($t_f = 2.4$). Two values have been reported according to the vacuum content in the skins (μ_0).

$$\sigma_{br} = k \frac{EI}{I} (1 - \mu_0)^2 10^{-3} = 303 \text{ [MPa]} \quad (\mu_0 = 0)$$

$$\sigma_{br} = k \frac{EI}{I} (1 - \mu_0)^2 10^{-3} = 48.4 \text{ [MPa]} \quad (\mu_0 = 0.6)$$

Where:

- EI [Nmm^2 / mm] is the flexural stiffness of the sandwich laminate by millimetre of width. It is obtained by summing the contribution of the skin and core layers, as required by the standard;
- I [mm^4 / mm] is the inertia of the sandwich laminate by millimetre of width. It is obtained by summing the contribution of the skin and core layers, as required by the standard;

- $E[N/mm^2]$ is the Young's modulus of the considered element (core, skin);
- μ_0 vacuum content of skins. It should be equal to 0 if no information is available;
- k is a coefficient dependent on the type of reinforcement and matrix used. It has been taken as 12.5 for laminates using carbon fibre and epoxy resin. It is worth mentioning that the resin by which the fibre is impregnated is not of the epoxy type but is a thermoplastic material (PA12).

It is well known that the highest bending strength is obtained for the lower vacuum content in the skins ($\mu_0 = 0$). The manufacturing process has thus to be oriented to reduce the vacuum content in the skins and, in general, in the whole structure.

The analysed structure would comply with the RINA requirements if the vacuum content in AMHSR skins was 60% or more, considering as reference the minimum normal stress in the skins at failure (among all the tested specimens). Since the additive manufacturing process is prone to defects, such a value may be reasonable. However, since no information is available, and since, in any case, such value would be too high, the AMHSR structure is currently non-compliant with Classification Society Rules for FPVs.

A comparison among the minimum requirements imposed by RINA [49] for commonly employed core types, traditionally manufactured honeycomb from Hexcel and AMHSR honeycomb properties is carried out in Table 13.

The minimum shear specifications from RINA and the shear properties of traditionally manufactured honeycombs depend on the employed core type and density. Therefore, the comparison is carried out by choosing similar density values, when possible. Moreover, the weaker honeycomb direction is selected as a reference.

Table 13: Shear response comparison – AMHSR vs RINA and EXCEL

	Core type	Density [kg/m^3]	Shear stress limit [MPa]	Shear modulus [MPa]
<i>RINA</i> <i>requirements</i>	Balsa wood	144	1.64	129
	Expanded PVC foam	140	2.3	64
	Expanded PUR foam	140	1.1	13
<i>Hexcel</i>	Aluminium 5052 Flex-Core F80-.0025-8.0	128	1.8	213
	Fiberglass Flex-Core HRP/F50-5.5	88	1.2	124
<i>AMHSR</i>	Nomex Flex-Core HRH-10/F50-5.5	88	1.2	39
	Chopped fibre-reinforced nylon honeycomb	140	1.3	17.8

The comparison reveals that the AMHSR honeycomb core complies with Classification Society rules if the minimum requirements for the expanded Polyurethane (PUR) foam are considered. At the same time, it is not compliant if the other listed materials (balsa wood, PVC) are taken as a reference. Moreover, their shear response is lower w. r. t. the honeycomb core materials traditionally employed in industries. The highest differences are encountered for the shear modulus, while the limit shear stresses for the core are comparable.

The analysis carried out in Chapter 6 has shown the core shear failure is not incepted for AMHSR beams ($l_s / b_s > 3$), while it is a relevant failure mode for AMHSR panels ($l_s / b_s < 3$). Therefore, the lower shear performances of AMHSR honeycomb impact the displacement under load. The higher shear sensitivity of AMHSR has been indeed seen in section 7.1, where the displacement under load was far higher than that of traditionally employed structural solutions.

From the comparison conducted, one of the weakest structural features of AMHSR is, together with the compressive response of the skins, the shear response of the core. This finding is related to the employed AM technique and to the used core base material. The shear modulus of the honeycomb is indeed linearly associated with the

interlaminar shear modulus of its base material, while the shear stress limit is related to its interlaminar shear strength. Therefore, to obtain superior properties w. r. t. currently employed structures, the research must focus on improving the core interlaminar shear response.

7.3 DISCUSSION

The present chapter has addressed to which extent Additive Manufactured Honeycomb Sandwich can be applied as structural elements in Fast Patrol Vessels (FPV) and has established a benchmark w. r. t. Classification Society Rules and traditional structures currently employed in the maritime field.

The main findings of the activities are the following:

- to employ AMHSR structures in the midship section of FPV, a re-design of the midship section is necessary to lower the compressive stresses to a suited AMHSR limit. Currently, the analysed AMHSR structures are not suited to be employed as structural elements, even if such a re-design would be conducted. However, an optimal combination of the base materials mechanical properties has been found to achieve an outstanding weight reduction of three times, by keeping the same structure encumbrances;
- the structural displacement under load and the cost of the structure are two orders of magnitude higher w. r. t. traditionally employed steel T profiles. The difference in displacement is related to the higher sensitivity of AMHSR to the shear load, due to the low shear performances of the core. The difference in costs is due to the hardware considered for the analysis (desktop 3D printer) and to the readiness of the raw materials market, which are not yet prone to large structure manufacturing;
- the minimum bending strength requirement from RINA rules for FPV is dependent on the vacuum content in the skins. The structure would comply with the RINA requirements if the vacuum content in AMHSR skins was 60% or more. However, since no information is available, the structure is currently non-compliant with Classification Society Rules;
- the AMHSR honeycomb shear performances are above the minimum requirements of the Classification Societies Rules for the PUR foam cores. However, they are lower if other typically employed core materials are considered. Moreover, their shear response is lower w. r. t. traditionally manufactured honeycomb cores. The highest differences have been found in

shear moduli, while the shear limit stresses are comparable. As core shear failure hardly occurs for sandwich beams, this finding mainly influences the response of AMHSR beams in terms of shear stiffness, and thus, of displacement under load.

From the study conducted, it can be stated that to achieve the integration of AMHSR structures in navy ships, there is the need to face the following main challenges:

- the structural weaknesses of the skins, which cause the low wrinkling stress and the low interlaminar shear strength, need to be mitigated. If such structural problems would be solved, this would lead to the inception of skin compression failure and to the improvement of their compressive strength. The skins will thus be exploited up to their maximum capacity, which, in turn, will be enhanced. Improving the compressive response of the skins is the key to achieve compliance with Classification Societies Rules and to obtain a structure that withstands typical compressive loads acting in FPV midship sections;
- the interlaminar shear response of the AMHSR honeycomb core needs to be enhanced. For sandwich beams, the main goal is to increase the shear stiffness and thus reduce the structural displacement under load. In addition to the above, the core shear strength needs to be considered for sandwich panels. Improving the interlaminar shear response of the core is the key to fully match minimum material requirements imposed by Classification Society Rules and to obtain comparable (or superior) performances w. r. t. traditionally employed honeycomb cores. This problem needs to be faced choosing proper core base materials and manufacturing procedures;
- the total cost of the structure, together with the manufacturing time, needs to be carefully controlled. This can be done by choosing proper raw materials and by implementing a purposely developed manufacturing process (e.g., RAM), which is also oriented to mitigate the identified structural weaknesses.

This chapter has demonstrated the development of optimal and validated design methods is the key to achieve outstanding structural performances. Moreover, the utilization of such methods to identify key design parameters, such as structural weaknesses or base material requirements, is of unprecedented importance to enhance performances and to guide the development of materials and manufacturing procedures.

8 CONCLUSIONS

The main objective of the present PhD thesis has been to understand to which extent the key enabling technology of Robotic Additive Manufacturing (RAM) can be employed to produce multi-functional and multi-material composite structures with outstanding performances, oriented to specific structural applications. In particular, the work deals with Additive Manufactured Honeycomb Sandwich (AMHS) structures to be employed as structural elements in navy ships.

The first task of the PhD work has dealt with the development of the conceptual design of a Robotic Additive Manufacturing (RAM) platform tailored to satisfy the main needs of the maritime sector (Chapter 4). Such a platform leverages Fused Deposition Modelling (FDM) based techniques for Fiber Reinforced Plastic (FRP) additive manufacturing. Such techniques have been identified, according to specific indicators, as promising Additive Manufacturing (AM) methods for structural applications in the maritime sector (section 4.1). The conceptual design of a hybrid RAM platform has been developed in terms of design and manufacturing workflow, where additive and subtractive manufacturing techniques, optimal design methods and robotics are combined to achieve a flexible, smart, low-cost and low-waste process (section 4.2). Finally, key research areas to be addressed to fully integrate RAM technology in the maritime sector have been highlighted (section 4.3). In this regard, particular attention has to be dedicated to validated optimal design methods as key tools to achieve outstanding structural performances and to guide the development of innovative manufacturing techniques and materials.

The second task of the PhD work has concerned the assessment of the potential of FDM based techniques for FRP additive manufacturing (Chapter 5), which have been previously identified as promising solutions for RAM applications. The tensile response of FRP specimens, produced through a purposely selected AM technique, has been analysed through a systematic testing campaign. In particular, the influence of fibre reinforcement type (chopped and continuous carbon fibres), AM deposition path and post-manufacturing treatments (annealing) on the mechanical properties of additive manufactured FRPs has been evaluated (section 5.2). Moreover, the potential applicability of additive manufactured FRPs to marine structures has been assessed, by comparison with minimum material requirements imposed by Classification Society Rules and with traditionally manufactured composites (section 5.3). According to the study, the mechanical properties of continuous FRPs are approximately seven times higher than chopped FRPs ones. Moreover, such properties are greatly affected by the deposition path and altered by the annealing

treatment. In particular, the tensile response is more than doubled if the deposition path is aligned with the load direction, while the annealing post-manufacturing treatment enhances it by approximately 10%. The analysis of Classification Society Rules revealed the current achievable fibre volume fraction does not match the one imposed for the production of the specimens. Despite such findings, interestingly, continuous FRPs produced by AM match the minimum structural requirements imposed by the standards in terms of tensile response. Moreover, their mechanical properties are comparable to some of the traditionally manufactured composites. However, such properties are currently lower than the ones of composite structures manufactured using traditional methods.

The PhD work has proceeded with the development of an optimal design methodology for raw Additive Manufactured Honeycomb Sandwich (AMHSR) subjected to flexural loads (3-point bending condition) and with the assessment of the potential of purposely developed sandwich solutions (Chapter 6). The design procedure leverages an Evolutionary Multi-Objective Optimization (EMOO) routine, which identifies the optimal structure according to specific objectives and constraints (section 6.4). The analytical formulations utilized in the optimization process have been derived using a combined analytical and experimental approach (section 6.2). A systematic testing campaign has been conducted on specimens manufactured through the previously analysed multi-material AM technique (section 6.3). The most relevant finding of this work is the development of purposely conceived analytical formulations to predict the structural response. In particular, the formulation to predict the load-displacement relation has been developed, containing the error below 10% in the design range. Moreover, the work provides formulations to predict the load at failure and the expected failure mode. Specific failure criteria have indeed been developed for skin and core failure. The skin fails in a combined failure mode, which considers delamination as a promoter of wrinkling, while the core fails by interlaminar shear. The other part of the work has demonstrated the flexural response may be greatly enhanced by purposely developed design solutions, while keeping almost the same geometry, constituent materials and mechanical properties. It has been indeed found that embedding a raw sandwich structure (produced by AM) within a plastic shell increases the flexural response by approximately 50%.

The final task of the PhD work has addressed to which extent raw Additive Manufactured Honeycomb Sandwich (AMHSR) can be applied as primary structural stiffeners in navy ships (Fast Patrol Vessels). Moreover, solid benchmarks w. r. t.

traditional structures and Classification Society Rules have been established (Chapter 7). To demonstrate the capabilities of AMHSR, an already designed and manufactured Fast Patrol Vessel (FPV) has been taken as a reference. A currently employed steel primary stiffener and its associated plate have been extracted from the midship section and replaced by AMHSR (section 7.1). To establish benchmarks w. r. t. Classification Society Rules and traditional structures, the bending and shear performances of AMHSR have been compared to minimum requirements imposed by Classification Society Rules and to traditionally manufactured honeycomb cores (section 7.2). It has been found that, to employ AMHSR structures in the midship section of steel FPVs, a re-design of the midship section is necessary to lower the compressive stresses to a suited AMHSR limit. Currently, the analysed AMHSR structure are not suited to be employed as structural elements, even if such a re-design would be conducted. However, an optimal combination of the mechanical properties of sandwich base materials has been found to achieve a weight reduction of three times by keeping the same structure encumbrances. This is an outstanding result, in contrast to the fact the structural displacement under load and the cost of the structure are two orders of magnitude higher w. r. t. traditionally employed steel T profiles. The analysis of Classification Society Rules for FPVs revealed the structure is currently non-compliant with the rules in terms of bending strength, as no information on the vacuum content in the skins is available. In contrast, the AMHSR honeycomb shear performances are above the minimum requirements imposed by the Classification Societies Rules for the PUR foam cores. However, they are lower if other typically employed core materials in navy ships are considered. Moreover, their shear response is lower w. r. t. traditionally manufactured honeycomb cores.

Given the above framework, it can be stated that the combination of validated optimal design methods, additive manufacturing and robotics has the potential to provide innovative multi-material and multi-functional structures, such as AMHS, that possess outstanding structural performances and thus the ability to enhance navy vessels capabilities. Moreover, it has been demonstrated the development of validated design methods is of outmost importance to provide guidelines and requirements to enhance manufacturing techniques and raw materials.

It is finally worth mentioning that to fully integrate innovative structural solutions and manufacturing technologies, such as AMHS and RAM, there is the need to face a few challenges. The most relevant ones are listed in the following section as future research routes to be addressed.

8.1 FUTURE RESEARCH ROUTES

The future research routes to be addressed to fully integrate multi-material and multi-functional sandwich structures, produced by the RAM technology, in navy vessels are the following:

- development of sandwich base materials (constituents of skin and core) that match specific mechanical properties requirements, in relation to the application. Such requirements can be set by validated design methods in relation to the structural specifications of the component and by the Classification Society Rules. The developments should be oriented towards environmentally friendly materials, whose utilization may lead to sustainable marine structures and manufacturing methods. Moreover, such materials may embed different types of fillers, enabling the multifunctionality of the structure (e.g., fire resistance, radar invisibility, etc.);
- development of a deposition methodology that aims to enhance the sandwich structural response, fulfilling material requirements. In particular, both the materials to be used and the deposition technique need to be tailored to mitigate the structural weaknesses that have emerged from the study, such as low skin wrinkling limit stress and low interlaminar shear response of the skins and of the core;
- development of an application-oriented RAM platform for sandwich production, which integrates the above-mentioned depositing methodology, to achieve a flexible, smart, low-cost and low-waste process;
- development and validation of optimal design procedures for additive manufactured sandwich beams and panels subjected to different loading conditions (e.g., uniaxial compression, lateral pressure);
- development and validation of a design procedure to achieve the full midship section design leveraging the single structural element response;
- development and validation of design procedures for structural joints, localized loads and load introductions (e.g., inserts);
- development of a RAM process to achieve the full midship section manufacturing, to be conducted by assembling the structural elements which constitute its geometry.

REFERENCES

- [1] B. Esmailian, S. Behdad, and B. Wang, “The evolution and future of manufacturing: A review,” *J. Manuf. Syst.*, vol. 39, pp. 79–100, 2016, doi: 10.1016/j.jmsy.2016.03.001.
- [2] J. Plocher and A. Panesar, “Review on design and structural optimisation in additive manufacturing: Towards next-generation lightweight structures,” *Mater. Des.*, vol. 183, 2019, doi: 10.1016/j.matdes.2019.108164.
- [3] Y. Li, G. Jia, Y. Cheng, and Y. Hu, “Additive manufacturing technology in spare parts supply chain: a comparative study,” *Int. J. Prod. Res.*, vol. 55, no. 5, pp. 1498–1515, 2017, doi: 10.1080/00207543.2016.1231433.
- [4] D. Santos González and A. González Álvarez, “Additive Manufacturing Feasibility Study & Technology Demonstration,” *Eur. Def. Agency*, pp. 1–187, 2018.
- [5] E. Peterson, “Recent Innovations in Additive Manufacturing for Marine Vessels,” *Marit. Technol. Res.*, vol. 4, no. 4, p. 257491, 2022, doi: 10.33175/mtr.2022.257491.
- [6] G. Palomba, S. Scattareggia Marchese, V. Crupi, and Y. Garbatov, “Cost, Energy Efficiency and Carbon Footprint Analysis of Hybrid Light - Weight Bulk Carrier,” *J. Mar. Sci. Eng.*, no. 10, p. 957, 2022, doi: <https://doi.org/10.3390/jmse10070957>.
- [7] G. Palomba, P. Corigliano, V. Crupi, G. Epasto, and E. Guglielmino, “Static and Fatigue Full-Scale Tests on a Lightweight Ship Balcony Overhang with Al/Fe Structural Transition Joints,” *J. Mar. Sci. Eng.*, vol. 10, no. 10, 2022, doi: 10.3390/jmse10101382.
- [8] G. Palomba, G. Epasto, L. Sutherland, and V. Crupi, “Aluminium honeycomb sandwich as a design alternative for lightweight marine structures,” *Ships Offshore Struct.*, vol. 17, no. 10, pp. 2355–2366, 2022, doi: 10.1080/17445302.2021.1996109.
- [9] T. D. Ngo, A. Kashani, G. Imbalzano, K. T. Q. Nguyen, and D. Hui, “Additive manufacturing (3D printing): A review of materials, methods, applications and challenges,” *Compos. Part B Eng.*, vol. 143, no. December 2017, pp. 172–196, 2018, doi: 10.1016/j.compositesb.2018.02.012.

- [10] M. Dinovitzer, X. Chen, J. Laliberte, X. Huang, and H. Frei, “Effect of wire and arc additive manufacturing (WAAM) process parameters on bead geometry and microstructure,” *Addit. Manuf.*, vol. 26, no. February, pp. 138–146, 2019, doi: 10.1016/j.addma.2018.12.013.
- [11] P. Urhal, A. Weightman, C. Diver, and P. Bartolo, “Robot assisted additive manufacturing: A review,” *Robot. Comput. Integr. Manuf.*, vol. 59, no. May, pp. 335–345, 2019, doi: 10.1016/j.rcim.2019.05.005.
- [12] M. L. L. and B. K. S. W. Lourens Gerrit Blok, “Fabrication and Characterisation of Aligned Discontinuous Carbon Fibre Reinforced Thermoplastics as Feedstock Material for Fused Filament Fabrication,” *Materials (Basel)*, 2020, doi: 10.1002/pc.25711.
- [13] J. Zhang, Z. Zhou, F. Zhang, Y. Tan, Y. Tu, and B. Yang, “Performance of 3D-printed continuous-carbon-fiber-reinforced plastics with pressure,” *Materials (Basel)*, vol. 13, no. 2, 2020, doi: 10.3390/ma13020471.
- [14] J. Li, Y. Durandet, X. Huang, G. Sun, and D. Ruan, “Additively manufactured fiber-reinforced composites: A review of mechanical behavior and opportunities,” *J. Mater. Sci. Technol.*, vol. 119, pp. 219–244, 2022, doi: 10.1016/j.jmst.2021.11.063.
- [15] A. Adumitroaie, F. Antonov, A. Khaziev, A. Azarov, M. Golubev, and V. V. Vasiliev, “Novel continuous fiber bi-matrix composite 3-D printing technology,” *Materials (Basel)*, vol. 12, no. 18, pp. 1–10, 2019, doi: 10.3390/ma12183011.
- [16] A. V. Azarov *et al.*, “Development of a two-matrix composite material fabricated by 3D printing,” *Polym. Sci. - Ser. D*, vol. 10, no. 1, pp. 87–90, 2017, doi: 10.1134/S1995421217010026.
- [17] A. Taşdemir and S. Nohut, “An overview of wire arc additive manufacturing (WAAM) in shipbuilding industry,” *Ships Offshore Struct.*, vol. 0, no. 0, pp. 1–18, 2020, doi: 10.1080/17445302.2020.1786232.
- [18] W. Zhao-Hui, D. Ji-Wang, Z. Ming-Hua, and F. Xiu-Min, “Survey on Flexible Shipbuilding Technologies for Curved Ship-Blocks,” *Procedia Eng.*, vol. 174, pp. 800–807, 2017, doi: 10.1016/j.proeng.2017.01.225.
- [19] A. Vahedi Nemani, M. Ghaffari, and A. Nasiri, “Comparison of microstructural characteristics and mechanical properties of shipbuilding steel plates fabricated by conventional rolling versus wire arc additive manufacturing,” *Addit. Manuf.*, vol. 32, no. December 2019, 2020, doi: 10.1016/j.addma.2020.101086.

- [20] P. Muller, G. Rückert, and P. Vinot, “On the benefits of metallic additive manufacturing for propellers,” *Sixth Int. Symp. Mar. Propulsors smp’19, Rome, Italy*, no. May, 2019.
- [21] S. Ford and M. Despeisse, “Additive manufacturing and sustainability: an exploratory study of the advantages and challenges,” *J. Clean. Prod.*, vol. 137, pp. 1573–1587, 2016, doi: 10.1016/j.jclepro.2016.04.150.
- [22] L. Yuan *et al.*, “Fabrication of metallic parts with overhanging structures using the robotic wire arc additive manufacturing,” *J. Manuf. Process.*, vol. 63, no. November 2019, pp. 24–34, 2021, doi: 10.1016/j.jmapro.2020.03.018.
- [23] M. Ziółkowski and T. Dyl, “Possible applications of additive manufacturing technologies in shipbuilding: A review,” *Machines*, vol. 8, no. 4, pp. 1–34, 2020, doi: 10.3390/machines8040084.
- [24] W. Tao and M. C. Leu, “Design of lattice structure for additive manufacturing,” *Int. Symp. Flex. Autom. ISFA 2016*, pp. 325–332, 2016, doi: 10.1109/ISFA.2016.7790182.
- [25] G. Epasto, G. Palomba, D. D’Andrea, E. Guglielmino, S. Di Bella, and F. Traina, “Ti-6Al-4V ELI microlattice structures manufactured by electron beam melting: Effect of unit cell dimensions and morphology on mechanical behaviour,” *Mater. Sci. Eng. A*, vol. 753, no. November 2018, pp. 31–41, 2019, doi: 10.1016/j.msea.2019.03.014.
- [26] J. G. Monteiro *et al.*, “Evaluation of the effect of core lattice topology on the properties of sandwich panels produced by additive manufacturing,” *Proc. Inst. Mech. Eng. Part L J. Mater. Des. Appl.*, vol. 235, no. 6, pp. 1312–1324, 2021, doi: 10.1177/1464420720958015.
- [27] S. Abrate, G. Epasto, E. Kara, V. Crupi, E. Guglielmino, and H. Aykul, “Computed tomography analysis of impact response of lightweight sandwich panels with micro lattice core,” *Proc. Inst. Mech. Eng. Part C J. Mech. Eng. Sci.*, vol. 232, no. 8, pp. 1348–1362, 2018, doi: 10.1177/0954406218766383.
- [28] R. Kaminski, T. Speck, and O. Speck, “Biomimetic 3D printed lightweight constructions: A comparison of profiles with various geometries for efficient material usage inspired by square-shaped plant stems,” *Bioinspiration and Biomimetics*, vol. 14, no. 4, 2019, doi: 10.1088/1748-3190/ab202f.
- [29] P. Tran, T. D. Ngo, A. Ghazlan, and D. Hui, “Bimaterial 3D printing and numerical analysis of bio-inspired composite structures under in-plane and

- transverse loadings,” *Compos. Part B Eng.*, vol. 108, pp. 210–223, 2017, doi: 10.1016/j.compositesb.2016.09.083.
- [30] B. Wu *et al.*, “A review of the wire arc additive manufacturing of metals: properties, defects and quality improvement,” *J. Manuf. Process.*, vol. 35, no. February, pp. 127–139, 2018, doi: 10.1016/j.jmapro.2018.08.001.
- [31] M. Shehadeh, Y. Shennawy, and H. El-Gamal, “Similitude and scaling of large structural elements: Case study,” *Alexandria Eng. J.*, vol. 54, no. 2, pp. 147–154, 2015, doi: 10.1016/j.aej.2015.01.005.
- [32] P. M. Bhatt, R. K. Malhan, A. V. Shembekar, Y. J. Yoon, and S. K. Gupta, “Expanding capabilities of additive manufacturing through use of robotics technologies: A survey,” *Addit. Manuf.*, vol. 31, no. August 2019, p. 100933, 2020, doi: 10.1016/j.addma.2019.100933.
- [33] D. Zenkert, “An Introduction to Sandwich Structures,” 1995.
- [34] C. A. Steeves and N. A. Fleck, “Collapse mechanisms of sandwich beams with composite faces and a foam core, loaded in three-point bending. Part I: Analytical models and minimum weight design,” *Int. J. Mech. Sci.*, vol. 46, no. 4, pp. 561–583, 2004, doi: 10.1016/j.ijmecsci.2004.04.003.
- [35] C. R. Schultheisz and A. M. Waas, “Compressive failure of composites, Part I: Testing and micromechanical theories,” *Prog. Aerosp. Sci.*, vol. 32, 1996.
- [36] A. M. Waas and C. R. Schultheisz, “Compressive failure of composites, Part II: Experimental studies,” *Prog. Aerosp. Sci.*, vol. 32, 1996, doi: 10.1016/0376-0421(94)00003-4.
- [37] L. Fagerberg, “Wrinkling and compression failure transition in sandwich panels,” *J. Sandw. Struct. Mater.*, vol. 6, no. 2, pp. 129–144, 2004, doi: 10.1177/1099636204030475.
- [38] L. J. Gibson and M. F. Ashby, *Cellular solids*. 1989.
- [39] HexCel Composites, “Honeycomb sandwich design technology,” *HexWeb Honeycomb Sandw. Des. Technol.*, no. AGU 075b, pp. 1–28, 2000, [Online]. Available: <http://scholar.google.com/scholar?hl=en&btnG=Search&q=intitle:Honeycomb+sandwich+design+technology#1>.
- [40] S. CORE, “Best Practice Guide for Sandwich Structures in Marine Applications,” *Best Pract. Guid. Sandw. Struct. Mar. Appl.*, p. 279, 2013.

- [41] M. J. Reddy and D. N. Kumar, “Multi-Objective Optimization using Evolutionary Algorithms: An Introduction,” *Water Resour. Manag.*, vol. 20, no. 6, pp. 861–878, 2006.
- [42] Ivántabernero, A. Paskual, P. Álvarez, and A. Suárez, “Study on Arc Welding Processes for High Deposition Rate Additive Manufacturing,” *Procedia CIRP*, vol. 68, no. April, pp. 358–362, 2018, doi: 10.1016/j.procir.2017.12.095.
- [43] P. Magnoni, L. Rebaioli, I. Fassi, N. Pedrocchi, and L. M. Tosatti, “Robotic AM System for Plastic Materials: Tuning and On-line Adjustment of Process Parameters,” *Procedia Manuf.*, vol. 11, no. June, pp. 346–354, 2017, doi: 10.1016/j.promfg.2017.07.117.
- [44] S. W. Williams, F. Martina, A. C. Addison, J. Ding, G. Pardal, and P. Colegrove, “Wire + Arc additive manufacturing,” *Mater. Sci. Technol. (United Kingdom)*, vol. 32, no. 7, pp. 641–647, 2016, doi: 10.1179/1743284715Y.0000000073.
- [45] L. G. Blok, M. L. Longana, H. Yu, and B. K. S. Woods, “An investigation into 3D printing of fibre reinforced thermoplastic composites,” *Addit. Manuf.*, vol. 22, no. April, pp. 176–186, 2018, doi: 10.1016/j.addma.2018.04.039.
- [46] J. M. Chacón, M. A. Caminero, P. J. Núñez, E. García-Plaza, I. García-Moreno, and J. M. Reverte, “Additive manufacturing of continuous fibre reinforced thermoplastic composites using fused deposition modelling: Effect of process parameters on mechanical properties,” *Compos. Sci. Technol.*, vol. 181, no. June 2018, p. 107688, 2019, doi: 10.1016/j.compscitech.2019.107688.
- [47] T. N. A. T. Rahim, A. M. Abdullah, and H. Md Akil, “Recent Developments in Fused Deposition Modeling-Based 3D Printing of Polymers and Their Composites,” *Polym. Rev.*, vol. 59, no. 4, pp. 589–624, 2019, doi: 10.1080/15583724.2019.1597883.
- [48] A. Garg and A. Bhattacharya, “An insight to the failure of FDM parts under tensile loading: finite element analysis and experimental study,” *Int. J. Mech. Sci.*, vol. 120, no. September 2016, pp. 225–236, 2017, doi: 10.1016/j.ijmecsci.2016.11.032.
- [49] RINA, “Rules For the Classification of Fast Patrol Vessels, Part D, Materials and Welding,” 2007.

-
- [50] J. Butt and R. Bhaskar, “Investigating the effects of annealing on the mechanical properties of FFF-printed thermoplastics,” *J. Manuf. Mater. Process.*, vol. 4, no. 2, pp. 1–20, 2020, doi: 10.3390/jmmp4020038.
- [51] C. Militello, F. Bongiorno, G. Epasto, and B. Zuccarello, “Low-velocity impact behaviour of green epoxy biocomposite laminates reinforced by sisal fibers,” *Compos. Struct.*, vol. 253, no. March, p. 112744, 2020, doi: 10.1016/j.compstruct.2020.112744.
- [52] P.K. Mallik, *Fiber-Reinforced Composites*. 2007.
- [53] K. Deb, A. Pratap, S. Agarwal, and T. Meyarivan, “A fast and elitist multiobjective genetic algorithm: NSGA-II,” *IEEE Trans. Evol. Comput.*, vol. 6, no. 2, pp. 182–197, 2002, doi: 10.1109/4235.996017.
- [54] Y. Garbatov, S. Scattareggia Marchese, G. Palomba, and V. Crupi, “Alternative hybrid lightweight ship hull structural design,” in *Trends in Maritime Technology and Engineering Volume 1*, Taylor & Francis Group, Ed. London: CRC Press, 2022, pp. 99–107.
- [55] N. Almany, “Ship and Structural Design and Analysis of Offshore Patrol Vessel,” no. June, 2018.
- [56] RINA, “Rules for the Classification of Fast Patrol Vessels - Part B: Hull and Stability,” 2007.

LIST OF FIGURES

FIGURE 1: ADDITIVE MANUFACTURING PROCESSES	18
FIGURE 2: TYPICAL FDM PROCESS	21
FIGURE 3: INFLUENCE OF FIBRE TYPE ON CHOPPED FRP PROPERTIES (20 WT.%) [14]	22
FIGURE 4: INFLUENCE OF FIBRE WEIGHT ON CHOPPED FRP PROPERTIES [14]	22
FIGURE 5: INFLUENCE OF PRINT TEMPERATURE ON FRP PROPERTIES [14]	23
FIGURE 6: AM OF CONTINUOUS FIBRE THROUGH FDM [15].....	24
FIGURE 7: INFLUENCE OF FIBRE TYPE ON CONTINUOUS FRP PROPERTIES [14]	25
FIGURE 8: INFLUENCE OF FVF ON CONTINUOUS FRP PROPERTIES [14].....	26
FIGURE 9: POTENTIAL BENEFITS OF THE AM/RAM TECHNOLOGY FOR SHIPBUILDING	28
FIGURE 10: EXAMPLES OF RAM FOR MARINE APPLICATIONS.....	30
FIGURE 11: SANDWICH STRUCTURE MAIN CONSTITUENTS.....	33
FIGURE 12: THE “SANDWICH EFFECT” ON FLEXURAL RESPONSE [33]	34
FIGURE 13: GEOMETRY AND PROPERTIES OF SANDWICH	35
FIGURE 14: SANDWICH BEAM IN 3-POINT BENDING	36
FIGURE 15: APPROXIMATIONS IN SANDWICH THEORY [33]	38
FIGURE 16: SANDWICH TOTAL (A), BENDING (B) AND SHEAR DEFORMATION (C) [33]	39
FIGURE 17: FAILURE MODES IN SANDWICH BEAMS. (A) FACE YIELDING/FRACTURE, (B) CORE SHEAR FAILURE, (C AND D) FACE WRINKLING, (E) GENERAL BUCKLING, (F) SHEAR CRIMPING, (G) FACE DIMPLING AND (H) LOCAL INDENTATION [33]	40
FIGURE 18: FAILURE MODES FOR A SANDWICH BEAM LOADED IN BENDING [34]	40
FIGURE 19: EXAMPLE OF NON-DOMINATED SOLUTION SET [41]	47
FIGURE 20: RAM PLATFORM GENERAL LAYOUT	55
FIGURE 21: RAM PROCESS WORKFLOW	56
FIGURE 22: (A) AM OF CHOPPED FRP; (B) AM OF CONTINUOUS FRP	63
FIGURE 23: (A) ADDITIVELY MANUFACTURED CHOPPED FRP SPECIMENS, 0°; (B) ADDITIVELY MANUFACTURED CONTINUOUS FRP SPECIMENS, 0°	64
FIGURE 24: (A) PLANNED PRINTING PATH FOR CHOPPED FRP, 0°; (B) PLANNED PRINTING PATH FOR CHOPPED FRP, 90°	66
FIGURE 25: STRESS-STRAIN RELATIONSHIP OF CHOPPED FRP WITH DIFFERENT DEPOSITION PATTERNS	67
FIGURE 26: STRESS-STRAIN RELATIONSHIP OF ANNEALED AND NON-ANNEALED CHOPPED FRP (0°)	68

FIGURE 27: (A) FAILURE MODES UNDER TENSILE LOAD FOR CHOPPED FRP-0°; (B) FAILURE MODES UNDER TENSILE LOAD FOR CHOPPED FRP-90°	69
FIGURE 28: (A) FRACTURE SURFACE OF ANNEALED CHOPPED FRP-0°; (B) FRACTURE SURFACE OF ANNEALED CHOPPED FRP-90°	69
FIGURE 29: FRACTURE SURFACE OF RAW CHOPPED FRP, 0°	70
FIGURE 30: (A) PLANNED PRINTING PATH FOR CONTINUOUS FRP-0°; (B) PLANNED PRINTING PATH FOR CONTINUOUS FRP-90°	71
FIGURE 31: FLASH THERMOGRAPHY SETUP	72
FIGURE 32: STRESS-STRAIN RELATIONSHIP OF CONTINUOUS FRP WITH DIFFERENT DEPOSITION PATTERNS	72
FIGURE 33: STRESS-STRAIN RELATIONSHIP OF ANNEALED VS NON-ANNEALED CONTINUOUS FRP (0°)	74
FIGURE 34: TENSILE FAILURE MODES OF CONTINUOUS FRP, 0° (LEFT); TENSILE FAILURE MODES OF CONTINUOUS FRP, 90° (RIGHT)	75
FIGURE 35: (A) FRACTURE SURFACE OF CONTINUOUS RAW FRP, 0°; (B) FRACTURE SURFACE OF RAW CONTINUOUS FRP, 90°	75
FIGURE 36: (A) DAMAGED SPECIMENS—ANNEALED CONTINUOUS FRP, 0°; (B) DAMAGED SPECIMENS—RAW CONTINUOUS FRP, 0°	76
FIGURE 37: STRESS-STRAIN RELATIONSHIP OF CHOPPED AND CONTINUOUS FRP ORIENTED AT 0°	77
FIGURE 38: TENSILE TEST RESULTS VS RINA MINIMUM REQUIREMENTS	79
FIGURE 39: AMHSR (LEFT) VS AMHS (RIGHT)	83
FIGURE 40: 3D CAD MODEL OF AMHSR	84
FIGURE 41: ADDITIVE MANUFACTURING PROCESS OF AMHSR	85
FIGURE 42: EXAMPLE OF DISPLACEMENT EQUATION CALIBRATION	90
FIGURE 43: STRESSES IN A SANDWICH BEAM UNDER 3-POINT BENDING	91
FIGURE 44: WRINKLING-DELAMINATION FAILURE CRITERIA FOR AMHSR SKINS....	95
FIGURE 45: EXPERIMENTAL TEST SET-UP FOR 3-POINT BENDING.....	101
FIGURE 46: FLEXURAL RESPONSE – AMHS VS AMHSR	103
FIGURE 47: SPECIMENS FAILURE MODES - AMHS VS AMHSR.....	104
FIGURE 48: INFLUENCE OF SPECIMEN LENGTH ON AMHSR FLEXURAL RESPONSE .	106
FIGURE 49: WRINKLING-DELAMINATION FAILURE CRITERIA – LENGTH.....	107
FIGURE 50: COMBINED FAILURE MODES FOR LS=50 – CORE AND SKIN FAILURE	108
FIGURE 51: SKIN WRINKLING - LS/BS>3	108
FIGURE 52: SKIN DELAMINATION PROGRESSION - LS/BS>3.....	109
FIGURE 53: INFLUENCE OF SKIN THICKNESS ON AMHSR FLEXURAL RESPONSE.....	109
FIGURE 54: SPECIMEN INDENTATION FOR TF=2.4.....	110

FIGURE 55: WRINKLING-DELAMINATION FAILURE CRITERIA – SKIN THICKNESS	110
FIGURE 56: INFLUENCE OF CORE DENSITY ON AMHSR FLEXURAL RESPONSE	111
FIGURE 57: WRINKLING-DELAMINATION FAILURE CRITERIA – CORE DENSITY	112
FIGURE 58: INTEGRATION OF AHS IN THE MIDSHIP SECTION OF A BULK CARRIER..	118
FIGURE 59: REPLACEMENT OF T PROFILE PRIMARY STIFFENER WITH AMHSR PRIMARY STIFFENER	121
FIGURE 60: AMHSR (LEFT) VS T PRIMARY STIFFENER (RIGHT)	123
FIGURE 61: PARETO FRONTIER – COST VS WEIGHT	124
FIGURE 62: PARETO FRONTIER – TOTAL THICKNESS VS WEIGHT	125
FIGURE 63: PARETO FRONTIER – DISPLACEMENT VS WEIGHT	125